DOCTOR OF PHILOSOPHY

Holocene climate variability in UK waters based on Arctica islandica sclerochronology

Estrella Martinez, Juan

Award date:
2019

Awarding institution:
Bangor University

Link to publication

Holocene climate variability in UK waters based on *Arctica islandica* sclerochronology

Juan Estrella-Martínez

A thesis submitted in accordance with the requirements of the Bangor University

for the degree of

Doctor of Philosophy

School of Ocean Sciences

Bangor University

Wales

Supervised by:

Dr. Paul G. Butler

Dr. James D. Scourse

ABSTRACT

The temperature variability in the North Atlantic is known to be a major influence on the regulation of Northern Hemisphere climate. The north-eastward transport of waters from the subtropics by the North Atlantic Current modulates the European climate. Understanding this climate variability over extended timescales informs climate and ecosystem models. In turn, these allow the forecast of future climatic conditions and the improv the management food sources. In this work, two annually resolved climatic reconstructions and one ecological reconstruction for the northern North Sea based on *Arctica islandica* (ocean quahog) sclerochronology are presented. Sclerochronology is the study of physical and chemical variations in the accretionary hard tissues of organisms, and the temporal context in which they formed. The bivalve *A. islandica* is an excellent organism on which to carry out such studies as it shows clear annual increments in its aragonitic shell which grows in close isotopic equilibrium with the ambient waters.

In the ecological study, an Atlantic herring (*Clupea harengus*) recruitment reconstruction for the 1551-2005 (Common Era, CE) interval based on carbon stable isotope geochemistry ($\delta^{13}C$) is presented. The results indicate a link between $\delta^{13}C$ and recruitment mediated by the dissolved inorganic carbon and nutrition. The reconstruction suggests that there were five extended episodes of low recruitment levels before the 20th century. These results are supported by instrumental recruitment estimates and historical fish catch and export documentation.

In the first climatic study, a bottom water temperature (BWT) reconstruction for the 1551-2004 CE interval based on oxygen stable isotope geochemistry ($\delta^{18}O$) is presented. Sub-annual shell sampling suggests that the average *A. islandica* growing season in the northern North Sea goes from February to October. The reconstruction shows an average temperature of 7.20 °C for the past c. 500 years, with warming trends of 0.05 ± 0.02 °C decade^{-1} for the years 1640-1740 and 0.08 ± 0.02 °C decade^{-1} for the years 1880-2001, and a cooling trend of -0.11 ± 0.02 °C decade^{-1} for the years 1810-1910. These trends cannot be attributed to North Atlantic sea surface temperatures (SST). Between 9 and 54 % of variability in average Feb-Oct BWT can be explained by low frequency changes in the winter North Atlantic Oscillation (NAO). A BWT/SST regression analysis suggests that the thermal stratification in the northern North Sea is susceptible to local

storm activity, while persisting under calmer conditions and storms passing through the central and southern North Sea.

In the second climatic study, a BWT and relative water stratification reconstruction during the 8.2 ka event (8,200 years before 1950 CE, cal BP) based on $\delta^{18}O$ and $\delta^{13}C$ is presented. The results indicate that a sudden sea level rise (SSLR) event-driven column stratification occurred between ages 8320-8220 cal BP. Thirty years later, cold conditions inhibited water column stratification but an eventual incursion of sub-Arctic waters into the North Sea re-established density-driven stratification. The water temperatures reached their minimum of ~3.8 °C 55 years after the SSLR. Intermittently-mixed conditions were later established when the sub-Arctic waters receded.

Through these studies it is demonstrated that molluscan sclerochronological records can contribute to climatic and ecological investigations in different timescales. These studies show how factors like sea level, water mass and storminess can all contribute to the strength of the seasonal water column stratification and how primary production affects the $\delta^{13}C$ of the dissolved inorganic carbon and the herring recruitment.

DECLARATION AND CONSENT

Details of the Work

I hereby agree to deposit the following item in the digital repository maintained by Bangor University and/or in any other repository authorized for use by Bangor University.

Author Name: Juan Estrella-Martínez

Title: Holocene climate variability in UK waters based on *Arctica islandica* sclerochronology

Supervisor/Department: Paul G. Butler, James D. Scourse/School of Ocean Sciences

Funding body (if any): EU Framework Programme 7 (FP7), Marie Curie International Training Network ARAMACC (604802)

Qualification/Degree obtained: Doctor of Philosophy

This item is a product of my own research endeavours and is covered by the agreement below in which the item is referred to as "the Work". It is identical in content to that deposited in the Library, subject to point 4 below.

Non-exclusive Rights

Rights granted to the digital repository through this agreement are entirely non-exclusive. I am free to publish the Work in its present version or future versions elsewhere.

I agree that Bangor University may electronically store, copy or translate the Work to any approved medium or format for the purpose of future preservation and accessibility. Bangor University is not under any obligation to reproduce or display the Work in the same formats or resolutions in which it was originally deposited.

Bangor University Digital Repository

I understand that work deposited in the digital repository will be accessible to a wide variety of people and institutions, including automated agents and search engines via the World Wide Web.

I understand that once the Work is deposited, the item and its metadata may be incorporated into public access catalogues or services, national databases of electronic theses and dissertations such as the British Library's EThOS or any service provided by the National Library of Wales.

I understand that the Work may be made available via the National Library of Wales Online Electronic Theses Service under the declared terms and conditions of use (http://www.llgc.org.uk/index.php?id=4676). I agree that as part of this service the National Library of Wales may electronically store, copy or convert the Work to any approved medium or format for the purpose of future preservation and accessibility. The National Library of Wales is not under any obligation to reproduce or display the Work in the same formats or resolutions in which it was originally deposited.

Statement 1:

This work has not previously been accepted in substance for any degree and is not being concurrently submitted in candidature for any degree unless as agreed by the University for approved dual awards.

Signed .... (candidate)

Date 14th of December 2018

Statement 2:

This thesis is the result of my own investigations, except where otherwise stated. Where correction services have been used, the extent and nature of the correction is clearly marked in a footnote(s).

All other sources are acknowledged by footnotes and/or a bibliography.

Signed .... (candidate)

Date 14th of December 2018

Statement 3:

I hereby give consent for my thesis, if accepted, to be available for photocopying, for inter-library loan and for electronic storage (subject to any constraints as defined in statement 4), and for the title and summary to be made available to outside organisations.

Signed .... (candidate)

Date 14th of December 2018

NB: Candidates on whose behalf a bar on access has been approved by the Academic Registry should use the following version of Statement 3:
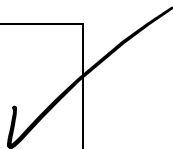
Statement 3 (bar):

I hereby give consent for my thesis, if accepted, to be available for photocopying, for inter-library loans and for electronic storage (subject to any constraints as defined in statement 4), after expiry of a bar on access.

Signed …………………………………………… (candidate)

Date …………………………………………………

Statement 4:

Choose <u>one</u> of the following options

a) I agree to deposit an electronic copy of my thesis (the Work) in the Bangor University (BU) Institutional Digital Repository, the British Library ETHOS system, and/or in any other repository authorized for use by Bangor University and where necessary have gained the required permissions for the use of third party material.	✓
b) I agree to deposit an electronic copy of my thesis (the Work) in the Bangor University (BU) Institutional Digital Repository, the British Library ETHOS system, and/or in any other repository authorized for use by Bangor University when the approved bar on access has been lifted.	
c) I agree to submit my thesis (the Work) electronically via Bangor University's e-submission system, however I opt-out of the electronic deposit to the Bangor University (BU) Institutional Digital Repository, the British Library ETHOS system, and/or in any other repository authorized for use by Bangor University, due to lack of permissions for use of third party material.	

Options B should only be used if a bar on access has been approved by the University.

In addition to the above I also agree to the following:

That I am the author or have the authority of the author(s) to make this agreement and do hereby give Bangor University the right to make available the Work in the way described above.

That the electronic copy of the Work deposited in the digital repository and covered by this agreement, is identical in content to the paper copy of the Work deposited in the Bangor University Library, subject to point 4 below.

That I have exercised reasonable care to ensure that the Work is original and, to the best of my knowledge, does not breach any laws – including those relating to defamation, libel and copyright.

That I have, in instances where the intellectual property of other authors or copyright holders is included in the Work, and where appropriate, gained explicit permission for the inclusion of that material in the Work, and in the electronic form of the Work as accessed through the open access digital repository, *or* that I have identified and removed that material for which adequate and appropriate permission has not been obtained and which will be inaccessible via the digital repository.

That Bangor University does not hold any obligation to take legal action on behalf of the Depositor, or other rights holders, in the event of a breach of intellectual property rights, or any other right, in the material deposited.

That I will indemnify and keep indemnified Bangor University and the National Library of Wales from and against any loss, liability, claim or damage, including without limitation any related legal fees and court costs (on a full indemnity bases), related to any breach by myself of any term of this agreement.

Signature: ……………………………………………………………

Date : 14th of December 2018

ACKNOWLEDGEMENTS

TABLE OF CONTENT

4. Analysis of the persistence of seasonal stratification in the northern North Sea using a bottom water temperature reconstruction of the last 455 years 65

5. 8.2 ka event North Sea hydrography determined by bivalve shell stable isotope geochemistry 95

LIST OF FIGURES

1. INTRODUCTION

1.1 MOTIVATION

1.1.1 Determining past climatic conditions

Temperature variability in the North Atlantic is known to be a major influence on the regulation of Northern Hemisphere climate. The north-eastward transport of waters from the subtropics by the North Atlantic Current and the subsequent loss of heat to the atmosphere has a key role in controlling regional conditions over Europe. Weather and climate observations in the form of historical log books and precise instrumental records inform global and regional climate models, which incorporate this material to produce forecasts and estimate the potential impacts of human activity on climate and *vice versa*. However, an accurate partition of climatic variability between that caused by external forcing (including anthropogenic forcing) and that caused by internal feedbacks requires understanding of the full range of timescales and periodicities represented in the climate system.

In places with extended human occupation, historical log books can provide a window to the past. However, not all past cultures had a tradition to record the daily weather (not to mention written records at all) and the vast majority of the Earth's surface has never been occupied by humans. In these cases, one must draw upon natural archives that reflect climate variability within them. By understanding how these archives respond to a wide variety of environmental conditions, we can study their physical and chemical properties and draw conclusions about the climate of the past – by proxy.

There are numerous proxy archives in nature. Ice sheets have been studied since the 1950s with the expressed intention to reconstruct past climate conditions (Jouzel, 2013) as their chemical properties reflect the atmospheric conditions when they were accreting. Lake sediments can be used to reconstruct past productivity and erosional inputs, among other things (Edwards and Whittington, 2001; Hiriart-Baer et al., 2011). Oceanic sediments can help determine past sea temperatures and changes in water composition (Eiriksson et al., 2006; Ellison et al., 2006; Thornalley et al., 2009). Stalagmites encode past precipitation within their chemical composition (Lachniet, 2009; Vieten et al., 2018; Winter et al., 2015). All these proxies provide valuable information about past climatic conditions, but they are all limited in one key aspect: Time.

The temporal resolution of many proxies can vary dramatically. Ice sheets can provide annual resolution but the chronology on which the data obtained from them is based is susceptible to a number of uncertainties (Andersen et al., 2006). Sediment records can cover millennia, but their temporal resolution is not normally higher than decadal as they are highly dependent on accumulation rates that may change dramatically over the time they have been deposited. Stalagmites depend on radioisotope age models which have an intrinsic uncertainty that can vary from decades to centuries. Only one terrestrial climate archive achieves long temporal coverage, annual resolution and little-to-no temporal uncertainty: Tree-rings.

The use of tree-rings (dendrochronology) as a climate proxy has long been established (Worbes, 2002). Rings are annual in nature as trees grow in very specific seasons which, as a result, changes the colour of the wood and allows us to see them. Single trees can live for hundreds of years and knowing the date of wood collection allows the assignment of a year to every ring. Uncertainties in ring counting can be ruled out by measuring the width of every ring from many trees with overlapping lifespans and matching the widths among all trees, a technique called "cross-matching". The study of physical changes such as ring width and wood density (Büntgen et al., 2006; Esper et al., 2007) and chemical changes such as isotopic composition and trace element incorporation (Treydte et al., 2006; Vaganov et al., 2013) allow for very detailed palaeoclimatic reconstructions. Although dendrochronological studies can be applied to reconstruct oceanic variability (Gray et al., 2004), the study of the calcium carbonate accretions of marine organisms, sclerochronology, represents the oceanic analogue to the techniques applied to the study of tree rings.

At the 1st International Sclerochronology Conference, 'sclerochronology' was defined as:

> *"[…] the study of physical and chemical variations in the accretionary hard tissues of organisms, and the temporal context in which they formed. Sclerochronology focuses primarily upon growth patterns reflecting annual, monthly, fortnightly, tidal, daily, and sub-daily increments of time entrained by a host of*

environmental and astronomical pacemakers. Familiar examples include daily banding in reef coral skeletons or annual growth rings in mollusk shells [...]" (Jones et al., 2007).

The accretionary bands (increments) of bivalve molluscs have been used to assess past climatic conditions since the late 1960s (Clark, 1968). Many bivalve species show this periodic growth and dendrochronological cross-matching techniques have been applied to a number of them since the 1980s (Jones, 1981). Of these species, the ocean quahog (*Arctica islandica*) is one of the most widely studied.

Cross-matched increment series (increment chronologies) from *A. islandica* shells can be produced using specimens that lived in communities separated by tens of kilometres (Butler et al., 2009a). Because of this and the statistical robustness of the increment chronologies derived from its shell, *A. islandica* has been dubbed "the tree of the sea" (Witbaard, 1997). The work presented here is one of the latest developments in *A. islandica* sclerochronology and North Sea palaeoceanography. The reconstructions presented here of temperature, water mass and ecosystem functioning in two epochs, the early Holocene and the Common Era, further demonstrate the applicability of molluscan sclerochronological records to the study of climatic variability.

1.1.2   General information about *Arctica islandica*

Arctica islandica is an exceptionally long-lived bivalve mollusc, commonly living more than one hundred years (Butler et al., 2013; Schöne et al., 2005a). Population studies have shown that it is widely distributed around the margin of the North Atlantic Ocean, from the New England and Iceland coasts to the British Isles, the North Sea and the Norwegian, Danish and Swedish coasts (Dahlgren et al., 2000; Pace et al., 2017; Witbaard and Bergman, 2003; Zettler et al., 2001). Water temperature and food availability seem to be major controlling factors on this distribution (Morton, 2011; Witbaard, 1996; Witbaard et al., 1999; Witbaard and Bergman, 2003). These factors also seem to contribute to the size and growth rates of the individuals that make up the communities.

A. islandica has typical size ranges between 8 and 13 cm (Figure 1.1; Tyler-Walters and Sabatini, 2017). Maximum growth rates occur early in life. In sizing research carried out in the 1980s, specimens recovered off Long Island (USA) grew at a rate of 5.0 mm yr^{-1} from age 3 to age 8, after which the specimens showed a reduced growth rate (Ropes et al., 1984). In Iceland, growth rates between years 10 and 27 were reported to be 2.0 mm yr^{-1} (Thorarinsdóttir and Jacobson, 2005). Populations in the North Sea showed maximum growth rates between 2.9 mm yr^{-1} and 1.8 mm yr^{-1} (Witbaard et al., 1999). These maximum growth rates appear to be related to sexual maturity (Thorarinsdóttir and Jacobson, 2005).

A. islandica is a suspension/surface deposit feeder, with short siphons located at the sediment/water interface when laying at its natural position within the sediment (Morton, 2011). It lives burrowed within the top few centimetres of soft/muddy sandy sediment (Morton, 2011; Tyler-Walters and Sabatini, 2017) where it remains motionless most of the time. However, some specimens have been found to burrow to depths up to 14 cm in the winter time (Thorarinsdóttir et al., 2009). Nevertheless, the passive lifestyle has been said to contribute to the longevity of the animal (Morton, 2011). Many other studies have described the biology, development and longevity of *A. islandica* (Lutz et al., 1982; Mann and Wolf, 1983; Munro and Blier, 2012; Oeschger and Storey, 1993; Ungvari et al., 2011). The work presented here is developed, however, by studying only *A. islandica*'s shell.

1.1.3 The shell of the ocean quahog

A. islandica's shell is normally thick and heavy. It has a brown-to-dark brown periostracum that easily peels away from dry shells (Figure 1.1). The colours of these 'naked' shells range from white to pale brown. Accretionary structures in *A. islandica*'s shell have been studied for many years. Growth bands were initially studied at the outer surface of the shells. It was not until 1980 that Thompson et al. analysed the growth increments by studying the cross-sectional area of cut and polished shells. In their study, Thompson et al. (1980) argued for the annual periodicity of the increments by (1) analogy to *Spisula solidissima*, another bivalve with annual increments (Jones, 1981); (2) the onset of sexual maturity; (3) a longitudinal study and; (4) an in-situ settlement and recovery study. Thompson et al. (1980) was also the first to show the synchronised shell growth between multiple specimens. Later, a radioisotope study confirmed the annual nature of the observed growth increments (Turekian et al., 1982).

Figure 1.1 From left to right: Top, side and inside view of *A. islandica* shells.
The side view shows the two articulated valves of a single specimen.

The living animal forms its shell in chemical disequilibrium with the ambient water which allows the formation of the aragonite polymorph of $CaCO_3$ (Marin et al., 2012). Schöne (2013) summarised of *A. islandica*'s shell formation. Specialised cells, supersaturation of $CaCO_3$, elemental transport to calcification sites while maintaining acidic balance to avoid premature precipitation, among many others all form part of a complex mechanism that is not completely understood (Marin et al., 2012). On the other hand, much more is known about the chemical characteristics of *A. islandica*'s shell.

1.1.4 Oxygen and carbon stable isotope geochemistry of the *A. islandica* shell

Carbonates are one of the most studies phases in stable isotope geochemistry. Relative oxygen isotope ratios ($\delta^{18}O$; see Section 2.7) of marine carbonates provide information about water temperature and land ice volume while relative stable carbon isotope ratios ($\delta^{13}C$; Section 2.7) provide information about biological productivity conditions. For the successful interpretation of $\delta^{18}O$ and $\delta^{13}C$ as environmental signals it is first necessary to consider three questions (Sharp, 2017):

1. Does *A. islandica* precipitate its shell in isotopic equilibrium with the ambient water?

   Most elements in the *A. islandica* shell are subject to vital effects and their incorporation are modulated to various degrees by the organism (Schöne, 2013). The opposite is true when examining the composition of stable isotopes of oxygen and carbon. There is unambiguous evidence that *A. islandica* deposits its shell in oxygen isotopic equilibrium with the ambient water (Schöne et al., 2005a; Weidman et al., 1994).

   The evidence is less clear in the case of $\delta^{13}C$. Two studies arrived at conflicting results when examining the *A. islandica* vital effects (growth rates) on $\delta^{13}C$ (Butler et al., 2011; Schöne et al., 2005a). However, an analysis of 21 shells from Iceland found that growth rates effects represent only a small component of the $\delta^{13}C$ variability in the first 30 years of the animal's life (Reynolds et al., 2017a). For the rest of the shell, $\delta^{13}C$ from *A. islandica*'s shell has been shown to be proportional to the $\delta^{13}C$ of the dissolved inorganic carbon ($\delta^{13}C_{DIC}$) in the water column (Figure 1.2; Beirne et al., 2012).

2. Do the shells show signs of diagenesis?

   Diagenesis is defined in the Glossary of Geology (Neuendorf et al., 2005)) as:

   "All the chemical, physical, and biologic changes undergone by a sediment after its initial deposition, and during and after its lithification, exclusive of surficial alteration (weathering) and metamorphism […] It embraces those processes (such as compaction, cementation, reworking, anthogenesis, replacement, crystallization, leaching, hydration, bacterial action, and formation of concretions) that

5

occur under conditions of pressure (up to 1 kb) and temperature (maximum range of 100 °C to 300°C) that are normal to the surficial or outer part of the Earth's crust."

Diagenesis affects $\delta^{18}O$ and $\delta^{13}C$ in aragonite by isotopic exchange with the ambient fluids. However, diagenesis is mainly present in material that is poorly preserved (Cochran et al., 2010), which can be avoided by paying attention to the taphonomic characteristics of the shells (Section 2.3.1).
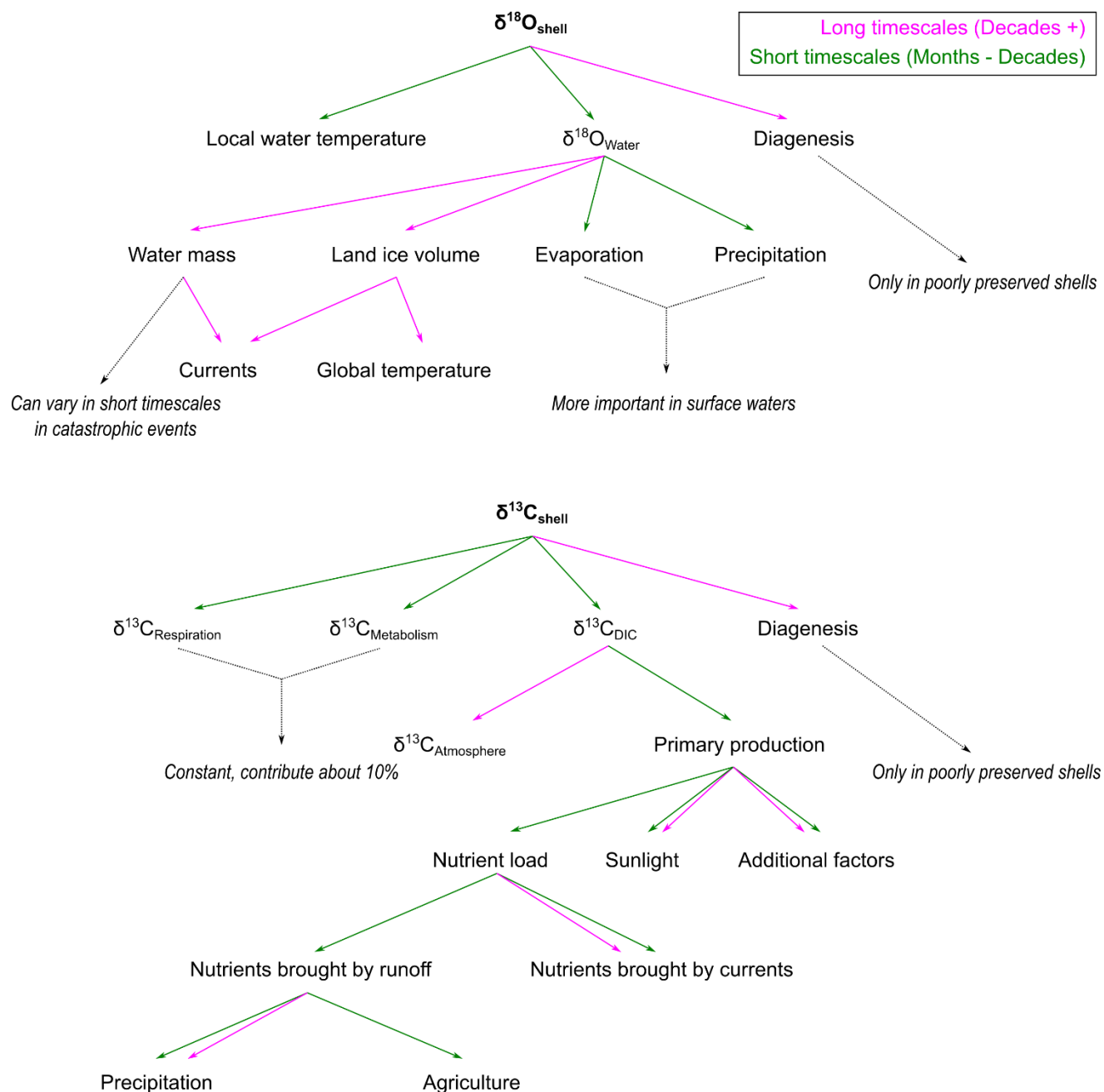
Figure 1.2 Non-exhaustive diagram of the processes affecting $\delta^{18}O$ and $\delta^{13}C$ in the shell of *Arctica islandica*. Processes at each level are sources of variability and need to be accounted for before making environmental interpretations.

6

3. What was the $\delta^{18}O$ of the ambient water at the time of increment growth?

This question only concerns $\delta^{18}O$. This is because $\delta^{18}O$ in marine carbonates is affected by changes in water temperature and changes in the water mass (Figure 1.2; Sharp, 2017 and refences therein). The changes in water mass are approximated by changes in salinity (Harwood et al., 2008; Sharp, 2017) and are a function of ocean currents, land ice volume, evaporation and precipitation. The latter two, however, are much more important in surface waters. Bottom waters are less affected by evaporation/precipitation processes and are also less prone to alteration due to runoff. Similarly, water mass changes due to ocean current variability and changes in land ice volume take place in time scales longer than the typical life of *A. islandica*. However, in catastrophic situations like the drainage of the glacial lake Agassiz-Ojibway, when a large volume of fresh water entered the North Atlantic, the $\delta^{18}O$ of the ambient water can change significantly within decades. An independent estimate of ambient water $\delta^{18}O$ is needed before interpreting the shell's $\delta^{18}O$ as a temperature signal.

1.2 THE NORTH SEA

Many of the studies carried out using the shell of *A. islandica* have been based on material from the North Sea. Studies range from the building of the first increment chronologies from live-collected organisms (Witbaard et al., 1997; Witbaard and Duineveld, 1990) and from fossil shells (Scourse et al., 2006a), the first theorised climatological meaning of the increment widths (Schöne et al., 2003; Witbaard, 1996; Witbaard et al., 2003), the probing of the spatial extension of a common signal among different *A. islandica* communities (Butler et al., 2009a) to multiple stable isotope studies (Dunca et al., 2009; Schöne et al., 2004, 2005c; Witbaard et al., 1994). This is because the environmental conditions and substrates found in the North Sea are ideal for the development of healthy *A. islandica* communities. This wealth of proxy material shows that the North Sea is one of the few areas in the high latitudes where high resolution palaeoceanographical reconstructions can be carried out.

1.2.1 Geology

The general topography of the North Sea bed originated from the deep geological structure influence on the patterns of basin subsidence and uplift (Lamb et al., 2018). The finer-scale shape of the continental shelf is a result of multiple glacial periods when terrestrial material was eroded from the surrounding continental masses (Busschers et al., 2007; Graham et al., 2011). The material was deposited on the shelf or

in deeper waters at the continental slope. The modern North Sea is dominated by low sediment input bottom current reworking of the sediments (Balson et al., 2001).

Most of the modern sediment is composed of reworked substrates. These form large areas of sand and gravel and accumulate in the form of extensive sandbanks and finer sand waves. Soft muds that cover the flat areas in deeper water also form part of the modern seascape. These are of particular interest as they provide an excellent substrate for *A. islandica* settlement.

The North Sea is relatively shallow, with an average depth of 74 m (Otto et al., 1990). This depth is not equally distributed as there is a north-south and east-west depth gradient. If we disregard the Norwegian Trench (where the greatest depths are found), then the north-south gradient becomes more prominent, with the northern North Sea characterised by depths of 100 to 200 m (Figure 1.2; IOC et al., 2003). The shallow depth of the North Sea largely determines its properties and hydrography.
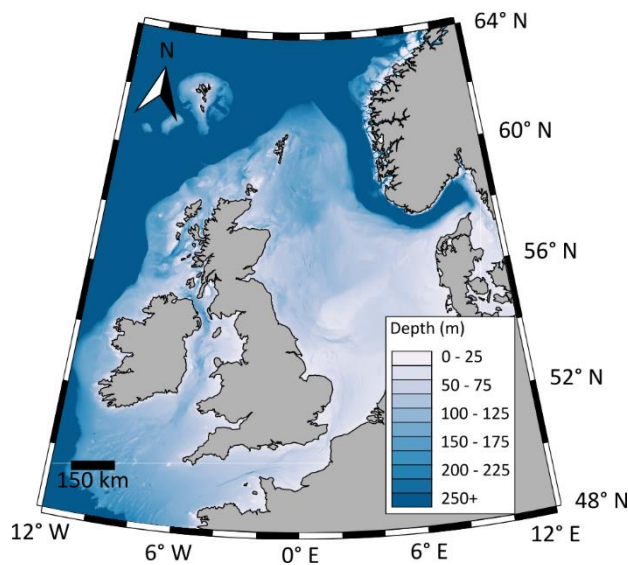
Figure 1.3 Bathymetry map of the waters surrounding the British Isles.
The map shows the North Sea depth gradient, increasing depth when moving from south to north (IOC et al., 2003).

1.2.2 Circulation

Currents in the North Sea are mainly affected by the average wind field, non-linear tidal dynamics and bathymetry (Blaas et al., 2001; Otto et al., 1990; Sušelj et al., 2010; Winther and Johannessen, 2006). The combination of these result in a cyclonic circulation, with the main inflow coming from the north through the western slope of the Norwegian Trench along with secondary inflows through the Fair Isle Channel and east of Shetland (Turrell et al., 1996; Winther and Johannessen, 2006) and a tertiary inflow through the English Channel (OSPAR, 2000). The integrated Fair Isle Channel and east of Shetland inflow is of the same magnitude of the primary inflow through the western slope of the Norwegian Trench (1.0 Sv vs. 1.23 Sv)

(Winther and Johannessen, 2006) while the tertiary inflow through the Channel is much smaller (0.06 Sv) (OSPAR, 2000). Conversely, the vast majority of the outflow is through the Norwegian Coastal Current (OSPAR, 2000; Otto et al., 1990; Turrell et al., 1996; Winther and Johannessen, 2006).

Numerical models have been applied to calculate the flushing time of the North Sea. Early estimates placed the average for the whole sea at one year (ICES, 1983; Otto et al., 1990). More recent measurements of radionuclides tracers place this figure closer to 500 days, however (OSPAR, 2000). These values are far from constant and are complicated by the relative importance of the factors controlling water movements. For example, when aeolian forcings are prominent, the flushing times tend to be shorter whereas conditions dominated by tidal or density forcings tend to produce longer flushing times (Blaas et al., 2001).

Semi-diurnal tides are the most energetic component of water transport within the North Sea (Otto et al., 1990). Three amphidromic points arise from the combination of the M2 and S2 components: One at the south coast of Norway, one at the eastern tip of the Dogger Bank and one near the Southern Bight (Otto et al., 1990; Sündermann and Pohlmann, 2011). A recent study found that the tidal currents show an extensive range of strength from a few cm/s in the Skagerrak to 67 cm/s in the Fair Isle Channel for the M2 component (Vindenes et al., 2018).

While tidal currents are strong and prevalent along much of the North Sea, especially in shallow and coastal areas, wind stress is an also an important source of circulation variability. The northern European wind fields are largely controlled by the governing atmospheric pressure gradient, namely, the North Atlantic Oscillation (NAO) (Hurrell et al., 2003; Luterbacher et al., 2001). The NAO consists of two opposite strength pressure poles, the low-pressure pole residing in the vicinity of Iceland and Greenland and the high pressure pole residing seasonally between the Azores, the Iberian Peninsula and the British Isles (Feldstein, 2007). The Fair Isle Channel and east Shetland inflows, for example, show a strong positive correlation (r>0.50, p<0.01) with the NAO from December to July at the weekly time-scale (Winther and Johannessen, 2006). This implies a similarly strong wind/inflow relationship.

1.2.3 Temperature

Unlike currents, the temperature distribution of the North Sea is rather simple. With approximate mean temperatures of 9.5 °C (Becker and Schulz, 2000; OSPAR, 2000), the North Sea waters are slightly colder than the adjacent North Atlantic (9 – 11 °C) (Grey et al., 2000). There is a south-north gradient showing warmer average sea surface temperatures (SST) in the south flowing out of the English Channel (Figure 1.4a). The SST decreases from ~12 °C at the exit of the Channel to ~9 °C at the waters adjacent to

Shetland (Becker and Schulz, 2000; Berx and Hughes, 2009). The temperature difference between bottom and surface waters varies by latitude but generally lies between 2 – 3 °C (Berx and Hughes, 2009).

Bottom water temperatures (BWT) are more evenly distributed with an approximate mean of 7 °C (Berx and Hughes, 2009) with the north and central areas being much colder than the southern areas (Figure 1.4b). Figure 1.6a shows three BWT time series: The Fladen Ground (ICES, 2014) and Utsire Station A (ICES, 2016) in the north and the Skagerrak (OSPAR, 2000) in the southeast. The two northern sites are much more similar to one another than to the south-eastern site, yet all three show similar sub-decadal trends which evidences the longer term regular distribution of BWT.
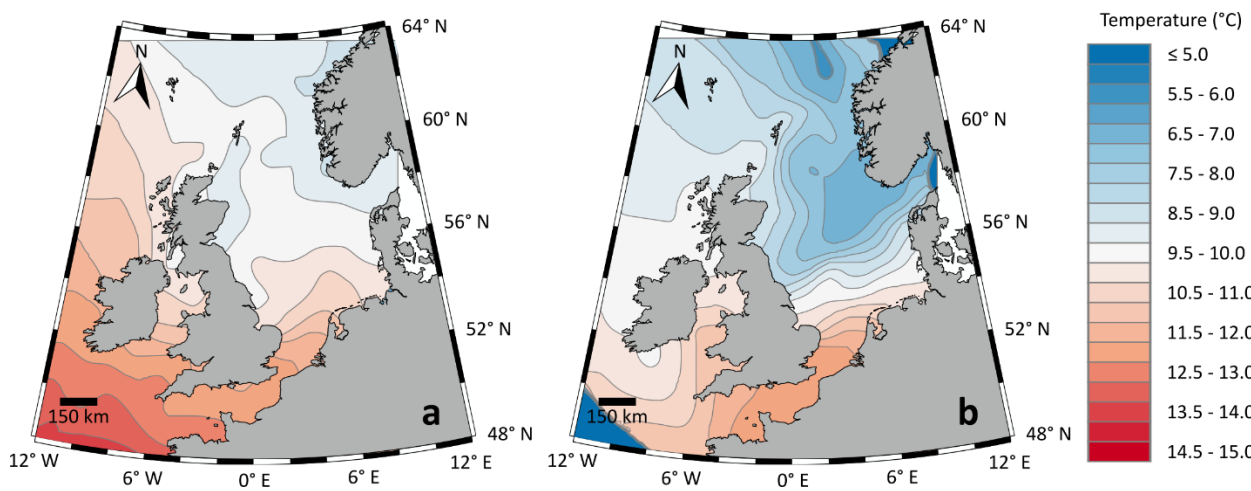
Figure 1.4 Annual average temperatures from 1970 to 2000 of the waters surrounding the British Isles.
The sea surface temperatures show the inflow of warm Atlantic waters through the British Channel (a). Bottom water temperatures are colder on average and show a more zonal pattern (b). Data adapted from Berx and Hughes, (2009).

Seasonally, the warmest SST occur between the months of August and September quite evenly across the whole Sea ranging between ~16 °C in the south and ~12 °C in the north (Becker and Schulz, 2000; Berx and Hughes, 2009). BWT maxima are lagged with respect to SST maxima by 1 – 2 months and do not occur coevally across the Sea. This is because of the development of a strong thermocline that impedes mixing in the summer months; the northern and central areas water columns are only mixed from November to April (ICES, 2014; Sprintall and Cronin, 2001; van Leeuwen et al., 2015), the southern areas remain tidally mixed year-round (Otto et al., 1990; van Leeuwen et al., 2015), while the waters in the Norwegian Trench tend not to mix at all (van Leeuwen et al., 2015).

1.2.4 Salinity

The salinity distribution of the North Sea is also quite simple. In general, the surface salinity increases from 33.15 PSU to 35.93 PSU from the Skagerrak towards the Fair Isle Channel (Figure 1.5a) (Berx and Hughes, 2009; Harwood et al., 2008). This gradient is mainly controlled by the outflow from the Baltic Sea with some influence of runoff at the Norwegian fjords (Harwood et al., 2008). Approximately half of the Atlantic water that enters the North Sea mixes with fresher water before it leaves through the Norwegian Coastal Current (Winther and Johannessen, 2006) which is evident in the Skagerrak-Fair Isle Channel surface salinity gradient (Harwood et al., 2008).
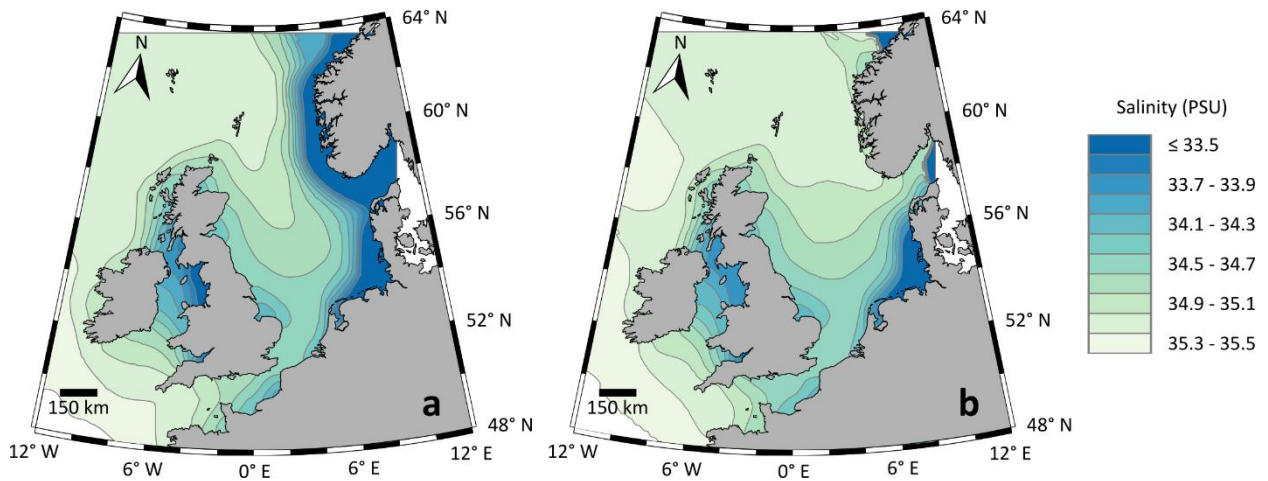
Figure 1.5 Annual average salinity of the waters surrounding the British Isles.
The sea surface salinity pattern in the North Sea is mainly controlled by the water flowing out of the Skagerrak and shows a strong zonal gradient (a). The zonal gradient is less pronounced at the bottom waters, where the salinity is more evenly distributed. Data adapted from Berx and Hughes (2009).

The zonal salinity gradient is less pronounced at the bottom of the North Sea, where a more meridional gradient is evident (Figure 1.4b; Berx and Hughes, 2009; Harwood et al., 2008), a feature that can be observed for the past 60 years (Figure 1.5b; ICES, 2016, 2014; OSPAR, 2000). This is related to the summer thermocline development mentioned above. The salinity range at the bottom is similar to the surface. However, the reduced surface/bottom exchange in the Skagerrak and Norwegian Trench mean that the salinity of the water exiting the Baltic Sea has limited influence over the salinities at the bottom of the North Sea and the meridional salinity gradient observed represents salinities from the North Atlantic waters in the north and salinities from English Channel waters mixing with the European runoff in the south.
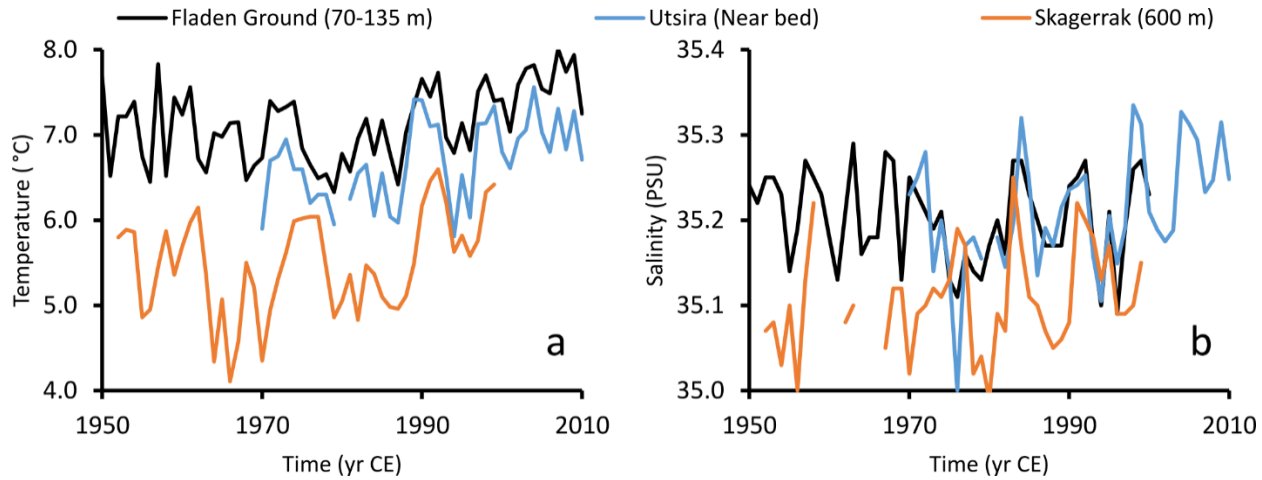
Figure 1.6 Instrumental bottom temperature and salinity time series of two northern (Fladen Ground, Utsira) and one eastern (Skagerrak) site in the North Sea.
The northern sites show a more similar bottom water temperature throughout the last 50 years while the eastern site has been consistently colder (a). The bottom water salinity shows more similarity between the northern and the eastern sites (b). Data from ICES (2016, 2014) and OSPAR (2000).

1.2.5 Palaeoceanography and palaeoclimatology

From the perspective of *high-resolution* climatic reconstructions, the North Sea is rather understudied. A literature search for North Sea temperature reconstructions yields only two works from the south and central regions (Schöne et al., 2004, 2005c). Both reconstructions are based on stable isotope geochemistry of aragonitic material ($\delta^{18}O_{arag}$) extracted from the shells of *A. islandica* specimens and were undertaken at sub-annual resolution.

The southern work (Schöne et al., 2004) makes an effort to reconstruct sea surface temperatures (SST) at the Amrum Bank (54.764° N, 7.273° E) from the 1880s to the 1980s. The reconstruction (Figure 1.7) is based on material extracted from a single shell and the age model is based on shell increment counting. While the obtained reconstruction is in good agreement with observational and modelled data for the region, Schöne et al. (2004) warn about the water effects ($\delta^{18}O_{water}$) on $\delta^{18}O_{arag}$ thermometry. These either need to be estimated from salinity values for the area or accounted for using a different proxy measurement. The latter option is difficult to achieve as there is conflicting evidence about the use of $\delta^{18}O_{water}$-independent proxies from *A. islandica* (Foster et al., 2009; Schöne et al., 2011b). Accordingly, Schöne et al. (2004) applied a constant offset into the SST calculation that represented the 1954-1973 $\delta^{18}O_{water}$ average at the collection site. Although Schöne et al. (2004) did not reconstruct SST before instrumental records, they demonstrated the potential of *A. islandica* stable isotope geochemistry as a viable high resolution water temperature estimator.
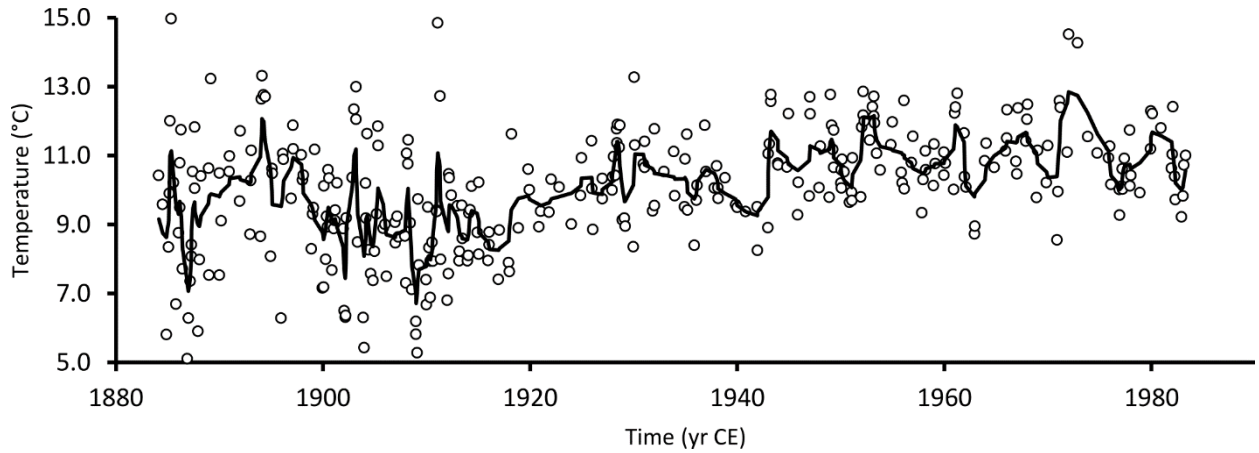
Figure 1.7 Sub-annual sea surface temperature reconstruction from the southern North Sea based on *A. islandica* stable isotope geochemistry.
The black line shows the seasonal data filtered with a 15-point Gaussian low-pass filter. Data from Schöne et al. (2004).

The work based on material from the central region of the North Sea applies the same concepts and techniques first applied for the southern region. Here Schöne et al. (2005c) presented a sub-annual bottom water temperature (BWT) reconstruction derived from twelve *A. islandica* shells (Figure 1.8) collected alive at an approximate depth of 50 m on the eastern section of the Dogger Bank (56° N, 4° E). The reconstruction covers the years 1880-2001 and the age model is based on annual increment counting. In similar fashion to the SST reconstruction, Schöne et al. (2005c) applied a constant $\delta^{18}O_{water}$ offset into their BWT calculation. In this case, however, the application of a constant $\delta^{18}O_{water}$ is more justified as bottom water salinity at the North Sea has an annual amplitude of less than 0.4 PSU (Section 1.2.4; Berx and Hughes, 2009). The BWT reconstruction shows high levels of similarity to the BWT instrumental series. As the bottom water instrumental records are much scarcer than surface records, Schöne et al. (2005c) research uncovered previously unknown BWT variability at the North Sea and showed that bottom temperatures rose at a rate of 0.09 °C decade^{-1} during the 1880-2001 interval.
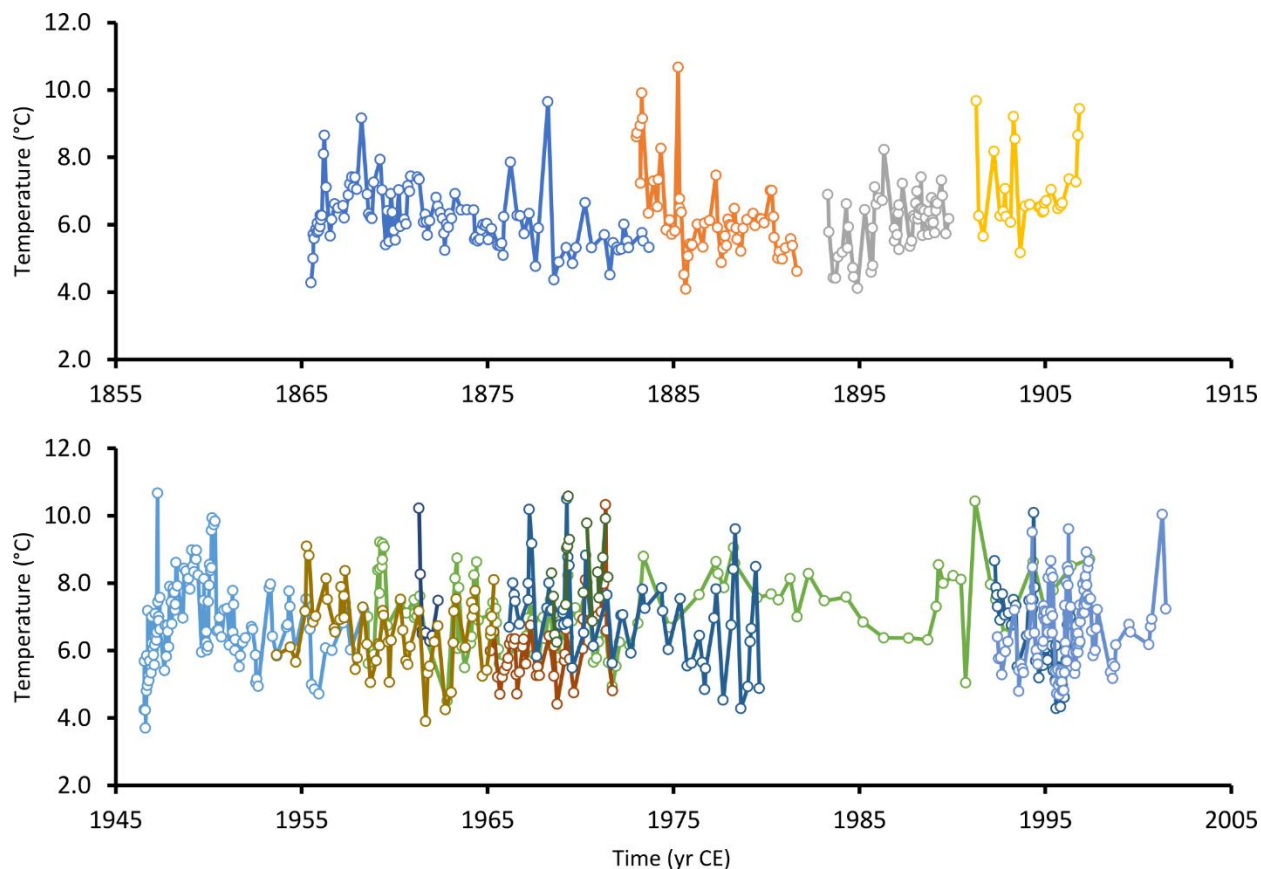
Figure 1.8 Sub-annual bottom water temperature reconstruction from the central North Sea based on *A. islandica* stable isotope geochemistry.
The reconstruction is based on multiple specimens (different colours). Data from Schöne et al. (2005c).

Other investigations that have produced lower resolution data have concentrated along the Norwegian margin. Eiriksson et al. (2006) produced a benthic foraminifera $\delta^{18}O$ series from two sediment cores. That study showed indications that bottom water temperatures in the 20th century were warmer than the rest of the Common Era (CE). While very valuable, the age model used by Eiriksson et al. (2006) was not adequately described as only two out of six radioisotope dates used in their study were ever published (Hebbeln et al., 2006), and the supplementary dating methods are mentioned without detail. Climatic interpretations from this record, thus, can only be qualitative and trends can only be analysed at temporal scales longer than the typical sediment core uncertainties.

Another environmental reconstruction based on a sediment core from the Norwegian margin centres around the 8.2 ka event (Klitgaard-Kristensen et al., 1998). The 8.2 ka event (8,200 years before 1950 CE) was an abrupt return to cold conditions in the Northern Hemisphere in the early Holocene when the Earth's climate was warming after the termination of the most recent glaciation. This cold event is usually defined by lower stable oxygen isotope values and a reduced ice accumulation rate in Greenland ice cores (Rasmussen

et al., 2007). Although this event has been extensively described in the context of the Greenland ice cores and across the wider North Atlantic (Came et al., 2007; Ellison et al., 2006; Rasmussen et al., 2007; Thomas et al., 2007; Thornalley et al., 2009), its expression in the Atlantic shelf seas is less well documented. Klitgaard-Kristensen et al. (1998) undertook the effort of quantitatively describing the water temperature changes in the northern North Sea. Although this work reconstructed the environmental variability during the 8.2 ka event at sub-decadal scale, only c.80 years benefit from this high temporal resolution. The rest of the record has the more typical multidecadal resolution of sediment cores. This, along with the temporal uncertainties from the age model, only allows for the examination of longer trend climatic changes in the North Sea.

The applications of the currently available North Sea palaeoceanographic reconstructions are somewhat limited. For instance, climatic models often require both long and highly resolved reconstructions to serve as verification and validation. Without appropriate boundary conditions, a model could potentially predict erroneous climatic responses to changes in atmospheric CO_2 concentration or oceanic current strength variability. Similarly, ecosystem models could stand to benefit from high resolution environmental reconstructions, as they operate over shorter time scales than climate models. A better constrained ecosystem model can help assess the status and response to environmental pressure of economically important North Sea fish stocks such as the Atlantic herring (Dickey-Collas, 2016).

1.2.6 North Sea herring fishery

The Atlantic herring (*Clupea harengus*) has been a source of wealth and nutritional stability for the countries bordering the North Sea going at least as far back as the Middle Ages (Pitcher and Lam, 2014). Recruitment variability, i.e. the number of juvenile fish that survive from egg production to join the stock, is known to be a crucial contributor to stock productivity (Pinnegar et al., 2016). In the past 50 years, the European fishing industry suffered severe economic impacts on two occasions. Herring recruitment failure in the 1970s led to a collapse of the fish stock and temporary closure of the fishery. In the 2000s, reduced recruitment levels caused the fisheries management agencies to reduce the total allowable catch of the North Sea stock by half (Corten, 2013). This has led to a number of investigations that seek to predict future herring recruitment levels using climatic and fish population factors. These have found that water temperature is a poor predictor of herring recruitment (Akimova et al., 2016; Bogstad et al., 2013) while other models constructed lack a mechanism to explain the interaction between climate variability and recruitment (Axenrot and Hansson, 2003; Gröger et al., 2010).

Recruitment models would stand to benefit from access to long-term recruitment variability data. High quality catch records exist for Dutch, Scottish and Swedish herring fisheries (Alheit and Hagen, 1996; Corten,

1999; Coull, 1990, 1986; Höglund, 1978; Jones et al., 2016; Poulsen, 2010, 2008). While these records have been used to assess the climatic impacts on herring migratory patterns ((Alheit and Hagen, 1996; Corten, 1999), they may not always be useful as a guide to estimate recruitment levels as this also requires information about levels of natural and fishing mortality (Tester, 1955).

One of the hypotheses investigated in this work is that a herring recruitment reconstruction is possible by using the information encoded in the chemical composition of the *A. islandica* shells. Such a reconstruction would not only provide the longer time scale needed to understand the interaction between climatic parameters and stock densities but would also demonstrate that molluscan sclerochronological records can contribute to the study of ecosystem functioning.

1.3 OBJECTIVES

Sündermann and Pohlmann (2011) summarised future research needs identified at the International North Sea conferences in Hamburg in 1996 and in Wilhelmshaven in 2000. Of these needs, the determination of the interaction between the North Sea and North Atlantic and of the interaction between physical and biological subsystems were deemed to be important challenges for marine science and socio-economics. These challenges adequately frame the following objectives of this work:

1. Establish a relationship between dissolved inorganic carbon, primary production and Atlantic herring population dynamics and use this to reconstruct Atlantic herring recruitment variability for the past 500 years.
2. Reconstruct the bottom water temperature variability of the northern North Sea for the past 500 years and establish the degree to which it is related to atmospheric and water temperature variability in the wider North Atlantic.
3. Reconstruct North Sea hydrographic variability during the early Holocene, a time of sudden and extreme variability in the Northern Hemisphere.

This cumulative thesis is composed of three manuscripts. The author contributions follow the 'CRediT taxonomy' developed by the Consortia Advancing Standards in Research Administration Information (CASRAI, https://casrai.org/credit/; Brand et al., 2015).

Manuscript I:

Reconstruction of Atlantic herring (*Clupea harengus*) recruitment in the North Sea for the past 455 years based on the δ^{13}C from annual shell increments of *Arctica islandica*

Juan Estrella-Martínez, Bernd R. Schöne, Ruth H. Thurstan, Elisa Capuzzo, James D. Scourse, and Paul G. Butler

Writing – original draft: J.E-M.; *Writing – review & editing*: All authors; *Conceptualisation*: J.E-M., P.G.B, J.D.S.; *Investigation*: J.E-M.; *Methodology*: J.E-M., P.G.B, J.D.S, B.R.S.; *Resources*: P.G.B., J.D.S, B.R.S.; *Formal analysis*: J.E-M.; *Validation*: J.E-M., R.H.T, E.C.; *Visualisation*: J.E-M.; *Data curation*: J.E-M.; *Supervision*: P.G.B, J.D.S.

This manuscript was published in the journal *Fish and Fisheries* in March 2019.

Manuscript II:

Analysis of the persistence of seasonal stratification in the northern North Sea using a bottom water temperature reconstruction of the last 455 years

Juan Estrella-Martínez, Bernd R. Schöne, James D. Scourse, and Paul G. Butler

Writing – original draft: J.E-M.; *Writing – review & editing*: All authors; *Conceptualisation*: J.E-M., P.G.B, J.D.S.; *Investigation*: J.E-M.; *Methodology*: All authors; *Resources*: P.G.B., J.D.S, B.R.S.; *Formal analysis*: J.E-M.; *Validation*: J.E-M., J.D.S, B.R.S; *Visualisation*: J.E-M.; *Data curation*: J.E-M.; *Supervision*: P.G.B, J.D.S.

This manuscript has been reviewed in the journal *Paleoceanography and Paleoclimatology* and returned for revisions in June 2019. The version included here has been submitted for further reviews.

Manuscript III:

8.2 ka event North Sea hydrography determined by bivalve shell stable isotope geochemistry

Juan Estrella-Martínez, Philippa L. Ascough, Bernd R. Schöne, James D. Scourse, and Paul G. Butler

2. MATERIALS AND METHODS

2.1 INTRODUCTION

This work builds upon the study originally carried out by Butler et al. (2009a). In that study, Butler constructed an *A. islandica* increment chronology using the shells of five live-collected specimens. The studies developed in Chapters 3 and 4 incorporate the material used by Butler et al. (2009a) and adds more shells with the intention of extending the "Site B" (see below) chronology.

The methods and materials section covers six broad areas: 1) site selection and shell collection; 2) AMS radiocarbon dating; 3) processing of the shell material; 4) increment measurement, standardisation and crossmatching; 5) chronology construction and assessment; 6) micromilling and stable isotope geochemistry; and 7) source and description of the data used for comparison with the geochemistry results.

2.2 SITE SELECTION

As described in Section 1.2, the North Sea is a relatively oceanographically simple shelf sea. In order to ensure that the environmental signal affecting the *A. islandica* shell growth was not disproportionately affected by local variability, it was thought desirable that the collection site for the shells which were to be used to construct the growth-increment chronology should be in the water column more representative of the average North Sea/North Atlantic waters rather than in a water column that would be influenced by coastal processes.

20

Some of the densest populations of *A. islandica* in the North Sea inhabit hydrographically dynamic environments towards the south (Oyster Ground) in shallow waters (~30 m; Witbaard and Bergman, 2003), where they can be subject to disturbance events, including storms, intra-annual fluctuations in salinity and heat waves. Large environmental fluctuations in an area can reduce synchronous growth in an *A. islandica* population and mask any common environmental signal (Epplé et al., 2006). The southern *A. islandica* populations are also vulnerable to fish/shellfish trawling activities (Witbaard and Bergman, 2003). On top of reducing the adult population, trawling activities can disturb the growth of the remaining younger specimens, as their shells are not as robust as those of the mature specimens (Witbaard and Bergman, 2003).

Another area of the North Sea with a known population of *A. islandica* is the Dogger Bank. As mentioned in Section 1.2.5, this population has been used for palaeoceanographic studies. However, the population density is one of the lowest in the North Sea (Witbaard and Bergman, 2003), meaning that the effort required to obtain enough shell material to potentially cover a long temporal interval (that is, longer than what Schone 2005 did) can be rather prohibitive.

In contrast, the Fladen Ground in the Northern North Sea (approximately between latitudes 58.0° to 60.0° N and longitudes -1.0° to 2.0° E) has a population density two to three orders of magnitude higher than those in the south. The higher number of specimens greatly improves the chances of obtaining shells that cover longer temporal intervals. Another advantage is that the Fladen Ground is comparatively less trawled than the Oyster Ground and the Dogger Bank (Witbaard and Bergman, 2003). Due to its greater depth, the Fladen Ground is also hydrologically stable, with the water column becoming thermally stratified between the months of May and November (ICES, 2014; van Leeuwen et al., 2015). The bottom average annual temperature range has stayed under 2 °C since the 1950s (Berx and Hughes, 2009; ICES, 2014), while the bottom average annual salinity range stayed under 0.4 PSU since the 1950s as well (Berx and Hughes, 2009; ICES, 2014). This suggests that the environmental conditions reflected in the shells of *A. islandica* collected in the Fladen Ground are likely to represent those of the main water mass in the North Sea (i.e., North Atlantic water, see Sections 1.2.2-1.2.4) with very little coastal influence. The large *A. islandica* population density along with its hydrographical stability makes the Fladen Ground an ideal site for sclerochronological studies and the subject of this dissertation.

2.2.1 Shell collection

Live A. islandica specimens along with articulated and single valves were dredged from the seabed from two sites in the Fladen Ground at coordinates 58.831° N, -0.356° E at a depth of 115 m (Site A) and 58.994° N, 0.291° E and at a depth of 123 m (Site B, Figure 2.1). Shells from Site A were collected during a cruise of the RV *Scotia* in 2001 and shells from Site B were collected during a cruise of the RV *Prince Madog*, the former as part of the EU HOLSMEER project (Scourse 2006). For the RV *Prince Madog* cruise, a bespoke rigid-toothed dredge was deployed, 1 metre wide with a 1.5 cm mesh, designed to retain medium and large bivalves (Figure 2.2). Prior to deployment, potential sites were surveyed using side-scan sonar in order to assess the state of the seabed and to avoid obstacles.
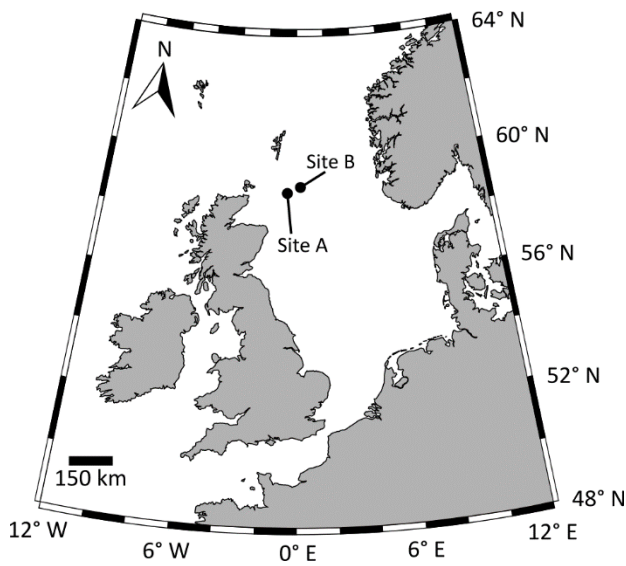
Figure 2.1 Approximate location of *A. islandica* sampling sites.
The shells were collected at the Fladen Ground in the years 2001 and 2004.

Specimens collected alive were sacrificed by freezing inside individual plastic bags (Butler et al., 2009a). The articulated and single valves collected were scrubbed to remove encrustations, washed in seawater, air-dried and placed in labelled plastic bags. In the laboratory the live-collected specimens were thawed, the flesh removed, and the shells washed and air-dried. The taphonomic characteristics of the single valves (periostracum preservation, condition of the outer shell rim, ligament condition, degree of bioerosion and boring and nacre condition) were recorded in a spreadsheet.

Figure 2.2 Deployment of the Arctica dredge.
The dredge was designed to retain medium and large bivalves. The deployment pictured here is from a cruise in 2014.

Sixteen shells from Site B were used for the studies developed in Chapters 3 and 4. Ten shells from Site A were used for the study developed in Chapter 5.

2.3 ACCELERATOR MASS SPECTROMETRY RADIOCARBON DATING

Although *A. islandica* specimens regularly live for hundreds of years, it is not always possible to rely exclusively on live-collected specimens to construct a multi-century record. To solve this, it is necessary to add shells from specimens that lived before dredging. Unless the shells are obtained from a museum collection with known provenance and date of death, it is necessary to identify which shells fall into the targeted period that is to be covered by the chronology (last 500 years and early Holocene; Section 1.3). A first approximation to the age of the shell can be obtained by accelerator mass spectrometry (AMS) radiocarbon dating, commonly known as ^{14}C-dating. AMS dating can determine the date of deposition of the analysed material within a 200 to 300 year range. This constrains the relative stratigraphic position that a given shell can occupy when building a chronology and has the added advantage of reducing the chances of random crossmatching with other shells of known age.

2.3.1 Shell selection for AMS dating

In line with the aims of the investigations presented in this dissertation and the objectives established in Section 1.3, the intention of shell selection for AMS dating was to identify shells from specimens which

were alive in the past 500 years and during the early Holocene. Two primary criteria for the selection of radiocarbon dating candidates were applied:

1. Size. The largest shells were presumed to come from the most long-lived specimens (Kilada et al., 2007). All of the shells used in the studies presented in this dissertation except for two had shell heights > 70.0 mm (Figure 2.3).
2. Taphonomic characteristics. A scale for the date of death of a specimen according to the shell condition (Butler, 2009; Nielsen, 2004).

Shell condition	Estimated antiquity
Paired valves	Months to years
Single valve: > 90% periostracum present, intact hinge ligament	Years to decades
Single valve: <90% periostracum present, degraded hinge ligament	Decades to centuries
Single valve: Absent periostracum and hinge ligament	Centuries to millennia

The working assumption was that shells from animals that lived back to the 1500s CE would be classified into the first three categories while shells from animals that lived in the early Holocene would be classified in the fourth category.
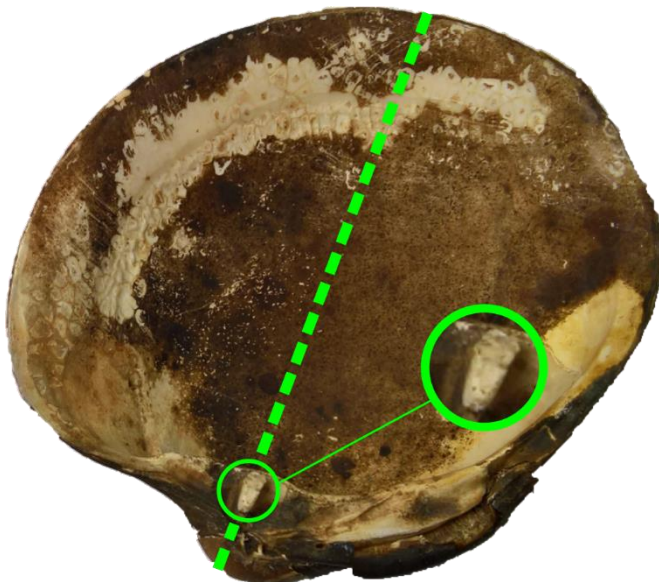
Figure 2.3 Inside view of *A. islandica* left valve showing the maximum shell height (green dashed line).
Left valves contain a 'tooth' in the umbonal region (inset).

Radiocarbon dating of the shells used throughout this dissertation was carried out in the years 2004 and 2005. This was carried out on the umbonal shell portion (deposited in early ontogeny) of nine of the

sixteen valves from Site B (the other seven valves belonged to live-collected specimens, five of which were described by Butler et al., 2009a). Samples for radiocarbon dating of the ten shells examined from Site A came from the ventral portion (deposited late in ontogeny).

The material was submitted to the Natural Environment Research Council Radiocarbon Laboratory (East Kilbride, United Kingdom) or the Accelerator Mass Spectrometry ^{14}C Dating Centre (University of Aarhus, Denmark) where it was processed using the methods described in Butler et al. (2009b) prior to ^{14}C analysis.

2.4 SHELL PROCESSING

In order to carry out the measuring of shell increments, the shells first need to be prepared for transmitted/reflected light microscopy. All shells were sectioned using a standard procedure (Butler et al., 2009a; Ropes, 1984; Scourse et al., 2006a).

In summary, a central strip of a given shell 1-2 cm wide is removed with a rough saw and embedded in epoxy resin. Once hardened, the embedded shell is cut through the maximum shell height using a Buehler ISOMET 5000 precision saw (cut rate 14 mm/minute at 5000 rpm) to expose the growth increments in the hinge and margin regions. One half of each resin block was then ground using progressively finer grinder pads (P120, P400, P1200 and P1200/4000) and polished using a 3 μm diamond paste.

What follows is the production of flat replicas of the shell's cross section to enhance visibility of the individual growth increments under the microscope using transmitted light. Once a satisfactory polished cross section is obtained (no visible scratches on the shell and surrounding resin with the naked eye), the section is etched in 0.1M hydrochloric acid for one minute and later rinsed with distilled water and air-dried for 24 hours in a fume hood. The dry etched surface is then flooded with an ethyl acetate solution and a 0.35 μm thick sheet of acetate film is applied and let to air-dry inside a fume hood for 45 minutes. The acetate peel is gently removed from the shell, trimmed, and mounted between microscope slides.

During the course of this work it was determined that the production of acetate replicas is not necessary for a good number of shells if the increments are to be measured on the ventral margin. This is because there is enough contrast between the growth increments and their boundaries (i.e., growth checks or growth lines) when examined under the microscope using reflected light. The contrast is sometimes enhanced when the shell is illuminated using dark field mode. This was the preferred method of microscopy for the study presented in Chapter 5.

2.5.1 Imaging and measuring

High-resolution images of the peels or resin blocks were taken using a Lumenera Infinity 3 camera attached to a microscope. The images were taken using a x5 magnification lens for the resin blocks (ventral margin) and a x10 magnification lens for the acetate peels (Figure 2.4). The computer software ImagePro Premier 9.1 was used to stitch the smaller images into single continuous images that contained either the complete ventral margin or the complete umbo of the shells examined. Each peel was stored and referenced for increment measurements.
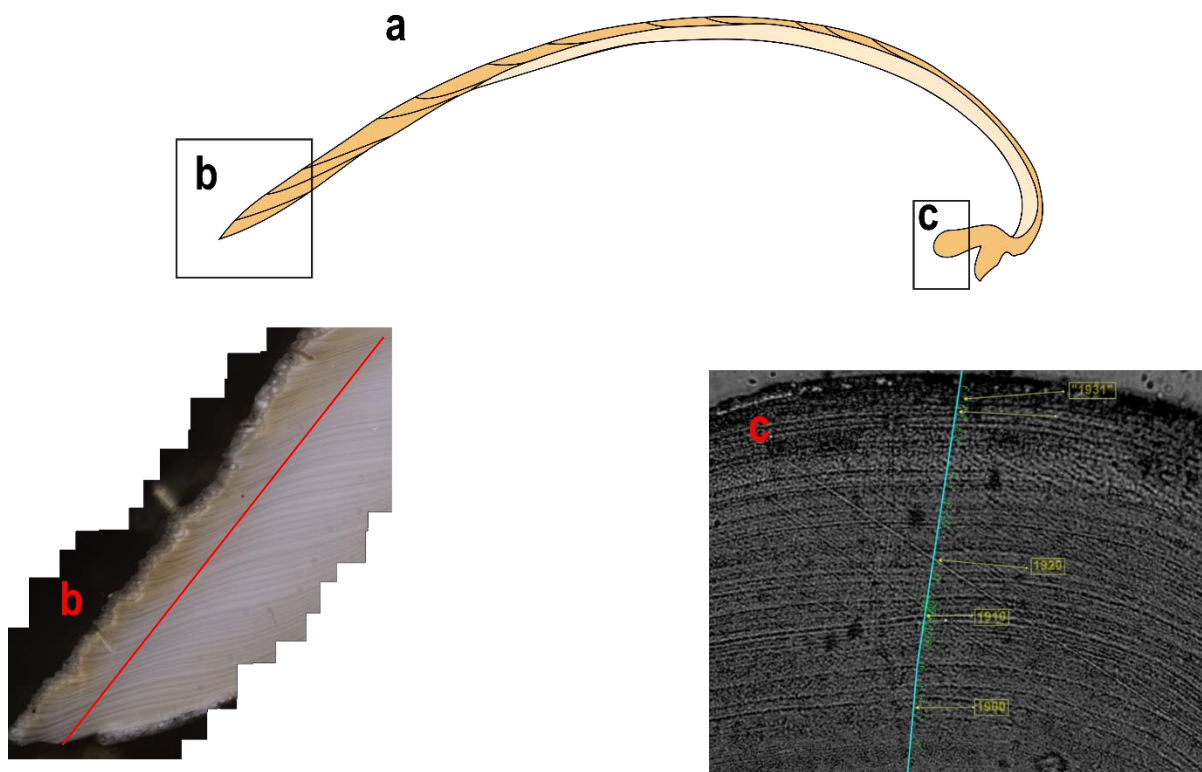
Figure 2.4 Cross section of and *Arctica islandica* shell.
The illustration shown in (a) depicts a typical cross section of an *A. islandica* shell. The increments found in the ventral margin (b) can often be analysed and measured using reflected light microscopy. The increments found in the umbo (c) are more densely packed and a higher magnification is required to study them. The red line in (b) and light blue line in (c) shows the axis on which measurements of the increments would be carried out.

ImagePro Premier has a tool that allows the interactive measurements of the increments. The width of these is measured from increment boundary to increment boundary. In the case of measurements taken in the umbo, these are done along the apex of the arch traced by the increments (Figure 2.4c). In the case of the ventral margin, the measurements are taken along an axis parallel to the outer shell surface (Figure 2.4b).

The measurements from each image were exported into individual spreadsheets and stored alongside the shell images.

2.5.2 Standardisation and detrending

An increment growth chronology is taken to be the average of the relative growth of multiple shells over an extended time duration. The operative term in the last statement is the phase "relative growth." Relative to what? Like many living organisms, *A. islandica* shows a decreasing growth trend with age. Juvenile specimens grow at a much higher rate than mature specimens for a given year (Figure 2.5). This decrease in growth can be estimated using a general negative exponential function with the form

$$G = Ae^{-bt} + K$$

where A is a scaling constant, e is Euler's number, b is the decaying growth rate, t is the time in years (either ontogenetical or calendar) and K is a positive constant that serves as an asymptote. The relative growth mentioned above is then the ratio of the measured increment width and the estimated growth:

$$R = M/G$$

Comparing the increments deposited in the mature years of one specimen to the increments deposited in the juvenile years of another quickly becomes unwieldy (Figure 2.5**a**). Doing the same exercise but using R calculated for both specimens makes the comparison much easier (Figure 2.5b). This is known as the ratio method, and it was employed in the dendrochronology field for the better part of the 20th century. However, the ratio method tends to amplify the variability in the slow-growing years of the specimens (Figure 2.5b, Cook and Peters, 1997). Cook and Peters (1997) suggest abandoning the ratio method altogether and instead first stabilise the variance of the raw increment measures with an adaptive power transformation (P_M). This stabilisation of the variance is what is referred to as "standardisation" in this dissertation. After standardisation, Cook and Peters (1997) recommend subtracting G from the transformed increment widths (P_M – G) for every shell (Figure 2.5c). The subtraction of the estimated growth is what is referred to as "detrending." The residuals from the detrending procedure (growth indices) are then compared.
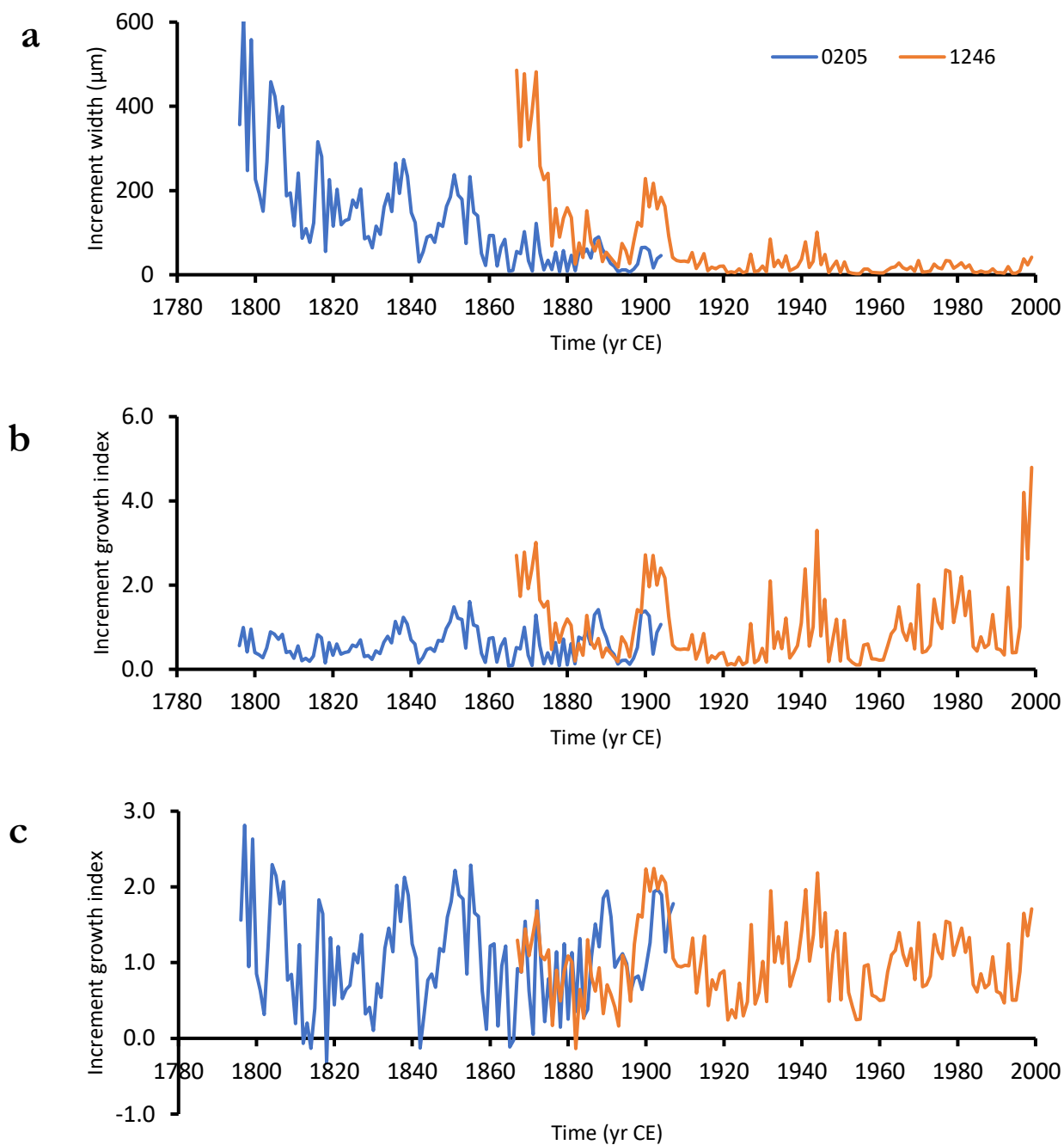
Figure 2.5 Raw *Arctica islandica* increment measurements and detrended indices.

The raw measurements show a characteristic negative trend as the mollusc age increases (a). Detrending the raw measurements using the ratio method tends to amplify the slow-growing years (b). On the other hand, stabilising the variance with an adaptive power transformation and then subtracting the modelled growth from the transformed measurements produces results that are easier to compare (c) between specimens. The measurements showed here are an example and not necessarily the final measurements used in the following chapters.

2.5.3 Crossmatching

The working assumption of chronology building in sclerochronoloy is that the relative growth of individuals from within a community is responding to a common environmental signal. The relative growth of every individual in the community for a given year should be comparable. Hence, a positive correlation between the growth indices calculated from individuals with overlapping lifespans is expected.

The crossmatching procedure puts into practice the working assumption and expectations. To crossmatch two specimens it is first necessary to know their approximate time of death, be it because one or both were caught alive or by AMS radiocarbon dating. In this investigation the increment widths for every specimen were measured and compared with the MATLAB program SHELLCORR (Butler, 2009; Butler et al., 2009a; Scourse et al., 2006a).

SHELLCORR provides a visual representation of running correlations between individual shell index series lagged relative to one another (Figure 2.6). In the default SHELLCORR code, positive correlations between shells series are represented with warm colours (yellow to bright red) while negative correlations are represented with cool colours (green to dark blue). Two shells with the same amount of increments measured in their common lifespan with similar growth patterns would be represented in SHELLCORR as a bright red stripe at lag-0, indicating a successful crossmatch. When the red stripe deviates from lag-0, either entirely or in sections, it usually means that the measurement of one of the shells is missing an increment (either because it is too thin or too faint), one extra ring was identified in one of the shells (known as a disturbance line, usually the result of shell damage by predator attack or stress) or that the date of death was incorrectly assigned to one or both of the shells. Disagreements between pairs of shells are resolved by comparing multiple shells that contain increments deposited at the time of disagreement. Finally, to avoid spurious correlations between otherwise unrelated specimens, at least 50 years of overlapping lifespan are required.
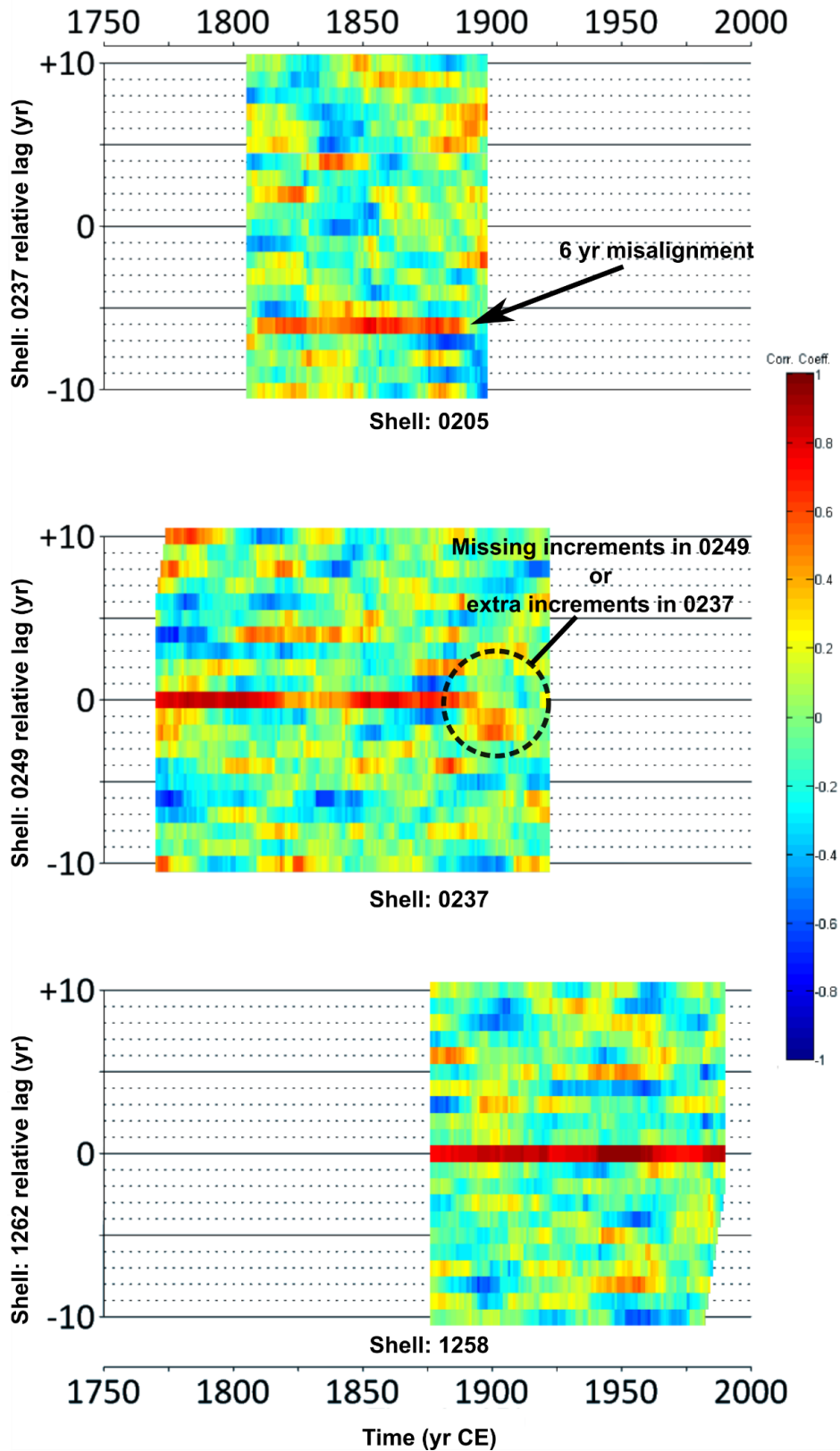
Figure 2.6 Output of three pairs of shells whose increment measurements were crossmatched using SHELLCORR. The extend of the plot in the horizontal axis denoted the common growth period of the pair of shells. The plots are generated when the compared shells measurements have been standardised and detrended. A strong positive correlation at lag-0 (vertical axis) implies that the shell pair has been correctly cross matched.

Once the shells have been crossmatched, the chronology building procedure can begin. The first step is to combine all the files that contain the increment measurements into a single file. The raw measurements were saved in text files (.txt) in two columns with the format TIME-MEASUREMENT with no headers. In the case of the shells used for the studies covering the last 500 years, the first column has units of year CE and the second column has units of micrometres. In the case of the shells used for the study covering the early Holocene, the first column has units of calibrated years before 1950 CE (often referred to as years before present). The software FMT (V 6.06) was used to combine all the text files into a single compact file (.cmp). Because FMT was originally developed for dendrochronology, it sometimes has trouble handling the increment measurements in micrometres (i.e., it does not expect the numbers to have so many digits). This is easily solvable by multiplying the measurements by 0.1 or 0.01 before creating the compact file (this functionality is built into FMT so there is no need to alter the text files themselves).

The next step is to process the compact file using the standard dendrochronology program ARTSAN (Cook and Krusic, 2014). ARTSTAN provides many options ranging from the type of input file to the type of mean calculation. The options selected within the program follow the methods described in the last two sections: The input file type is a compact file, the raw increment series are standardised using an adaptive power transformation and the raw measurements are detrended by subtracting a negative exponential function. If the negative exponential function results in a bad fit, the program was told to use a linear function with a negative slope instead. Finally, the increment growth indices from the individual shells are averaged using a biweight robust mean function. The robust function is preferred over an arithmetic mean because it is much less sensitive to outliers.

The strength of the chronologies was analysed with the standard dendrochronology and sclerochronology statistics $\bar{r}$ (the average inter-series correlation) and the expressed population signal (EPS; variance explained by a finite subsample of a population chronology, see Wigley et al., 1984). These statistics were calculated in ARSTAN in a 30-year sliding window with 29-year overlaps. The simpler mathematical formulation of EPS

$$EPS = \frac{n\bar{r}}{1 + (n-1)\bar{r}}$$

indicates that it is a function of the number of shells (n) in the sliding window and $\bar{r}$. A high EPS is usually interpreted as indicating the presence of a strong common environmental signal in the growth increment series of the sampled shell population (Buras, 2017; Butler et al., 2009a; Wigley et al., 1984). An EPS of 0.85 is commonly used as a threshold to indicate that a chronology is reasonably representative of the whole population (Buras, 2017).

There is some contention about the use of EPS when evaluating the strength of a chronology. Cook and Pederson (2011) comment that there is a considerable amount of biological uncertainty that is not represented by EPS. Buras (2017), on the other hand, offers a more careful reading of the work that introduced the EPS concept (Wigley et al., 1984) and concludes that EPS does not reveal whether the signal contained within an increment width chronology is closely related to a reconstructed environmental parameter or any source of common growth variation. Instead, Buras (2017) recommends the use of the subsample signal strength (SSS), also introduced by Wigley et al. (1984):

$$SSS = \frac{n_{win}(1 + (n_{chron} - 1)\bar{r})}{n_{chron}(1 + (n_{win} - 1)\bar{r})}$$

The n_{win} and n_{chron} in the equation for SSS represent the number of shells represented in the sliding window and the total number of shells contained in the chronology, respectively.

Using the $\bar{r}$, EPS and SSS statistics do not *really* say much about the correctness of the crossmatching exercise, only how well is a common environmental signal is represented within the growth pattern of the shells (Cook and Pederson, 2011). Because the studies presented in this dissertation use the chronologies solely as a stratigraphic template on which to base geochemical results (in other words, the chronologies are used as age models *only*), the Baillie-Pilcher t-value method (Baillie and Pilcher, 1973) was employed to determine the likelihood of obtaining spurious crossmatches between shells. This allows the assessment of temporal uncertainties in the chronologies. With this method, the correlation between pairs of shell indices is evaluated with a student t-test with N-2 degrees of freedom, where N is the number of overlapping years. A p-value is then calculated to determine the chances of getting the obtained correlation by chance.

2.7 MICROMILLING AND STABLE ISOTOPE GEOCHEMISTRY

A number of shells from each site were selected for micromilling (details in Chapters 3 and 5). The selection was based on temporal coverage of the individual shells and their taphonomic state, with preference given to the shells that showed the least erosion, the broadest increments and those that provided at least 10

years of temporal overlap between shell pairs. Milling was carried out on polished shell sections at the School of Ocean Sciences, Bangor University, using a computerised New Wave/Elemental Scientific micromill system fitted with a spherical tungsten carbide dental burr with a diameter of 300 μm at the tip. To minimise aragonite to calcite transformation due to heating and stress (Foster et al., 2008), the rotation speed was limited to 10-12 % of the maximum, equivalent to 3,710-4,450 rpm. The milling for every resin-embedded shell was carried out on the ventral margin section on the outer shell layer after the increments had been internally crossmatched (i.e. the increments found on the ventral margin of a given shell were crossmatched with those found in the hinge of the same shell) and after the outermost surface of the shells was physically removed to avoid contamination with remnants of the periostracum and resin (Schöne et al., 2017). To avoid chipping, the milling direction was from the periostracum surface of the outer shell towards the inner part of the shell, taking care not to incorporate material from the inner shell layer in the samples. The entirety of the outer layer in each annual increment was milled between the growth lines to an average depth of 100 μm.

All the powder extracted from a given increment was thoroughly homogenized before an aliquot of the sample was isotopically characterised with a Thermo Fisher MAT 253 continuous-flow isotope ratio mass spectrometer equipped with a GasBench II at the Institute of Geosciences, University of Mainz (Germany). Samples were reacted with water-free H_3PO_4 at 72 °C for 2 hours. Isotope data were calibrated against an NBS-19-calibrated Carrara marble standard ($\delta^{18}O$ = -1.91 ‰, $\delta^{13}C$ = +2.01 ‰). The 1σ external reproducibilities and internal precisions are given in and 5. Both isotope values were reported relative to the Vienna Pee Dee Belemnite standard (VBDB) in the δ notation:

$$\delta^L X = \left(\frac{\left(\frac{^L X}{^K X} \right)_{sample}}{\left(\frac{^L X}{^K X} \right)_{standard}} - 1 \right) \times 1000$$

Where X stands for the particular element being analysed (carbon or oxygen), L stands for the atomic mass of the less common naturally occurring isotope (13 for carbon, 18 for oxygen) and K stands for the atomic mass of the most common naturally occurring isotope (12 for carbon, 16 for oxygen).

The data used for comparison against the geochemistry results comes from a variety of sources. In Chapter 3 the $\delta^{13}C$ is used to reconstruct herring recruitment in the North Sea. Two data categories can be derived to do this: (1) Instrumental environmental data to prepare and test a calibration and (2) historical data to test the reconstruction in the times prior to when instrumental data existed.

1. Instrumental environmental data

      The instrumental environmental data comprises a diatom count in a sector of the North Sea that includes the Fladen Ground and two North Sea herring surveys. Monthly diatom abundance data for the years 1958 to 2015 was obtained from the Continuous Plankton Recorder (CPR) Survey, operated by the Sir Alister Hardy Foundation for Ocean Science. The CPR is a near-surface (10 m) plankton sampler voluntarily towed each month behind merchant ships on their normal routes of passage. The diatom abundance data was used as a proxy of diatom biomass in the Fladen Ground vicinity (Leblanc et al., 2012). The diatom count/biomass was selected because the phytoplankton community biomass of the North Sea is dominated by diatoms during the spring bloom (Halsband and Hirche, 2001; Nielsen and Richardson, 1989), representing primary production.

      Another instrumental data set used was the ICES (2018) herring stock assessment. The assessment covers the areas of the North Sea, the English Channel, the Skagerrak and the Kattegat. The ICES (2018) data provides a thorough look at the North Sea herring stock (considered a unit-stock, Mariani et al., 2005), showing estimates for recruitment, spawning stock biomass, natural mortality, fishing mortality, catch and landings at annual resolution from 1947 to 2017. Although the area covered by the stock assessment is significantly larger than the Fladen Ground region, catch statistics and spawning studies suggest that the majority of the herring recruitment occurs in the northern North Sea (Heath and Richardson, 1989; Lusseau et al., 2014; Richardson, 2017).

2. Historical data

      The historical data comprises the index "catch per unit effort" (CPUE) from the Netherlands (Poulsen, 2008), Lowestoft (east of England, Cushing, 1968), southeast Scotland (Jones et al., 2016) and the Peterhead district (east Scotland, Coull, 1986). CPUE is defined as

$$\frac{C}{E} = qN$$

where C represents the catch, E represents the effort, N is the fish density and q is the catchability coefficient (Arreguín-Sánchez, 1996; Poulsen and Holm, 2007). The effort can be defined in different

ways, ranging from the number of ships in a given year's fishing fleet, the total area of fishing net, or the ships' dimensions and power. For the purpose of the study presented in Chapter 3 is study, only the left-hand side of the CPUE equation was used. Chapter 3 goes into detail when describing the nature of the CPUE indices used, including how was the catch data compiled, what temporal resolution does it have, how was effort defined for each index and who calculated the indices.

In Chapter 4 the $\delta^{18}O$ is used to reconstruct bottom water temperatures in the North Sea. In this case the availability of the widely used Grossman and Ku (1986) palaeotemperature equation deemed the development of a calibration unnecessary. However, to test the results from the application of the Grossman and Ku (1986) equation to the $\delta^{18}O$ data, water temperature measurements taken in the Fladen Ground vicinity were used. The temperature measurements from 1947 to 2010 of the water between 0 and 135 m depth were extracted from the ICES CTD and bottle data database (available at http://ocean.ices.dk/HydChem/HydChem.aspx; last checked: 11-Dec-2017; ICES, 2014) from a 2° latitude by 2° longitude grid box centred at Site B. The available data for the depths between 70 and 135 metres were integrated and averaged to monthly resolution. This integrated depth was selected because it shows temperatures and salinities through time that suggest consistently mixed conditions.

The missing data were interpolated in five-year intervals. This was done by "sandwiching" the interval of interest between data of the five years prior and five years after said segment starting with 1950-1955. Then an 8-term Fourier regression was calculated using the complete 15-year interval and used to interpolate the missing data. The temperature of months when the value was replicated by less than the average monthly replicate of the 15-year interval minus 75% of the replicate standard deviation ($N_{month} < N_{15-year} - 0.75 * \sigma[N_{15-year}]$) was replaced by the value predicted by the Fourier interpolation. The replicate number for the interpolated months was assigned as $N_{month} = N_{15-year} - 0.75 * \sigma[N_{15-year}]$. The 75% factor in the standard deviation was selected to obtain a higher threshold in the number of replicates required to represent a given month.

To model realistic uncertainties for the averaged temperature data, first the monthly standard deviation for the years 1986-2010 was calculated prior to the interpolation exercise ($\sigma[T_{month, 1986-2010}]$). This segment was selected because it had the least amount of missing data and the average monthly temperature was commonly represented by more than 30 replicates. Then $\sigma[T_{month, 1986-2010}]$ was assigned for every month starting in January 1950. Finally, the uncertainty for a given month was obtained by multiplying $\sigma[T_{month, 1986-2010}]$ by a factor F calculated as $F = -0.178 * \ln(N_{month}) + 1.695$. This has the effect of multiplying $\sigma[T_{month, 1986-2010}]$ by 1.5 when N_{month} is 3 and by 1 when N_{month} is 50.

3. RECONSTRUCTION OF ATLANTIC HERRING (*CLUPEA HARENGUS*) RECRUITMENT IN THE NORTH SEA FOR THE PAST 455 YEARS BASED ON THE $\delta^{13}C$ FROM ANNUAL SHELL INCREMENTS OF *ARCTICA ISLANDICA*

Juan Estrella-Martínez[1], Bernd R. Schöne[2], Ruth H. Thurstan[3], Elisa Capuzzo[4], James D. Scourse[5], and Paul G. Butler[5]

[1]School of Ocean Sciences, Bangor University, Bangor, Wales, UK.
[2]Institute of Geosciences, Johannes Guttenberg University, Mainz, Germany.
[3]Centre for Ecology and Conservation, University of Exeter, Penryn, Cornwall, UK.
[4]Centre for Environment, Fisheries & Aquaculture Science (Cefas), Lowestoft, UK
[5]College of Life and Environmental Sciences, University of Exeter, Penryn, Cornwall, UK.

3.1 ABSTRACT

Understanding the recruitment variability of the Atlantic herring North Sea stock remains a key objective of stock assessment and management. Although many efforts have been undertaken linking climatic and stock dynamic factors to herring recruitment, no major attempt has been made to estimate recruitment levels before the 20th century. Here we present a novel annually-resolved, absolutely dated herring recruitment reconstruction, derived from stable carbon isotope geochemistry (δ^{13}C), from ocean quahog shells from the Fladen Ground (northern North Sea). Our age model is based on a growth increment chronology obtained from fourteen shells. Ten of these were micromilled at annual resolution for δ^{13}C analysis. Our results indicate that the anthropogenically-driven relative depletion of ^{13}C, the oceanic Suess effect (oSE), became evident in the northern North Sea in the 1850s. We calculated a regression line between the oSE-detrended δ^{13}C results (δ^{13}CṠ) and diatom abundance in the North Sea, the regression being mediated by the effect of phytoplankton on the δ^{13}C of the ambient dissolved inorganic carbon. We used this regression to build an equation mediated by a nutritional link to reconstruct herring recruitment using δ^{13}CṠ. The reconstruction suggests that there were five extended episodes of low recruitment levels before the 20th century. These results are supported by measured recruitment estimates and historical fish catch and export documentation. This work demonstrates that molluscan sclerochronological records can contribute to the investigation of ecological baselines and ecosystem functioning impacted by anthropogenic activity with implications for conservation and stock management.

3.2 INTRODUCTION

The North Sea herring has been a source of wealth and nutritional stability for the countries bordering the North Sea going at least as far back as the Middle Ages (Pitcher and Lam, 2014). Recruitment variability, i.e. the number of juvenile fish that survive from egg production to join the stock, is known to be a crucial contributor to stock productivity (Pinnegar et al., 2016). The socioeconomic impacts of extended low recruitment intervals were evidenced twice in the past 50 years. In the 1970s, herring recruitment failure led to a collapse of the fish stock and temporary closure of the fishery. Later, in the 2000s, reduced recruitment levels caused the fisheries management agencies to reduce the total allowable catch of the North Sea stock by half (Corten, 2013). While annual estimates of herring recruitment in the North Sea are available for the 20th and 21st centuries (Burd, 1978; ICES, 2018), understanding the long-term variability, magnitude and drivers of recruitment can inform management efforts to keep the stock at sustainable levels (Dickey-Collas et al., 2010; Simmonds, 2007).

38

In the classical view of the marine food-web in temperate seas, fisheries recruitment and production is linked to diatom blooms (in spring and autumn); particularly, the energy of the diatom bloom flows to fish, either directly (e.g. with large colonial diatoms; Chavez, Messié, & Pennington, 2011; Ryhter, 1969) or mediated through copepods (Cushing, 1989; Irigoien et al., 2002). In fact, the phytoplankton community biomass of the North Sea is dominated by diatoms during the spring bloom (e.g. (Halsband and Hirche, 2001; Nielsen and Richardson, 1989).

Other factors are also likely to contribute to fish recruitment and significant efforts have been undertaken to understand the drivers of recruitment variability in the North Sea. These include regression analyses between recruitment, stock densities and water temperature (Akimova et al., 2016; Bogstad et al., 2013), and models based on the interaction of major climatic variability modes such as the North Atlantic Oscillation (NAO) and the Atlantic Multidecadal Oscillation (AMO) and stock densities (Axenrot and Hansson, 2003; Gröger et al., 2010). Of these, Akimova et al., (2016) and Bogstad et al. (2013) agree that water temperature is a poor herring recruitment predictor. On the other hand, Axenrot and Hansson (2003) and Gröger et al. (2010) successfully modelled herring recruitment in their studies but these were limited to the second half of the 20th century and neither was able to provide an adequate mechanism to explain the interaction between modes of climatic variability and recruitment.

The difficulty of defining a mechanism that associates climatic variability with fish recruitment was evidenced in a study by Capuzzo et al. (2018). Although these authors found a significant positive correlation between primary production and recruitment levels in different fish stocks in the North Sea, they did not find a link between the NAO and primary production, instead relating the latter to riverine nutrient inputs and sea surface temperature. Riverine runoff is in turn influenced by the combined effects of the NAO and AMO (Hurrell, 1995; O'Reilly et al., 2017).

For periods before the 20th century, research has concentrated on fish landing reconstructions from historical records. High quality records exist for Dutch, Scottish and Swedish herring fisheries (Alheit and Hagen, 1996; Corten, 1999; Coull, 1990, 1986; Höglund, 1978; Jones et al., 2016; Poulsen, 2010, 2008). While these records have been used to assess the climatic impacts on herring migratory patterns (Alheit and Hagen, 1996; Corten, 1999), they may not always be useful as a guide to estimate recruitment levels as this also requires information about levels of natural and fishing mortality (Tester, 1955). To effectively address this information gap, we require a set of reliably dated proxy data that are tightly coupled to ecosystem variability, which extend at least as far back in time as the historical catch reconstructions, and that also cover the 20th and 21st centuries.

In this study we present an annual reconstruction of North Sea herring recruitment for the time interval 1551 to 2005 CE (hereafter all references to dates assume years CE) based on the stable carbon isotopes of shells of the ocean quahog from the Fladen Ground in the northern North Sea. The stable carbon isotope values (deviations of the ^{13}C:^{12}C ratio of a substance when compared to the ^{13}C:^{12}C ratio of a standard, δ^{13}C) from the ocean quahog's shell have been shown to be proportional to the δ^{13}C of the dissolved inorganic carbon (δ^{13}C$_{DIC}$) in the water column (Beirne et al., 2012) and to not be affected by ontogeny or growth-rates (Schöne et al., 2005c, 2011a). δ^{13}C$_{DIC}$ and DIC concentration in the North Sea are largely controlled by primary production and respiration (Bozec et al., 2006; Burt et al., 2016). Robust growth increment chronologies can be built from the annual increments in the ocean quahog's shell (Butler et al., 2009a, 2010, 2013; Schöne et al., 2003; Scourse et al., 2006a; Thompson et al., 1980; Witbaard, 1996) which provide an accurate age model for stable isotopic results. The work presented here reconstructs herring fish recruitment through the interpretation of temporally aligned δ^{13}C values of the ocean quahog's shell, through the relation between δ^{13}C$_{DIC}$ and the wider ecosystem in the North Sea.

In presenting this reconstruction we will (a) determine the timing of the anthropogenic-driven relative ^{13}C depletion in the North Sea (oceanic Suess effect) and determine a time-dependent mathematical formulation for it, (b) explore the relationship between the δ^{13}C from the shell of the ocean quahog and diatom abundance, and (c) associate this relationship with patterns of herring recruitment in the North Sea. As the first attempt to link molluscan sclerochronological data to wider ecosystem functioning, this work constitutes a novel application of ocean quahog sclerochronology.

3.3 MATERIALS AND METHODS

To reconstruct and test herring recruitment for the North Sea we adopted techniques used in different fields. First, we established our age model by applying crossdating techniques first developed by the tree-ring community and later adapted in the study of long-lived bivalves. We did this by extending an existing northern North Sea ocean quahog increment chronology (Butler et al., 2009a) to be used solely as an age model.

We then obtained geochemistry of stable carbon isotopes from the shells comprising this chronology and used it to build a continuous δ^{13}C time series covering the 1551-2005 interval. As modern marine δ^{13}C records show a characteristic negative trend related to the burning of fossil fuels (oceanic Suess effect, see below), we applied a modified technique routinely used in the tree-ring and bivalve-increment communities, i.e. detrending.

We calibrated the detrended $\delta^{13}C$ time series against 20th century measurements of diatom abundance and age-0 herring recruitment and used this calibration to reconstruct herring recruitment during the 1551-2005 interval. Finally, we tested our reconstruction with various independent historical records of catch per unit of effort.

3.3.1   Shell collection and processing

The ocean quahog shells used in this research were collected from the Fladen Ground in the northern North Sea at coordinates 58.994° N, 0.291° E. The collection was acquired by the RV *Prince Madog* in 2004. Figure 3.1 shows the approximate location of the collection site, together with average annual herring landings from 2012 to 2016 by the UK-registered fishing fleet. Given that the majority of herring spawning in the North Sea occurs in the vicinity of Orkney and Shetland in northern Scotland, near the Fladen Ground (Heath and Richardson, 1989; Lusseau et al., 2014), and the tendency of juvenile herring to stay in shallow waters before recruitment, it is not unreasonable to assume that an important part of recruitment would also occur in or nearby the Fladen Ground.
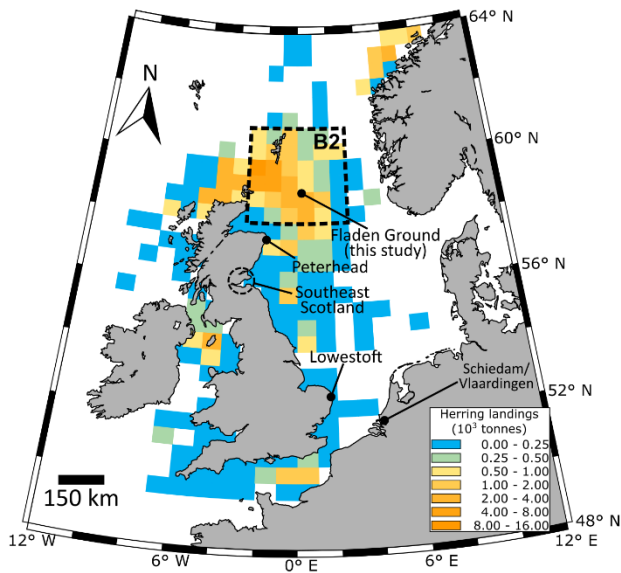
Figure 3.1 Approximate position of *A. islandica* sampling site.
The map shows the annual average herring landings by UK-registered ships between the years 2012-2016 (Richardson, 2017) per ICES standard rectangle.

We used a total of 16 shells, being a combination of live-collected specimens (five adults originally described in Butler et al., 2009a, and two juveniles), articulated valves and single valves. Once cleaned, the shells were sectioned using a standard procedure (Butler et al., 2009a; Scourse et al., 2006a). The polished surfaces of the shell sections were etched in 0.1 M HCl for one minute and the etched surfaces were copied onto acetate peel replicas (Ropes, 1984). The peels were viewed under transmitted light, and the imaging software package ImagePro Premier 9.1 was used to identify and measure the growth increments in the outer layer of the hinge and ventral margin of the shell.

3.3.2 Accelerator mass spectrometry radiocarbon dating and chronology construction

Radiocarbon dating was carried out on the umbonal shell portion (deposited in early ontogeny) of nine of the previously mentioned sixteen specimens (Scourse et al., 2006a). These were selected based on size (assuming that larger shells belonged to longer-lived animals, see Butler et al., 2009a and Kilada et al., 2007), and taphonomic characteristics that suggested the specimens were alive during the last millennium (Nielsen, 2004). Typically, the juvenile section in the ocean quahog's shell contains the broadest increments and, therefore, umbonal shell samples incorporate less than five years of growth (Helama et al., 2006; Scourse et al., 2006a). The material was submitted to the Natural Environment Research Council Radiocarbon Laboratory (East Kilbride, United Kingdom) or the Accelerator Mass Spectrometry [14]C Dating Centre (University of Aarhus, Denmark).

Our results are based on an extension of the Fladen Ground, Site B increment-width chronology (FGB) described by Butler et al. (2009a). FGB was selected as its extended version (1755-2003) is the longest of the five Fladen Ground chronologies described by Butler et al. (2009a), and because a substantial number of shells from that site have been radiocarbon-dated. The nine radiocarbon-dated specimens described above were put in relative stratigraphic order and then crossdated with the five specimens in FGB and among each other following the crossdating methods described by Butler et al. (2009a) and Scourse et al. (2006a). The final increment-width chronology was built using the standard dendrochronology software package ARSTAN (Cook and Krusic, 2014) by applying an adaptive power transformation to each shell series to stabilise the variance (Cook and Peters, 1997; Helama et al., 2006; Schöne, 2013) then detrending each series with a negative exponential function to account for ontogenetic effects before finally averaging the individual increment-width series with a bi-weight robust mean function (Butler et al., 2009a). Two juvenile (age <30 yr) live collected specimens were not crossmatched to FGB, but were independently dated by counting increments.

The strength of the chronology was analysed with the standard dendrochronology and sclerochronology statistics $\bar{r}$ (the average inter-series correlation) and the expressed population signal (EPS; variance explained by a finite subsample of a population chronology, see Wigley et al., 1984). These statistics were calculated in a 30-year sliding window. The simpler mathematical formulation of EPS

$$EPS = \frac{n\bar{r}}{1 + (n - 1)\bar{r}}$$

indicates that it is a function of the number of shells (n) and r̄. A high EPS is usually interpreted as indicating the presence of a strong common environmental signal in the growth increment series of the sampled shell population (Buras, 2017; Butler et al., 2009a; Wigley et al., 1984). An EPS of 0.85 is commonly used as a threshold to indicate that a chronology is reasonably representative of the whole population.

Dissertation-specific note
Additional to EPS, the subsample signal strength (SSS; variance explained by a finite subsample of a population chronology, see Buras, 2017 and Wigley et al., 1984) was also calculated. This is presented in Section 3.7.

Sensitivity to increment counting errors in the FGB extension were estimated by comparing the "smoothness" (Black et al., 2016) of the extension to that of the original Butler et al. (2009a) FGB version with an F-test on the year-to-year differences of the two segments. Both segments of the chronology are considered equally smooth if the variance of the year-to-year difference is not significantly different.

3.3.3 Micromilling and stable isotope analysis

Eight of the shells contained in the newly extended FGB were selected for isotopic analysis at annual resolution on the time interval from 1551 to 1980. The selection was based on temporal coverage of the individual shells and their taphonomic state, with preference given to the shells that showed the least erosion, the broadest increments and those that provided at least 10 years of temporal overlap between shell pairs. Two live-collected juvenile specimens were selected for micromilling at annual resolution for the time interval 1976-2005. These specimens came from the same site as the FGB shells but they were not incorporated into the chronology.

Milling was carried out on polished shell sections at the School of Ocean Sciences, Bangor University, using a computerised New Wave/Elemental Scientific micromill system fitted with a spherical tungsten carbide dental burr with a diameter of 300 µm at the tip. To minimise aragonite to calcite transformation due to heating and stress (Foster et al., 2008), the rotation speed was limited to 10-12 %, equivalent to 3,710-4,450 rpm. The milling for every resin-embedded shell was performed on the ventral margin section on the outer shell layer after the increments had been internally crossmatched (i.e. the increments found on the ventral margin of a given shell were crossmatched with those found in the hinge of the same shell) and after the outermost surface of the shells was physically removed to avoid contamination with remnants of the periostracum and resin (Schöne et al., 2017). Figure 3.2 shows a schematic of the micromilling process. To avoid chipping, the milling direction was from the surface of the outer shell towards the inner part of the

shell, taking care not to incorporate material from the inner shell layer in the samples. The entirety of the outer layer in each annual increment was milled between the growth lines to an average depth of 100 μm.
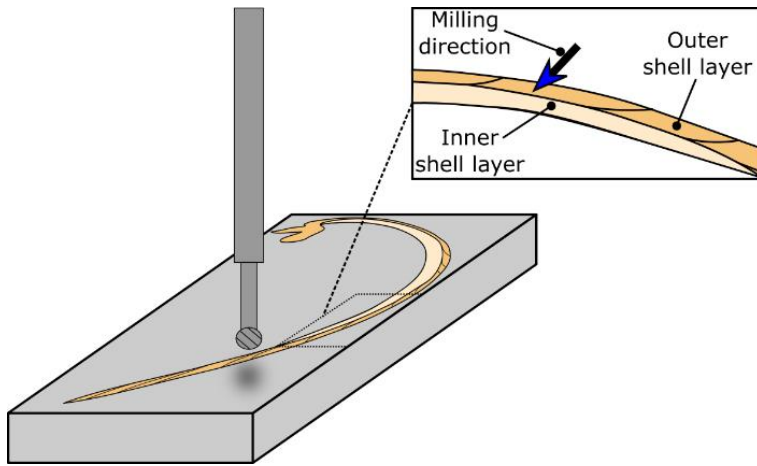
Figure 3.2 Schematic of the micromilling process.

All the powder extracted from an increment was thoroughly homogenized before an aliquot of the sample was isotopically characterised.

All the powder extracted from a given increment was thoroughly homogenized before an aliquot of the sample was isotopically characterised with a Thermo Fisher MAT 253 continuous-flow isotope ratio mass spectrometer equipped with a GasBench II at the Institute of Geosciences, University of Mainz (Germany). Samples were reacted with water-free H_3PO_4 at 72 °C for 2 hours. Isotope data were calibrated against an NBS-19-calibrated Carrara marble standard ($δ^{18}O$ = -1.91 ‰, $δ^{13}C$ = +2.01 ‰) with 1σ external reproducibility (accuracy based on 421 blindly measured NBS-19 samples) better than 0.04 ‰ for $δ^{18}O$ and 0.03 ‰ for $δ^{13}C$ and internal precision better than 0.06 ‰ for $δ^{18}O$ and 0.04 ‰ for $δ^{13}C$. Both isotope values were reported relative to the Vienna Pee Dee Belemnite standard. Note that we did not apply a correction for different acid fractionation factors of the shell samples (aragonite) and the reference material (calcite). For more detailed description and reasoning see Füllenbach et al. (2015).

We inspected the results against the average peak intensity given by the mass spectrometer and rejected those that showed abnormally high/low isotope values and those with intensities falling significantly outside the range of the reference materials. Lower-than-average peak intensities are related to insufficient mass in the carbonate powder sample.

3.3.4 Adjustment for the oceanic Suess effect

We approximated the oceanic Suess effect (oSE), i.e., the relative depletion of ^{13}C in carbonate material due to fossil fuel burning since the second half of the 19th century, using a weighted Fourier regression consisting of the two largest coefficients (Section 3.7). The weights were given by $1/σ^2$ where σ represents the internal $δ^{13}C$ precision for each sample. The purpose of this approximation is not to capture the entire variability of the oSE but, rather, determine its onset in the northern North Sea.

To emphasise the high frequency variability, we subtracted the oSE as given by our regression from the raw $\delta^{13}C$ data ($\delta^{13}C\dot{S}$, "$\delta^{13}C$ Sdot"). The $\delta^{13}C\dot{S}$ was weight-averaged into a single series before comparison with diatom assemblages or herring recruitment data.

3.3.5   Modern diatom and recruitment data

We used diatom abundance data as a proxy of diatom biomass at our site (Leblanc et al., 2012). Diatom abundance data was obtained from the Continuous Plankton Recorder (CPR) Survey, operated by the Sir Alister Hardy Foundation for Ocean Science. The CPR is a near-surface (10 m) plankton sampler voluntarily towed each month behind merchant ships on their normal routes of passage. We used the annual maximum diatom count from the CPR standard area B2 (Figure 3.1) for the years 1958 to 2005 (Johns, 2016).

Annual age-0 herring recruitment data for the years 1947 to 2005 was obtained from the International Council for the Exploration of the Sea (ICES) 2017 fish stock assessment for the North Sea, Skagerrak, Kattegat, and east English Channel, the so called "North Sea autumn spawners" (ICES, 2018). Annual age-2 recruitment for the years 1919 to 1973 was obtained from Burd (1978) for central and northern North Sea. The recruitment for the two areas was averaged into a single annual series. The Burd (1978) and ICES (2018) data overlap between the years 1953 and 1973 and, in general, show that the age-2 recruitment reported by Burd (1978) is ten times smaller than the age-0 recruitment (ICES, 2018). However, herring catch statistics from ICES (2017) show an approximate age-2:age-0 catch ratio of 5 to 1 in the overlapping time interval which suggests that the recruitment reported by Burd (1978) may be an underestimation. We thus scaled the Burd (1978) recruitment data by a factor of 10 before comparing to our analysis.

3.3.6 $\delta^{13}C\dot{S}$ calibration

The $\delta^{13}C\dot{S}$ data were compared to the *log-transformed* maximum diatom count (Johns, 2016) and *log-transformed* age-0 herring recruitment (ICES, 2018) (see Section 3.7 for detailed description and reasoning). The latter two were also compared against each other.

A cross calibration/verification (CCV) using reduced major axis (RMA) regressions was performed after removal of outliers in the $\delta^{13}C\dot{S}$ and herring recruitment and diatom count for the interval 1947-2015. The outliers were identified graphically in a modified box and whisker plot where the extent of the first and fourth quartiles (represented by the whiskers) is constrained to be less than 1.5 times the combined height of the second and third quartiles (represented by the box). Data outside this constraint is considered an

outlier. Three outliers were identified in MD and HR (1969, 1970, 1972, and 1975-1977, respectively) and one was identified in $\delta^{13}C\dot{S}$ (1979).

Six equations were generated from the CCV procedure: two equations relate $\delta^{13}C\dot{S}$ to maximum diatom count (MD), two relate MD to herring recruitment (HR) and two relate $\delta^{13}C\dot{S}$ to HR. The $\delta^{13}C\dot{S}$/MD and MD/HR equations that produced the residuals with the lowest heteroscedasticity were combined to generate an additional $\delta^{13}C\dot{S}$/HR equation which was compared with those generated from the regression procedure. We applied the $\delta^{13}C\dot{S}$/HR equation with the most significant statistics to the rest of the $\delta^{13}C\dot{S}$ series and further verified the results against the scaled version of the Burd (1978) record.

3.3.7 Comparison to historical data

As a mean to verify our reconstruction prior to the 20th century, the recruitment was also compared to historical catch per unit effort (CPUE, Garstang, 1900). CPUE is defined as

$$\frac{C}{E} = qN$$

where C represents the catch, E represents the effort, N is the fish density and q is the catchability coefficient (Arreguín-Sánchez, 1996; Poulsen and Holm, 2007). The effort can be defined in different ways, ranging from the number of ships in a given year's fishing fleet, the total area of fishing net, or the ships' dimensions and power. For the purpose of this study, we worked with the left-hand side of the CPUE equation only.

The CPUE calculations come from Dutch, Scottish, and English fisheries (Figure 1). The Dutch record (1604-1856) was compiled and calculated by Poulsen (2008) from the archives of the College van de Grote Visserij (CGV) which held a monopoly on the salted herring landings in the Netherlands from the late 1500s until the 1850s. The catch data compiled by Poulsen (2008) was registered in the southern towns of Schiedam and Vlaardingen. Poulsen (2008) used the fishing ships' dimensions and power as his unit of effort which remain consistent throughout the entire time series. The fishing vessels associated with the CGV carried hemp driftnets until 1859 (Poulsen, 2008) so the adoption of lighter cotton nets does not factor into the Dutch CPUE record.

The English record (1750-1789) was compiled by Cushing (1968) from "An historical account of the ancient town of Lowestoft" by Edmund Gillingwater in 1790. In his book, Gillingwater provides the "total

average of each owner's boat" which is the total catch by that owner divided by the number of boats. Cushing (1968) calculated the CPUE representing all fishermen and suggests that their nets were made of hemp.

Two Scottish CPUE records are presented. The first one is from southeast Scotland (1845-1889), compiled and calculated by Jones et al. (2016) from the archives of the United Kingdom Fishery Board (UKFB). Jones et al. (2016) used the total area of driftnet in a given year as their unit of effort. Using the total area of driftnet considers the adoption of lighter cotton nets introduced c.1860 (Coull, 1986).

The second Scottish CPUE record is from the Peterhead district in the north of Scotland (1835-1914). Herring cure records and number of fishing vessels were compiled by Coull (1986), presumably from the UKFB archives which covered all of Scotland for the interval of interest and recorded the landings of fish intended for cure (Jones et al., 2016). We calculated the Peterhead CPUE by assuming that the cured herring represented the great majority of the catch and divided it by the number of fishing vessels in a given year. Of all four CPUE used, this one is the weakest as it fails to consider technological developments.

The CPUE data used in this study were standardised into dimensionless indices to account for differences in definition of effort. We did this by subtracting the series average from every data point and dividing the result by the series standard deviation. This harmonisation only scales the CPUE data, so it can be plotted in a common axis. Correlation analyses are not affected by standardisation.

3.4 RESULTS

3.4.1 Chronology

We extended FGB to from its original start point of 1755 back to 1545 (Figure 3.3a). In general, the interval from 1545-1755 is represented by fewer shells than the interval from 1755-2003 (Figure 3.3b), with the average sample depth being 2.66 shells for the former and 6.49 shells for the latter. The interval from 1545 to 1588 is represented by only one shell.
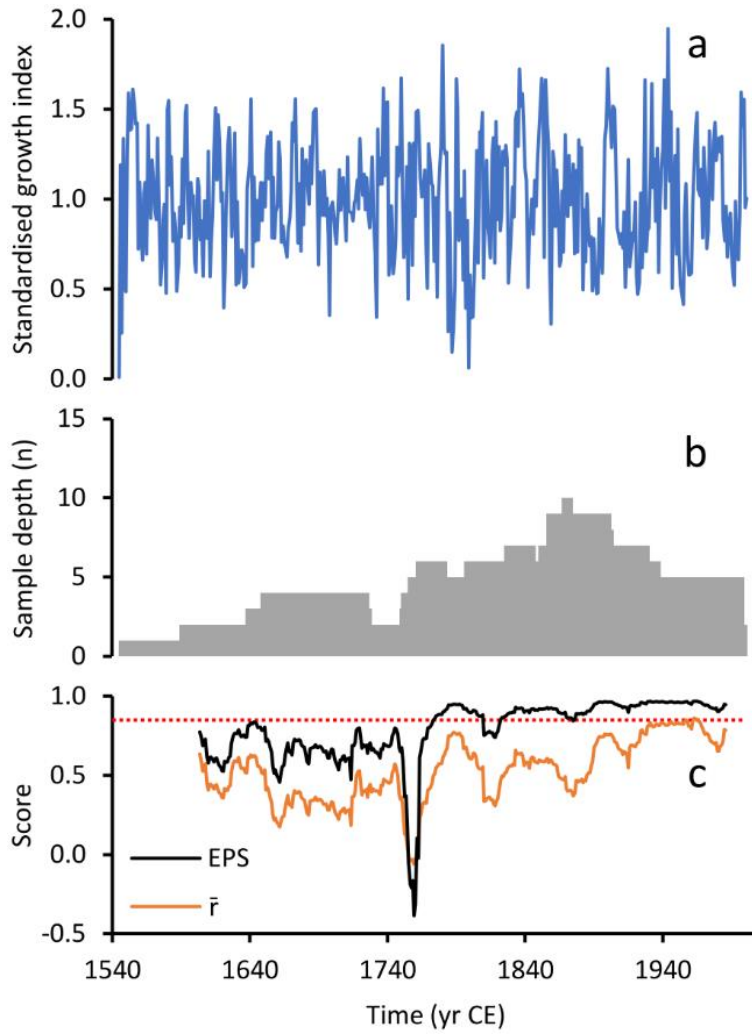
Figure 3.3 Fladen Ground Site B chronology. Newly extended chronology from Site B at the Fladen Ground (a). The extension of FGB (1545-1754) is composed of fewer shells (b) than its original iteration (1755-2001) and shows lower $\bar{r}$ and EPS scores (c). The dotted line in c represents the commonly used threshold value for EPS, 0.85.

We observed a decreased $\bar{r}$ and EPS (Figure 3.3c) in the 1545-1751 interval (average for the complete segment: $\bar{r}$ = 0.41, EPS = 0.67) when compared to 1764-2003 (average for the complete segment: $\bar{r}$ = 0.63, EPS = 0.91). These intervals are separated by an interval (1752-1763) of near-zero average values (average: $\bar{r}$ = 0.03, EPS = 0.02) which is represented by six shells, four of which settled during that time, showing biological ages between 3 and 15 years in 1763.

An F-test on the year-to-year differences (F = 1.20, $F_{Crit, p = 0.05}$ = 1.31) of the new segment of the chronology (1545-1751) and that originally constructed by Butler et al. (2009a) (1764-2003) suggests that our newly extended chronology has an increment counting error lower than 5% (Black et al., 2016), which allows us to confidently base our stable isotopic results on the age model provided by FGB.

48

3.4.2 Annual stable carbon isotopes

We obtained annual $\delta^{13}C$ results from 1551 to 1980 from eight shells in FGB, while results for 1975 to 2005 were obtained from two additional juvenile shells not contained in FGB. We were not able to achieve the target temporal overlap of ten years between shell pairs as single-increment sampling becomes increasingly difficult in later ontogeny as the increments get compressed into a smaller area. The average temporal overlap between specimens was nine years with a minimum of one year and a maximum of 26 years.

Following our sample-rejection convention in combination with samples that were under the detection limit of the machine and powder samples that were lost in the milling process, resulted in data being available for 422 out of the 455 years of temporal coverage. The longest hiatuses occur in the 20th century in the intervals between 1939-1944 and 1955-1959.
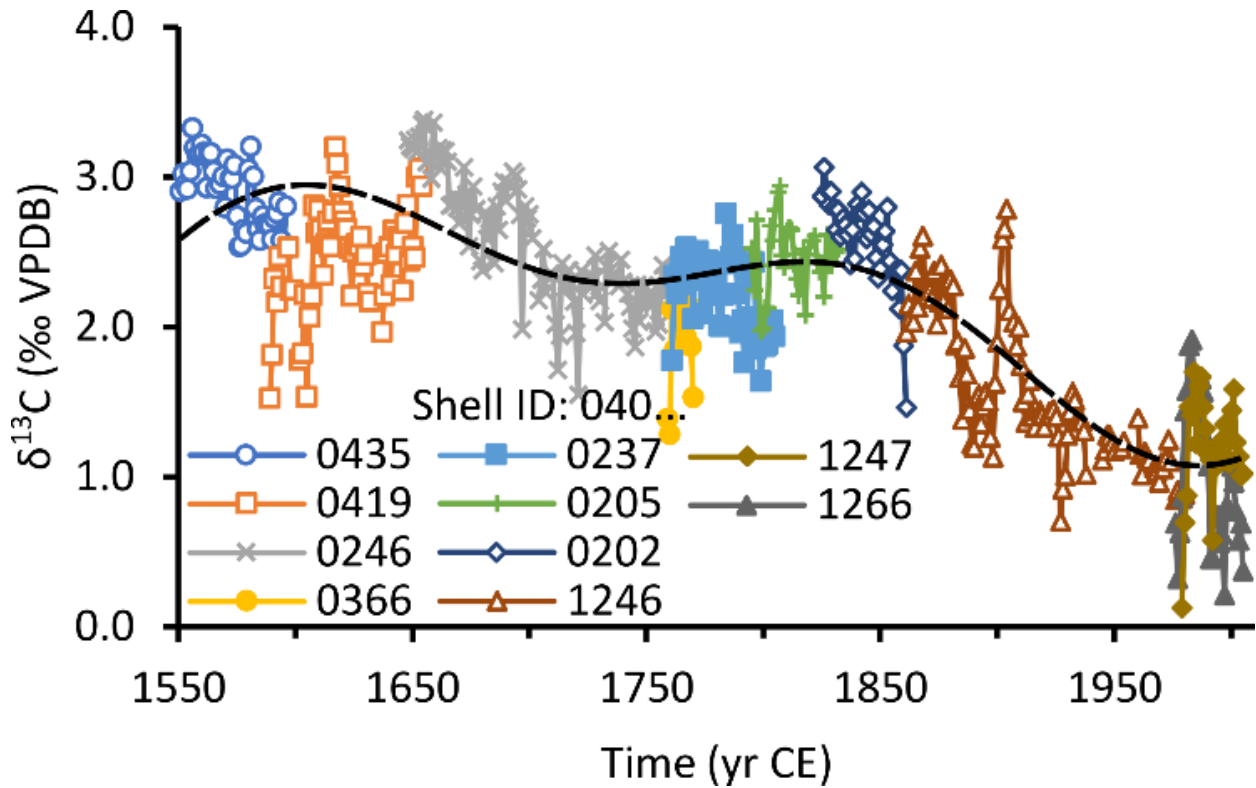
Figure 3.4 $\delta^{13}C$ results for every shell analysed.
The results show the relative depletion of $\delta^{13}C$ starting in the second half of the 19th century, i.e., the oceanic $\delta^{13}C$ Suess effect. The superimposed dashed line shows our weighted 2-term Fourier regression which suggests that the onset of the oceanic Suess effect at the Fladen Ground occurs c.1850.

The composite $\delta^{13}C$ results fall within the range 3.38 ‰ to 0.13 ‰ (Figure 3.4), the former occurring in 1655 and the latter in 1979. The results from the 19th to 21st century show a depletion of ^{13}C relative to times before the 19th century, reflecting the introduction of isotopically light carbon from the burning of fossil fuels into the oceanic dissolved inorganic carbon (DIC) pool and biogenic carbonate material (Butler et al., 2009b; Moore et al., 2000; Schloesser et al., 2009; Schöne et al., 2011a; Swart et al., 2010), the so-called $\delta^{13}C$ oceanic Suess effect (oSE). Our Fourier approximation of the oSE was highly significant, with a coefficient of determination of 0.71 (p < 0.0001). The first derivative of our approximation shows that consistent ^{13}C depletion began in c.1820. The second derivative shows that there was an increase in the rate of depletion in c.1850 from -0.0025 ‰ yr^{-1} (1817-1848) to -0.0104 ‰ yr^{-1} (1848-1914). We take this sudden change in depletion rate as the onset of the oSE at our location. The maximum rate of ^{13}C depletion occurs in 1914 (-0.0131 ‰ yr^{-1}). After that, the depletion slows down until it stops in 1986 after which we observe an average increase in $\delta^{13}C$ at a rate of 0.0028 ‰ yr^{-1} until 2005.
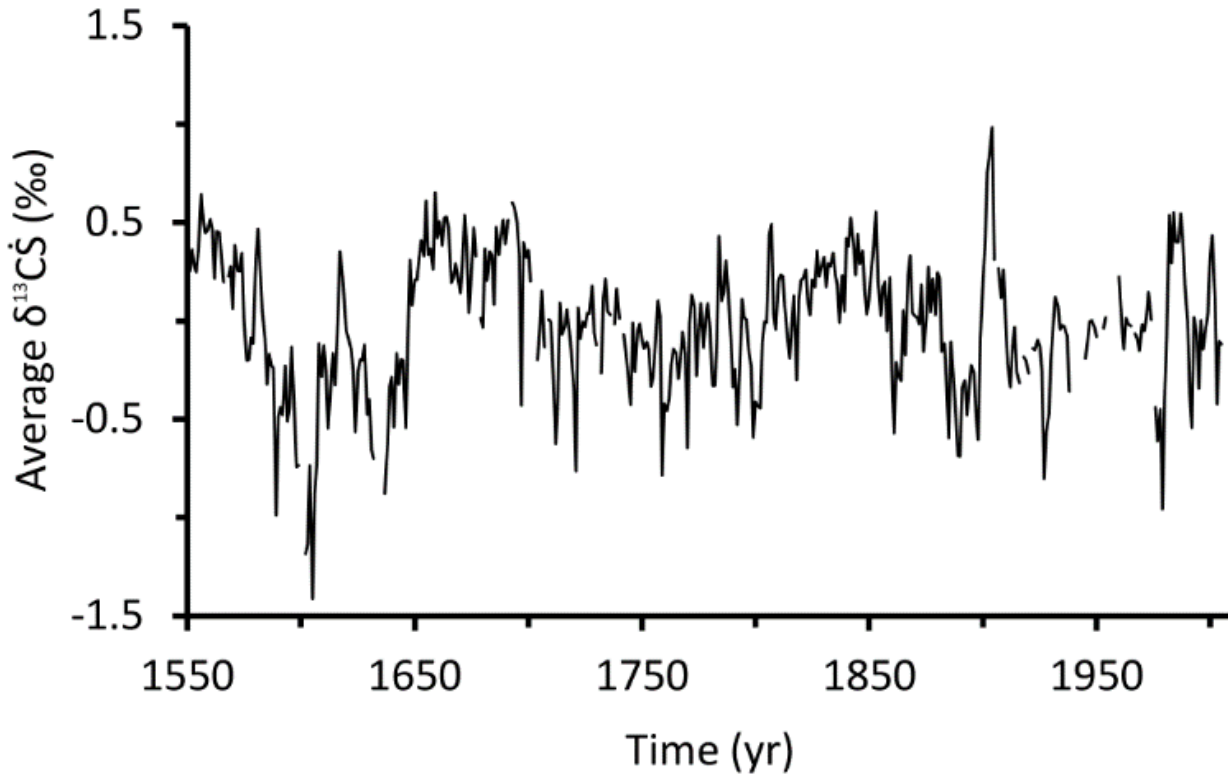
Figure 3.5 Weight-averaged $\delta^{13}C$ residuals from the oceanic Suess effect ($\delta^{13}C\dot{S}$).
The great majority of the uncertainties are smaller than the thickness of the line (not shown). $\delta^{13}C\dot{S}$ shows an average value of -0.04 ‰ with a standard deviation of 0.35 ‰. Extended intervals (≥ 4 yrs) with negative deviations greater than 1σ occur in the late 1500s to early 1600s, 1630s, and early and late 1800s. Extended intervals with positive deviations greater than 1σ occur in the 1550s, 1650s, late 1600s, 1840s, early 1900s and in the 1980s.

After subtraction of the Fourier regression from the individual shell $\delta^{13}C$, the residuals ($\delta^{13}C\dot{S}$) were weight-averaged (Figure 3.5). The resulting $\delta^{13}C\dot{S}$ series shows an average value of -0.04 ‰ with a standard deviation of 0.35 ‰.

3.4.3 $\delta^{13}C\dot{S}$-based maximum diatom abundance and herring recruitment estimates

We undertook two RMA linear regressions on the $\delta^{13}C\dot{S}$/MD data using the temporal intervals of 1962-1988 and 1988-2005 as cross calibration/verification (CCV) intervals. The same was done for the MD/HR and $\delta^{13}C\dot{S}$/HR pairs for the CCV intervals of 1959-1990/1991-2015 and 1960-1985/1985-2005, respectively. To obtain the highest correlations, MD was lagged by one year (i.e., $\delta^{13}C\dot{S}_{\tau\,=\,2000\,CE}$ was compared with $MD_{\tau\,=\,1999\,CE}$). We obtained the following equations:

$$MD_{\tau-1} = (0.4969 \pm 0.1021)\,\delta^{13}C\dot{S} + (5.540 \pm 0.0016) \tag{1}$$

$$MD_{\tau-1} = (0.5727 \pm 0.1024)\,\delta^{13}C\dot{S} + (5.546 \pm 0.0008) \tag{2}$$

$$HR = (1.253 \pm 0.2221)\,MD_{\tau-1} + (0.4119 \pm 1.565) \tag{3}$$

$$HR = (0.8934 \pm 0.1717)\,MD_{\tau-1} + (2.551 \pm 0.9031) \tag{4}$$

$$HR = (1.133 \pm 0.2228)\,\delta^{13}C\dot{S} + (7.386 \pm 0.0040) \tag{5}$$

$$HR = (0.6237 \pm 0.1193)\,\delta^{13}C\dot{S} + (7.493 \pm 0.0016) \tag{6}$$

HR and MD are log-transformed and all uncertainties in Equations 1-6 represent the standard error in slope and intercept. Table 1 summarises the equations' statistics and calibration intervals.

When applied to their respective verification intervals, Equations 1, 3 and 6 perform better than their counterparts, the linear-space standard deviation of residuals being 82.09 x 10^3 diatoms for Equation 1 and 183.62 x 10^3 diatoms for Equation 2, 16.85 x 10^9 recruits for Equation 3 and 17.65 x 10^9 recruits for Equation 4, and 19.34 x 10^9 recruits for Equation 5 and 16.50 x 10^9 recruits for Equation 6. The residuals from Equations 1, 3 and 6 also show the lowest levels of heteroscedasticity, given by the Breusch-Pagan score, meaning that they maintain a stable variability within their predictive range. However, by combining Equations 1 and 3 we derive an equation with lower residual heteroscedasticity, higher coefficient of determination and higher significance than those obtained from the equations derived from the RMA regressions:

$$HR = (0.6228 \pm 0.1690)\,\delta^{13}C\dot{S} + (7.356 \pm 1.991) \tag{7}$$

Equation 7 has a standard error of prediction of 11.60 x 10^9 recruits (equivalent to the standard deviation of residuals), the lowest of all the HR equations, calculated for the same calibration interval as for

Equation 6 (Figure 3.6a, Figure 3.6b). In the verification interval of 1960-1985, predictions made by Equation 7 fall within 24 x 10^9 recruits of the real value 62% of the time, compared to 57% for Equation 6.

Table 1. Summary statistics of Equations 1-7. Equation 7 is the result of substituting Equation 1 into Equation 3 and shows the highest coefficient of determination for herring recruitment, the smallest standard error of estimate and the residuals with the lowest heteroscedasticity.

Equation	Calibration interval	n	r^2	p_{Eq}	Standard error of estimate	Breusch-Pagan test on residuals	p_{BP}
1	1962-1988	18	0.3248	0.0135	163.0 x 10^{3} [†]	0.4703	0.4928
2	1988-2005	18	0.4888	0.0012	90.50 x 10^{3} [†]	1.044	0.3068
3	1959-1990	26	0.2461	0.0010	20.22 x 10^{9} [‡]	5.007	0.0252
4	1991-2015	26	0.0993	0.1168	15.02 x 10^{9} [‡]	12.86	0.0003
5	1960-1985	21	0.2650	0.0170	24.08 x 10^{9} [‡]	9.855	0.0017
6	1985-2005	21	0.3045	0.0095	12.62 x 10^{9} [‡]	0.6415	0.4232
7	-	41[§]	0.6242[§]	0.0013[§]	11.60 x 10^{9} [‡]	0.3486 [§]	0.5550

[†] Units: diatoms
[‡] Units: recruits
[§] Calculated for 1960-2005

As an independent verification of Equation 7, we used the scaled age-2 recruitment data from Burd (1978) for the northern North Sea (1919-1973). This comparison shows that Equation 7 overestimates the scaled recruitment by an average of 7.16 x 10^9 recruits (Figure 3.6b). The residuals, however, are normally distributed (W = 0.9865, p = 0.9135, JB = 0.0592, p = 0.9709) with a standard deviation of 5.80 x 10^9 recruits, well within the standard error of prediction.

In addition to the low recruitment levels during the early 2000s and the late 1970s, our reconstruction shows that there were five extended episodes (≥4 yr, interrupted by ≤2 yr) of low herring recruitment levels prior to the 20th century (1589-1607, 1629-1638, 1759-1762, 1799-1802, and 1885-1893). These were defined as values lower than the average 1551-2005 annual reconstructed recruitment (24.79 x 10^9 recruits) minus one standard deviation (13.02 x10^9 recruits). Similarly defined episodes of extended high recruitment levels occurred between 1552-1564, 1653-1665, 1681-1700, 1840-1847, 1901-1904, and 1982-1988. The average duration of the extended low recruitment episodes is 8.5 years and occur with an average periodicity of 69.2 years (this calculation includes the 1976-1980 episode). The average duration of extended high recruitment episodes is 10.8 years and occur with an average periodicity of 75.4 years.
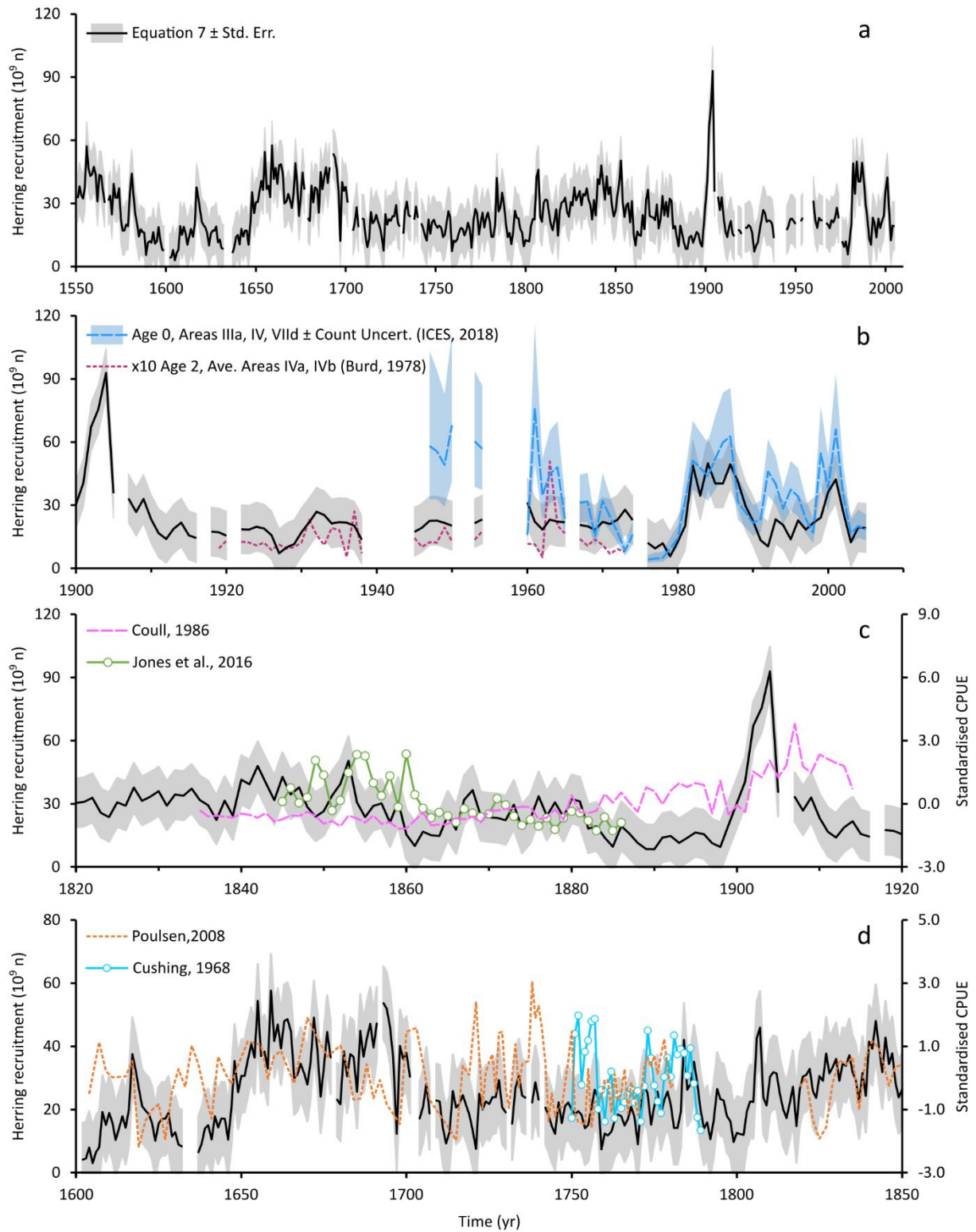
Figure 3.6 Reconstructed herring recruitment according to Equation 7.

Our reconstruction shows extended intervals of low recruitment from 1600-1650, most of the 1700s, 1860-1900 and most of the 1900s. (b) Reconstructed recruitment compared to instrumental recruitment for the 20th century. Measured recruitment data for time intervals when predicted data are not available has been omitted. The predictions made by Equation 7 lie within 24 x 10^9 recruits of the ICES, (2018) value 62% of the time. (c and d) Reconstructed recruitment compared to historical CPUE from the Scottish, English and Dutch fishing fleets.

3.4.4 Relationship to historical catch per unit effort

Our HR reconstruction shows positive correlations with the Dutch, English and Scottish CPUE standardised indices. When compared to the CPUE reconstruction of the Dutch herring fishing fleet, we find the strongest HR:CPUE correlation when the fishing occurs between one and three years after the herring recruitment (Figure 3.6c, Figure 3.7a). During the 17th century (1604-1698) the Dutch CPUE reconstruction has an average temporal resolution of 2.35 years and shows the weakest overall HR:CPUE correlation when analysed within ±5 years of recruitment (i.e., correlation analysis done by lagging the CPUE series five years before and five years after recruitment). The strongest correlation after recruitment occurs at a one year lag but does not show significance ($r = 0.23$, $p = 0.14$) while a significant HR:CPUE correlation is present when the fishing precedes the recruitment by 3 years ($r = 0.35$, $p = 0.03$). The 18th century CPUE data (1700-1781) has an average temporal resolution of 1.25 years and shows significant correlations with HR at lags between one year preceding recruitment and four years after, the most significant occurring two years after recruitment ($r = 0.47$, $p = 7.8 \times 10^{-5}$). The 19th century Dutch CPUE data, representing the years 1820-1855 at a two-year resolution, shows the strongest correlation to our HR reconstruction when fishing occurs one and three years after recruitment ($r = 0.47$, $p = 0.04$ and $r = 0.48$, $p = 0.04$).

A similar pattern arises when comparing our reconstruction to the English CPUE from Lowestoft (Figure 3.6d, Figure 3.7b). The Lowestoft CPUE has annual resolution from 1750-1789 and does not show significant correlation with HR within ±5 years of recruitment. If we expand the window to include year 6 after recruitment, however, we find a significant HR:CPUE correlation of 0.31 ($p = 0.049$).

The pattern of positive HR:CPUE correlations is also present in the Scottish fisheries (Figure 3.6c, Figure 3.7b). We found significant positive correlations with the southeast Scotland CPUE (Jones et al., 2016) for the years 1845-1871 (annual resolution) and our reconstruction at lags between one and four years after recruitment has taken place, the most significant occurring two years after recruitment ($r = 0.50$, $p = 0.0008$). The relationship is weaker but still significant when comparing against the CPUE derived from the Peterhead District for the years 1835-1914 (annual resolution, Coull, 1986), where we find significant correlations to our HR reconstruction when fishing occurs three and four years after recruitment ($r = 0.29$, $p = 0.009$ and $r = 0.24$, $p = 0.03$). If the Peterhead data are divided into two segments (1835-1870 and 1871-1914) and the correlation analysis is repeated, we find a significant correlation with our HR reconstruction when fishing occurs three years after recruitment ($r = 0.36$, $p = 0.04$) for the first segment. Similarly, a significant correlation when fishing occurs between two and five years after recruitment has taken place in the second segment, the most significant occurring three years after recruitment ($r = 0.57$, $p = 0.0001$).
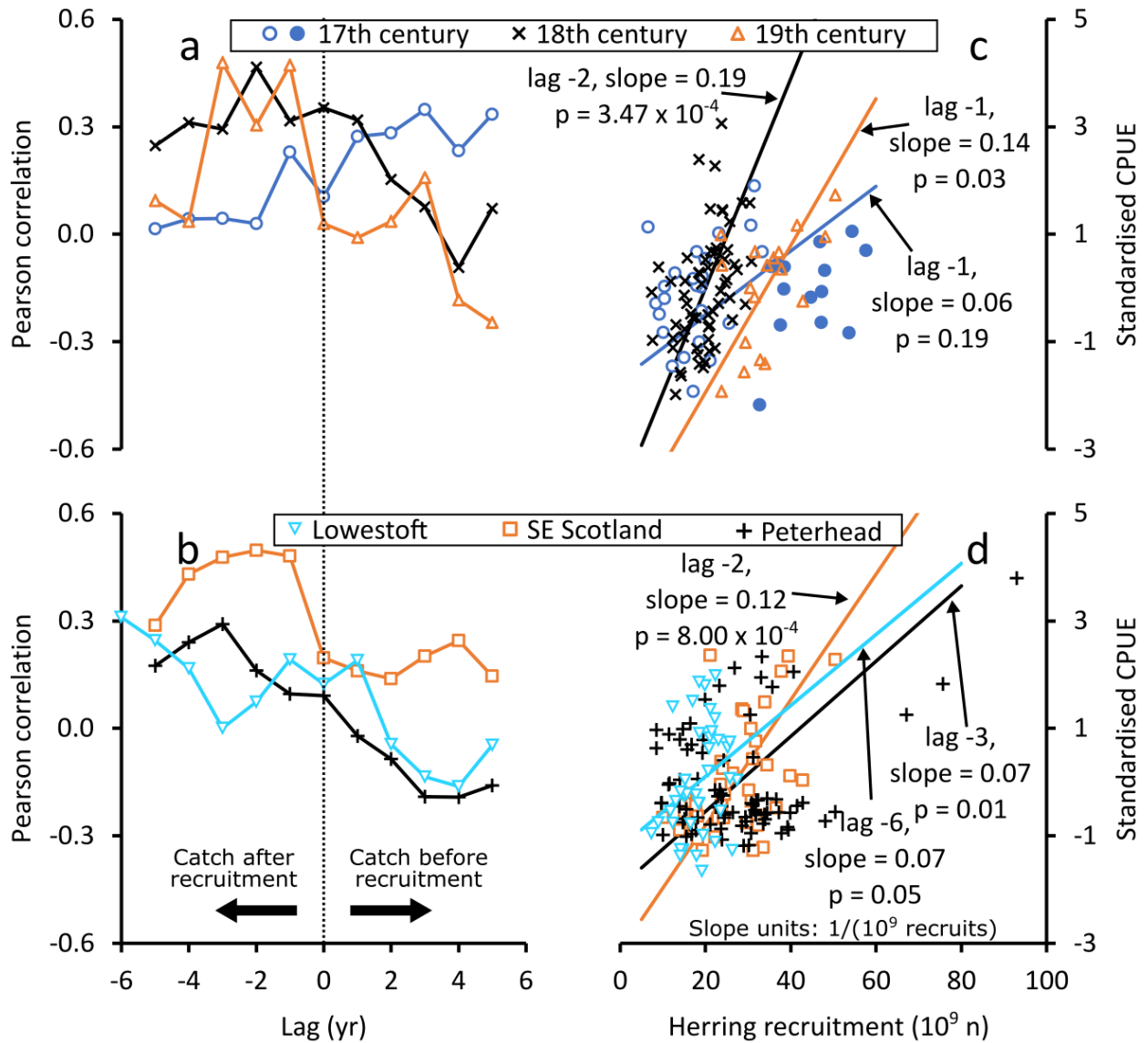
Figure 3.7 Relation between the reconstructed herring recruitment and CPUE from the Dutch (a), east English and east Scottish fishing fleets (b) at different lags before and after the year of recruitment.

There is a general indication that the strongest HR:CPUE correlation occurs between one and three years after recruitment. The strength of the HR and Dutch CPUE relationship varies according to the century, the weakest being in the 17th century, coincident with the Anglo-Dutch wars in the second part of the century (filled circles in c). HR is more strongly related to the SE Scottish CPUE (1845-1871) two years after recruitment has occurred while the relationship is stronger with the English CPUE six years after recruitment. The relationship is not as strong with the Peterhead District CPUE. This may be due to the amalgamation of the data before and after the introduction of cotton nets in the 1860s and decked fifie ships in 1870 (see text for details). The scatter plots in c and d show the CPUE data that has the strongest correlation after lagging.

3.5 DISCUSSION

3.5.1 Interpretation of chronology statistics

The newly added extension to the FGB chronology (1545-1754) shows lower $\bar{r}$ and EPS scores than those shown in the original Butler et al. (2009a) version (1755-2003). This may be due to the relatively lower sample depth (the number of shells available in the chronology) compared to the 1755-2003 interval. The near-zero $\bar{r}$ and EPS scores during the 1751-1763 in the new chronology are most likely due to the erratic growth during the juvenile years of the four specimens that settled during this time combined with the lower-than-average growth of the other two shells that cover the interval. This problem is sometimes circumvented by disregarding the first 20-30 years of growth when constructing *A. islandica* chronologies (Butler et al., 2010, 2009a), but the exclusion of juvenile years in this study would have meant a chronology with shorter temporal coverage and a rather long interval where the chronology would have been represented by only two shells (1728-1780).

Another possible explanation of the lower $\bar{r}$ and EPS scores in the 1545-1754 interval is error in growth increment counting (Black et al., 2016). However, the growth indices in this interval are not significantly smoother than those during the later interval when the EPS scores surpass the 0.85 threshold, as indicated by the F-test on the year-to-year differences. Black et al. (2016) showed that a chronology with a 5% rate of error in increment counting would be significantly smoother than one that has been correctly cross-matched. The same study, however, shows that a 1% error rate can induce great variability in the EPS score while still maintaining high levels of coherence with environmental signals. The F-test on our results implies that our newly extended chronology has an increment counting error lower than 5%, which allows us to confidently base our stable isotopic results on the age model provided by FGB.

3.5.2 Nutritional link between stable isotopic signal and abundance estimates

In 2012 Beirne et al. showed that $\delta^{13}C$ variability in the shell of the ocean quahog is controlled by $\delta^{13}C_{DIC}$ variability in the water column, itself being partly controlled by primary production. Equation 1 is used to reconstruct the maximum diatom abundance because, as primary production increases (during the spring diatom bloom, for example), ^{12}C is preferentially incorporated into the blooming biomass, leaving the ambient water enriched in ^{13}C (Gruber et al., 1999). The likely reason for the one-year lag in the maximum $\delta^{13}C\dot{S}$:MD correlation is the timing of the phytoplankton bloom and the onset of the water column stratification at the Fladen Ground. CPR data from the northern North Sea (Johns, 2016) indicates that the

56

MD occurs on average (1958-2015) late in April and is closely followed by the onset of thermal stratification (van Leeuwen et al., 2015; Warrach, 1998). The ocean quahog community at the Fladen Ground is, therefore, disconnected from the phytoplankton bloom for most of its growing season (February to August, see Schöne et al., 2005c) and only has access to the ^{12}C-depleted DIC from the previous year.

Similarly, the reconstruction of herring recruitment using Equation 3 depends on how well it can represent food availability for the fish. Capuzzo et al. (2018) showed that a decline in primary production in the North Sea for the years 1988-2013 produced a knock-on effect on higher trophic levels, indicating a bottom-up control of the local ecosystem. In their study, Capuzzo et al. (2018) found that the 25-year decline in primary production caused a decline in small copepod abundances which, in turn, caused a decline in fish recruitment in seven commercially-important fish stocks in the North Sea. The correlation (r = 0.45) between primary production and fish recruitment index observed by Capuzzo et al. (2018) is similar to that which we found between MD and HR (r = 0.50, Equation 3). The slightly stronger covariance is not surprising as small copepods show a preference for consuming diatoms (Frederiksen et al., 2006; Irigoien et al., 2002, 2000) while constituting a staple of North Sea herring diet (Last, 1989; Segers et al., 2007).

The HR:δ^{13}C$\dot{S}$ relationship shown in Equation 6 is more subtle. According to Kürten et al. (2013), North Sea copepods from the North Dogger Bank occupy higher relative trophic levels in February than during the rest of the year. The higher trophic position of the copepods corresponds to higher overall somatic δ^{13}C as they consume ^{12}C-depleted phospholipid-derived fatty acids. The small copepods are then preyed upon by juvenile herring (Last, 1989), also in February (Segers et al., 2007). As the food is being digested, high-magnesium carbonates with relatively high δ^{13}C values are precipitated within the fish intestine, later to be excreted in mucus-coated tubes and faecal pellets (Jennings and Wilson, 2009). These excretions fall though the water column while being rapidly degraded by zooplankton and bacteria (Hansen and Bech, 1996; Lampitt et al., 1990) and the high-Mg CaCO$_3$ precipitates contained within the excretions dissolves as they reach the benthos (Viitasalo et al., 1999; Woosley et al., 2012). This dissolved carbonate would change the overall local δ^{13}C$_{DIC}$ which would, in turn, be reflected in the ocean quahog's shell (Beirne et al., 2012). Most of this heavy high-Mg CaCO$_3$ will be precipitated in the intestines of age-0 to age-1 recruits when the fishing mortality rates are ~6% or higher, assuming a constant natural mortality rate of ~27% (Jennings and Wilson, 2009; Ricker, 1975).

By combining Equations 1 and 3 into Equation 7 we are explicitly including the diatom-mediated nutritional link between HR and δ^{13}C$\dot{S}$. Equation 7 is therefore to be preferred over Equation 6, which expresses a purely statistical relationship.

3.5.3   Dutch, English and Scottish herring industry in the context of recruitment variability

Our herring recruitment reconstruction (Figure 3.6a) is supported by a variety of historical records derived from different sources that cover different geographical extensions. The decline in recruitment observed from the second half of the 16th century until the beginning of the 17th century coincides with a decline in salted herring exports from east Scotland that began in 1541 at an average rate of -7.6 x10³ kg yr⁻¹ (Rorke, 2005, 2001). An apparent recruitment failure in the early 17th century is reflected in the Scottish herring exports to Sweden as the export per ship declined from 19.0 x 10³ kg in 1592 to 5.8 x 10³ kg in 1604 (Dow, 1969). No Scottish fish exports to Sweden were made in 1605-06 and the exports remained infrequent until 1616 (Dow, 1969), the year which, according to our reconstruction, the recruitment is fully stabilised and on a positive trend.

ICES (2018) data shows that, for the second part of the 20th century, there is a strong and significant correlation between recruitment and catch, especially when the catch occurs four years after recruitment has taken place ($r = 0.68$, $p << 0.01$). Thus, a general positive correlation between historical CPUE and reconstructed HR was expected. However, using the CPUE model defined in section 2.7 assumes a linear relation between catch and fish abundance which may not always be correct (Erisman et al., 2011; Harley et al., 2001). This is due to hyperstability, the tendency of CPUE remaining elevated as stock declines due to the schooling behaviour of fish. Hyperstability can be observed in overexploited stocks. Nevertheless, the historical data presented here comes from intervals when overexploitation of the complete North Sea herring stock was unlikely, and it is the only assessment tool available.

The change in the strength and significance of the Dutch CPUE:HR correlation is revealing when examining the historical catches within the biological context. For example, the Dutch CPUE:HR correlation is at its lowest during the 17th century. During this time, the Dutch fishing season started in June and lasted until January and the fishing fleet distributed its effort between Shetland, Scotland and Northern England from June to September while the rest of the season the fleet went south to the Dogger Bank, East Anglia and the English Channel (Poulsen, 2008). The apparent early 17th century recruitment failure, combined with the Anglo-Dutch wars in the second half of the 17th century, might have forced the Dutch fleet to spend more time fishing further south which would have caused a decoupling between recruitment in the northern North Sea and the fisheries records.

We observe a stronger CPUE:HR coupling in the 18th century when the fishing occurs two years after recruitment. As the Dutch fleet regained access to the Fladen Ground, the fishing season lasted from June to November and the Dutch spent the first two-thirds of the season in the northern North Sea between

Shetland, Scotland and northern England when they would land the majority of the fish for the season (Poulsen, 2008).

In the 19th century we observe the highest CPUE:HR correlation for our record for the Dutch fishing fleet (Poulsen, 2008). The strengthening of the correlation with the Dutch CPUE is likely related to the fishing patterns adopted in the 1800s. As was the case in the 18th century, the fishing season lasted from June to November and the fleet would spend its time between Shetland, Scotland and northern England and would not head much further south than the Dogger Bank. The fleet would dedicate the second half of the season to fishing in Scottish waters, with the months of October and November being spent in the Fladen Ground (Poulsen, 2008).

The case of the Lowestoft herring fishery CPUE stands out as the only one without a significant correlation with HR within ±5years of recruitment. As with the case of the Dutch fishery, this can be explained by the fishing practices adopted in Lowestoft. Here the fishing season was shorter than in the Dutch Republic, going from the 29th of September (Michelmas Day) to the 22nd of November (Martinmas Day) and the fishermen would stay within 70 km of the coast (Cushing, 1968). Cushing (1968) suggest that if the fish behaved in the 1700s as they did in the first half of the 20th century then the average age of capture was between five and eight years. The 6-year lag after recruitment required to obtain significance between our HR reconstruction and CPUE is in good agreement with this assumption.

The weaker Peterhead CPUE:HR correlation is most likely due to the definition of "effort" as the number of fishing boats at a given time when we calculated the Peterhead CPUE. This definition fails to consider the improvements in technology through time, such as the introduction of the decked fifie ships in the 1870s (Smylie, 1999) which were capable of going into open waters (Jenkins, 1913) and the adoption of cotton nets in the 1860s (Coull, 1986). Having to divide the record in segments before and after these technological improvements to obtain stronger correlations highlights the importance of the "effort" definition when working with CPUE data.

Jones et al. (2016) argues that the observed significant decline in standardised CPUE for the SE Scottish fleet at a rate of -0.057 yr^{-1} (p = 5.30 x 10^{-7}) in the years 1845-86 was due to over-exploitation of the fishery. Overexploitation by the SE Scottish fleet is rather unlikely, as the localised nature of fishing activities in Scotland (Harris, 2000; Jones et al., 2016) would have a limited effect on the herring stock as a whole. The similar significant decline in standardised CPUE observed in Peterhead (Coull, 1986) from 1835-70 (-0.051 yr^{-1}, p = 1.52 x 10^{-3}) strongly indicates a common cause rather than two local phenomena, especially because the North Sea herring are considered a unit-stock (Mariani et al., 2005). Our reconstruction, which shows a

decline in recruitment that lasted most of the second half of the 19th century, provides a plausible explanation for these two local negative trends. These results further suggest that declines in recruitment are not caused by fishing mortality in an under-exploited fish stock.

3.6 CONCLUSIONS

In this study we developed an absolutely-dated 455-year long carbon stable isotope series from the shells of the ocean quahog. This series is currently the longest in temporal extension for the region and it suggests that the onset of the oSE occurred in the early 1850s. By subtracting the oSE from the series we emphasised the high frequency variability in $\delta^{13}C$ ($\delta^{13}C\dot{S}$) and calculated a significant regression line between $\delta^{13}C\dot{S}$ and diatom abundance in the North Sea. The two quantities in this regression line are linked by the effect of phytoplankton primary production on $\delta^{13}C_{DIC}$. We used this regression to build an equation mediated by a nutritional link (diatom abundance) that allowed us to reconstruct herring recruitment in the North Sea using $\delta^{13}C\dot{S}$. Our reconstruction is supported by independent recruitment estimates, by historical CPUE documentation from the Netherlands, England and Scotland and by east Scotland fish exports.

Our work provides the longer time scale needed to understand the interaction between climatic parameters and stock densities. It also demonstrates that molluscan sclerochronological records can contribute to the study of the ecosystem functioning to which the socioeconomical stability of the countries surrounding the North Sea is ultimately tied.

3.7 SUPPLEMENTARY MATERIAL

3.7.1 Criteria for shell selection for ^{14}C dating

The shells were selected based on size (assuming that larger shells belonged to longer-lived animals, see Butler et al., 2009a; Kilada et al., 2007), and taphonomic characteristics that suggested the specimens were alive during the last millennium (Nielsen, 2004).

3.7.2 Subsample signal strength

The SSS mirrors the EPS for the complete duration of the record but it is shifted toward more positive values and never crosses the zero-line (Figure 3.8). For the interval 1545-1751, the average SSS is 0.74 (compared to average EPS of 0.67). In the interval 1752-1763 the average SSS is 0.36 whereas the average

EPS is 0.02. For the interval of the chronology mostly developed by Butler et al. (2009a) (1764-2003) the average SSS is 0.95 and the average EPS is 0.91.
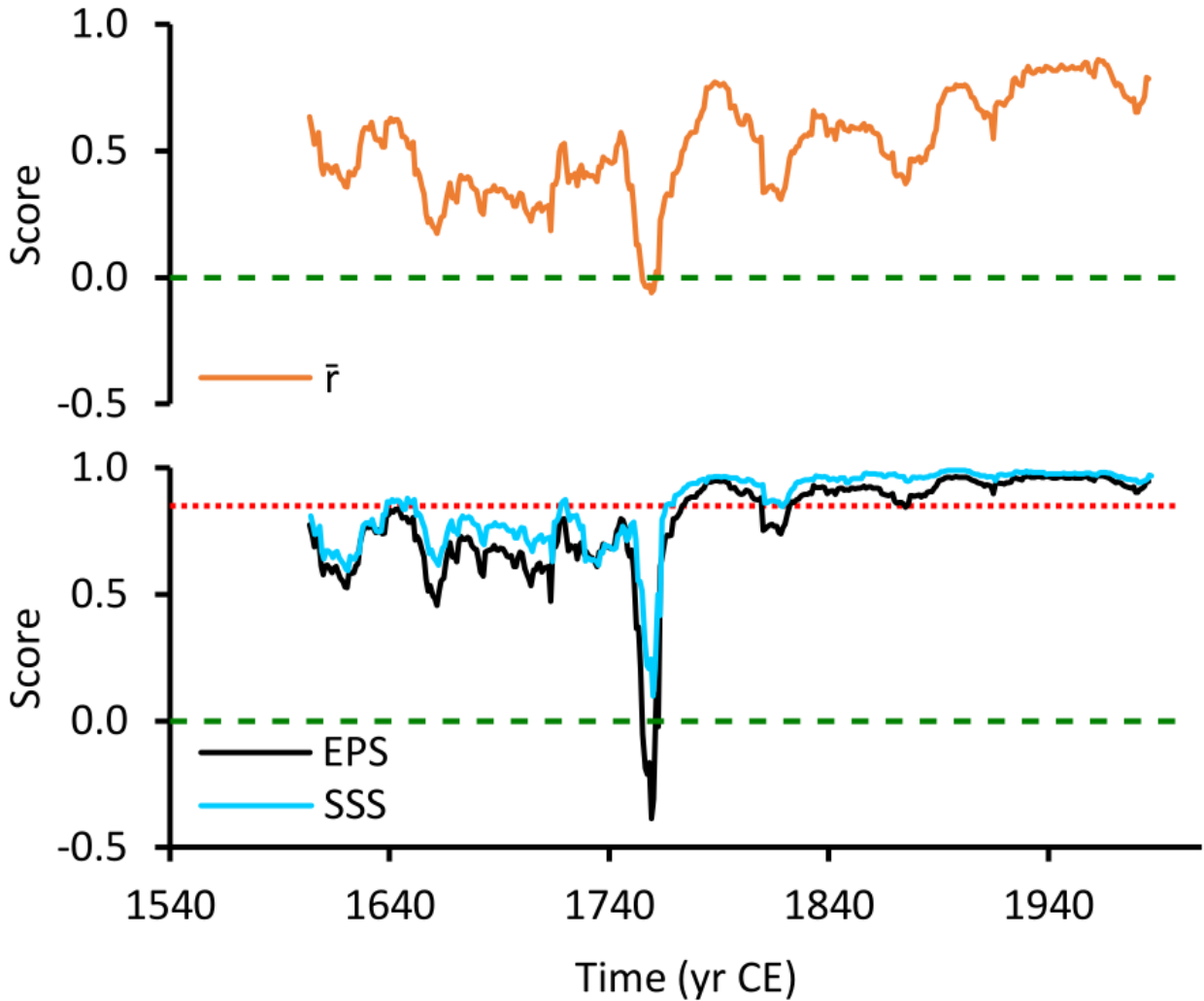
Figure 3.8 Subsample signal strength in relation to r̄ and expressed population signal.
The SSS mirrors the EPS for the complete duration of the calculation but it is shifted towards more positive values and it never becomes negative.

The reason that the SSS never reaches negative values lies on its mathematical definition (Section 2.6). Solving the SSS equation for r̄ shows that for a chronology composed of 14 shells an r̄ value of -0.077 is necessary to obtain an SSS of zero.

One must remember that the r̄, SSS and EPS scores do not offer much information about the correctness of the crossmatching exercise (Buras, 2017; Cook and Pederson, 2011). This is not to say that they offer no value. Buras (2017) concludes that the SSS should be used to estimate the loss of explanatory power of a transfer function based off the increment width chronology. This is not the case for this work as the FGB chronology is used exclusively as a stratigraphic template on which to base geochemical results. If a relation between the growth increment widths and $\delta^{13}C$ (or $\delta^{18}O$, see next two Chapters) was to be

61

established, then SSS could be used to scale the uncertainty of any environmental interpretation made with the $\delta^{13}C$ values. Such relation, however, does not seem to exist (Reynolds et al., 2017a; Schöne et al., 2005a).

3.7.3 Testing normality of measured diatom and recruitment data for calibration

We tested the normality of the maximum diatom abundance (MD) for the northern North Sea (Johns, 2016) and age-0 herring recruitment (HR) (ICES, 2018) in linear and log space for the temporal intervals of 1958-2015 and 1947-2017, respectively, using the Shapiro-Wilk W and the Jarque-Bera JB scores (Adefisoye et al., 2016). A normal distribution of the independent variable is an assumption of linear regressions. The data type (linear or log-transformed) that showed the highest scores for normality after justified removal of outliers (three, see below) were used for the calibration analysis.

Table S1. Summary statistics of the northern North Sea maximum diatom count and the herring recruitment. Both quantities show a strong normal distribution around the geometric mean after logarithmic transformation.

Parameter	Max. diatoms	Herring recruitment
Temporal coverage	1958-2016	1947-2017
Min (n)	85.00×10^3	49.55×10^9
Max (n)	12.75×10^3	92.52×10^9
Mean (n)	41.61×10^3	35.64×10^9
Stand. dev. (n)	22.42×10^3	18.07×10^9
Skewness	1.58	0.70
Kurtosis	3.57	0.20
Geom. mean (n)	36.52×10^3	30.96×10^9
Geom. stand. dev. factor	46.67	45.80

Linear MD shows a W score of 0.88 (p = 4.98×10^{-5}) and a JB score of 47.11 (p = 5.90×10^{-11}), failing both normality tests. Alternatively, the log-transformed MD shows a W score of 0.99 (p = 0.89) and a JB score of 0.84 (p = 0.66), suggesting a strong normal distribution. Similarly, linear HR after removal of the three lowest values (corresponding to the years 1975, 1976 and 1977, the years of lowest recruitment during the North Sea herring stock collapse of the 70s) shows a W score of 0.96 (p = 0.02) and a JB score of 5.17 (p = 0.08), passing only the Jarque-Bera normality test. The log-transformed HR data, excluding the aforementioned three years, shows a W score of 0.98 (p = 0.41) and a JB score of 1.63 (p = 0.44), showing a stronger normal distribution. Table S1 shows the summary statistics for the non-transformed instrumental data. The normal distribution of the log-transformed data occurs around the geometric mean values.

3.7.4 Oceanic Suess effect Fourier regression

$$f(t) = a0 + a1*cos(t*w) + b1*sin(t*w) + a2*cos(2*t*w) + b2*sin(2*t*w)$$

Where t represents time in years from 1551 to 2005

Coefficients (with 95% confidence bounds):
a0 =   2.144 (2.104, 2.184)
a1 =   0.6744 (0.6023, 0.7465)
b1 =   0.02685 (-0.6453, 0.699)
a2 =   -0.2644 (-0.945, 0.4162)
b2 =   -0.3463 (-0.9057, 0.213)
w =   0.01125 (0.01068, 0.01182)

Goodness of fit:
R-square: 0.7114
Adjusted R-square: 0.7084

4. ANALYSIS OF THE PERSISTENCE OF SEASONAL STRATIFICATION IN THE NORTHERN NORTH SEA USING A BOTTOM WATER TEMPERATURE RECONSTRUCTION OF THE LAST 455 YEARS

Juan Estrella-Martínez[1], Bernd R. Schöne[2], James D. Scourse[3], and Paul G. Butler[3]

[1]School of Ocean Sciences, Bangor University, Bangor, Wales, UK.

[2]Institute of Geosciences, Johannes Guttenberg University, Mainz, Germany.

[3]College of Life and Environmental Sciences, University of Exeter, Penryn, Cornwall, UK.

4.1 ABSTRACT

The development of seasonal stratification in epicontinental seas is a first-order hydrographic phenomenon with physical, biological, biogeochemical and geological impacts. Instrumental series of stratification dynamics are of very high resolution but they are limited to the very recent past. Millennial-length records, on the other hand, lack the temporal resolution required to assess the seasonal persistence of stratification under the influence of high frequency atmospheric forcings. Here we present a c.500-year, annually-resolved, absolutely-dated bottom water temperature (BWT) reconstruction derived from stable oxygen isotope geochemistry from *Arctica islandica* shells ($\delta^{18}O_{shell}$) collected at the Fladen Ground (FG, northern North Sea). Increments micromilled at annual resolution yielded a $\delta^{18}O_{shell}$ record for the interval 1551-2004 CE. Sub-annual sampling suggests that the average growing season at FG covers February to October. The reconstruction shows an average temperature of 7.20 °C for the past c. 500 years, with warming trends of 0.05 ± 0.02 °C decade^{-1} for the years 1640-1740 and 0.08 ± 0.02 °C decade^{-1} for the years 1880-2001, and a cooling trend of -0.11 ± 0.02 °C decade^{-1} for the years 1810-1910. These trends cannot be attributed to North Atlantic sea surface temperature (SST) trends. Between 9 and 54 % of variability in average Feb-Oct BWT can be explained by low frequency changes in the winter North Atlantic Oscillation (NAO). Higher frequency NAO variability does not show a consistent effect for any season. A BWT/SST regression analysis suggests that thermal stratification in the northern North Sea is susceptible only to local storm activity.

4.2 INTRODUCTION

Temperature variability in the North Atlantic exerts a major influence on the regulation of European climate. The north-eastward transport of warm water from the subtropical ocean by the North Atlantic Current and the subsequent loss of heat to the atmosphere in the mid- and high-latitude North Atlantic is well understood while analysis of instrumental observations demonstrates the key role of North Atlantic atmospheric dynamics in controlling regional climate over Europe. Such observations inform global and regional climate models, improving their forecasting skill and ability to estimate the potential impacts of human activity on climate and vice versa. However, attribution of climatic variability caused by external forcing (including anthropogenic forcing) and internal unforced variability requires understanding of the full range of time scales and periodicities represented in the climate system. Currently there is a lack of temporally highly resolved data that extend back before the start of any major anthropogenic influence.

While many seawater temperature reconstructions for the North Atlantic region are of multicentennial or multimillennial-length (Hald et al., 2011; Kabel et al., 2012; Klitgaard-Kristensen et al., 2001; Miettinen et al., 2012, 2011; Reynolds et al., 2017b, 2016), only a few have sufficient temporal resolution for the reliable analysis of high-frequency modes of variability such as the North Atlantic Oscillation. Fewer still represent bottom water conditions for regions that are characterised by seasonal stratification (Austin and Scourse, 1997; Schöne et al., 2005c; Scourse et al., 2002).

In epicontinental seas such as the North Sea, water temperature is mainly determined by vertical heat exchange with the atmosphere (Otto et al., 1990). In these regions, the development of thermally-stratified conditions in mid-spring and summer controls vertical exchange processes in the water column. It limits nutrient flow to the benthos and modulates the effects of atmospheric variability on bottom waters. The sensitivity of stratification to atmospheric forcings, however, remains poorly constrained. Understanding the variability and strength of thermal stratification is not only beneficial for climate modelling but also provides a more detailed physical baseline on which to base ecological and fisheries assessments (Corten, 2001; Sims et al., 2001; van Leeuwen et al., 2015).

In this study we present an annually-resolved bottom water temperature reconstruction for the time interval from 1551 to 2004 CE (hereafter all references to years assume years CE) based on the stable oxygen isotope geochemistry of shells of *Arctica islandica* from the Fladen Ground, northern North Sea. The use of $\delta^{18}O$ values from the shell of *A. islandica* for the reconstruction of seawater temperatures is already established for a range of sites around the North Atlantic Ocean (Mette et al., 2016; Reynolds et al., 2016; Schöne et al., 2005a; Weidman et al., 1994) and the North Sea (Schöne et al., 2004, 2005c; Witbaard et al., 1994). Robust growth chronologies can be built from the annual increments in the *A. islandica* shell (Butler et al., 2009a, 2010, 2013; Estrella-Martínez et al., 2019; Schöne et al., 2003; Scourse et al., 2006a; Thompson et al., 1980; Witbaard, 1996), providing an accurate and precise age model for the isotope results.

4.3 MATERIALS AND METHODS

4.3.1 Shell collection and processing

The *A. islandica* shells used in this research were collected from the Fladen Ground in the northern North Sea at coordinates 58.994° N, 0.291° E, at a mean depth of 123 metres (Figure 4.1). The collection was acquired during a cruise of the RV *Prince Madog* in 2004. Sampling was carried out using a custom-made dredge designed for the collection of bivalves of a wide array of sizes.
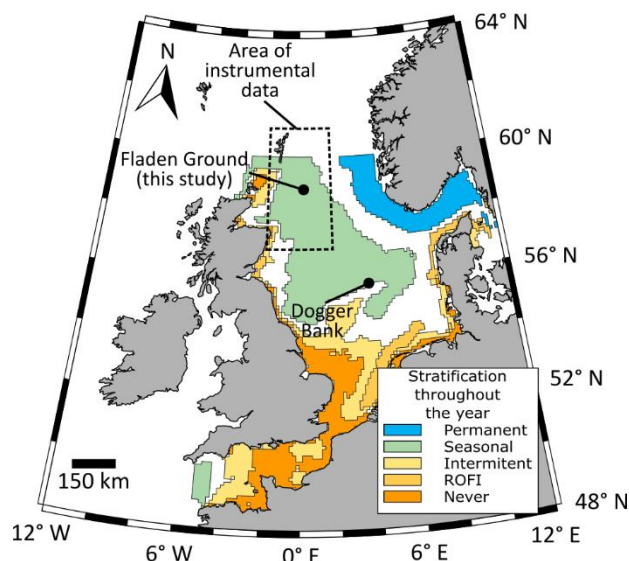
Figure 4.1 Approximate location of sites mentioned in this work.
The map shows the dominant stratification regimes in the North Sea (van Leeuwen et al., 2015). ROFI = Region of freshwater influence.

The shells were pre-processed on board and in the laboratory as described by Scourse et al. (2006). We used a total of 16 shells, being a combination of seven live-collected specimens and nine valves from dead specimens (empty articulated valves or single valves described in Butler et al., 2009a and Estrella-Martínez et al., 2019). Once cleaned, the shells were sectioned and acetate peel replicas were produced using standard procedures (Butler et al., 2009a; Ropes, 1984; Scourse et al., 2006a). The peels were examined under transmitted light, and the imaging software package ImagePro Premier 9.1 was used to identify and measure the growth increment widths in the outer shell layer of the hinge and ventral margin.

4.3.2   Absolute age model

Our age model is based on an *A. islandica* standardised growth increment chronology from the Fladen Ground, Site B (FGB) originally described in Butler et al. (2009a) and extended by Estrella-Martínez et al. (2019). FGB was selected as in its original version it was the longest of the five Fladen ground chronologies presented in Butler et al. (2009a), and because a substantial number of shells from that site had already been radiocarbon-dated. The chronology was constructed and extended by crossmatching fourteen of the specimens mentioned above using the visual crossmatching programme SHELLCORR (Scourse et al., 2006a) and the standard dendrochronology software package ARSTAN (Cook and Krusic, 2014). Two juvenile (age <30 yr), live-collected specimens were not crossmatched to FGB, but were independently dated by counting increments. Estrella-Martínez et al. (2019) estimated an increment counting error lower than 5%.

As an added test to FGB, we employed the Baillie-Pilcher t-value method (Baillie and Pilcher, 1973) to determine the likelihood of obtaining spurious crossmatches between shells. This allows the assessment of temporal uncertainties in the chronologies. With this method, the correlation between pairs of shell indices

is evaluated with a student t-test with N-2 degrees of freedom, where N is the number of overlapping years. A p-value is then calculated to determine the chances of getting the obtained correlation by chance. The correlation exercise was carried out using the power-transformed, detrended growth indices from every shell.

4.3.3   Micromilling and stable isotope analysis

Micromilling was carried out on the repolished sections of eight specimens used in the FGB chronology at the School of Ocean Sciences, Bangor University, using a computerised New Wave/Elemental Scientific micromill fitted with a tungsten carbide dental burr with a spherical tip of 300 μm diameter. These were selected for isotope analyses at annual resolution for the interval from 1551 to 1980 based on their individual temporal coverage, and their taphonomic state and size (Estrella-Martínez et al., 2019). The milling strategy was devised to allow a target temporal overlap of at least 10 years between shell pairs. Material for the interval from 1976 to 2004 was micromilled at annual resolution from the two juvenile live-collected specimens described above. One of these was selected for additional sampling at sub-annual resolution for the years 1979-2002 to aid in the determination of the *A. islandica* growing season at the Fladen Ground.

The annual-resolution micromilling strategy employed in this study was described by Estrella-Martínez et al. (2019): Micromilling was performed at the ventral margin of each shell after internal crossmatching i.e., increments found on the ventral margin were crossmatched with those found on the hinge of the same shell. The entirety of the increments sampled at annual resolution were milled between the growth lines to an average depth of 100 μm. A similar strategy was followed for the specimen sampled at sub-annual resolution. Each increment was sub-divided into sectors of approximately equal areas prior to micromilling. Each of these sectors was then milled to an average depth of 800 μm. The area of each sector represented, on average, 11% of the total area of a given increment.

All powder extracted from a given increment/sector was thoroughly homogenised before an aliquot of the sample was isotopically characterised with a Thermo Fisher MAT 253 continuous-flow isotope ratio mass spectrometer equipped with a GasBench II at the Institute of Geosciences, University of Mainz (Germany) following methods described in Colonese et al. (2017) and Estrella-Martínez et al. (2019). The 1σ external reproducibility (accuracy) based on 421 blindly measured NBS-19 samples was better than 0.04 ‰ and 0.03 ‰ for $\delta^{18}O$ and $\delta^{13}C$, respectively. The average internal precision error of the samples (computed from eight injections per analysis) was better than 0.06 ‰ for $\delta^{18}O$ and 0.04 ‰ for $\delta^{13}C$. Both isotope values are reported in per mil deviations relative to the Vienna Pee Dee Belemnite (VPDB) standard. No correction for different acid fractionation factors of shell samples (aragonite) and the reference material (calcite) was applied (Füllenbach et al., 2015).

We inspected the results against the average peak intensity given by the mass spectrometer and rejected those with showed abnormally high/low isotope values and those with intensities falling significantly outside the range of the reference materials.

4.3.4   Determination of increment growth timing using instrumental data

Instrumental temperature and salinity from 1947 to 2010 of the water between 0 and 135 m depth were extracted from the ICES CTD and bottle data database (available at http://ocean.ices.dk/HydChem/HydChem.aspx; last checked: 11-Dec-2017; ICES, 2014) from a 2° latitude by 2° longitude grid box centred at the collection site (Figure 4.1). The available data for the depths between 70 and 135 metres were integrated and averaged to monthly resolution. This integrated depth was selected because it shows temperatures and salinities through time that suggest consistently mixed conditions.

The missing data were interpolated in five-year intervals. This was done by "sandwiching" the interval of interest between data of the five years prior and five years after said segment starting with 1950-1955. Then an 8-term Fourier regression was calculated using the complete 15-year interval and used to interpolate the missing data. The temperature of months when the value was replicated by less than the average monthly replicate of the 15-year interval minus 25% of the replicate standard deviation ($N_{month} < N_{15\text{-year}} - 0.75*\sigma[N_{15\text{-year}}]$) was replaced by the value predicted by the Fourier interpolation. The replicate number for the interpolated months was assigned as $N_{month} = N_{15\text{-year}} - 0.75*\sigma[N_{15\text{-year}}]$. We selected the 75% factor in the standard deviation to obtain a higher threshold in the number of replicates required to represent a given month.

To model realistic uncertainties for the averaged temperature data, first the monthly standard deviation for the years 1986-2010 was calculated prior to the interpolation exercise ($\sigma[T_{month, 1986\text{-}2010}]$). This segment was selected because it had the least amount of missing data and the average monthly temperature was commonly represented by more than 30 replicates. Then $\sigma[T_{month, 1986\text{-}2010}]$ was assigned for every month starting in January 1950. Finally, the uncertainty for a given month was obtained by multiplying $\sigma[T_{month, 1986\text{-}2010}]$ by a factor F calculated as $F = -0.178*\ln(N_{month}) + 1.695$. This has the effect of multiplying $\sigma[T_{month, 1986\text{-}2010}]$ by 1.5 when N_{month} is 3 and by 1 when N_{month} is 50.

We converted the interpolated monthly 70 – 135 m salinity into $\delta^{18}O_{water}$ (Harwood et al., 2008) and solved an updated version of the classical palaeotemperature equation (Grossman and Ku, 1986) for $\delta^{18}O_{aragonite}$ to compute a theoretical or "synthetic" $\delta^{18}O$ ($\delta^{18}O_{syn}$) using the interpolated monthly 70 – 135 m temperature and salinity. The updated equation

$$T = 150.32 \, [\pm \, 3.94] - 4.35 \, [\pm \, 0.12] \, (\delta^{18}O_{aragonite} - \delta^{18}O_{water}) \qquad (1)$$

takes into consideration the latest determination of equivalence between the VSMOW and VPDB scales ($\delta^{18}O_{VPDB} = 0.97001 * \delta^{18}O_{VSMOW} - 29.99$‰; Brand et al., 2014; Coplen et al., 2002) and does not significantly alter the slope originally calculated by Grossman and Ku (1986). Quantities in square brackets represent the standard error. For a $\delta^{18}O_{aragonite}$ range of +2.0 ‰ to +4.0 ‰ (VPDB), the difference between the original equation calculated by Grossman and Ku (1986) and Equation 1 is between 0.03 °C and 0.06 °C for the $\delta^{18}O_{water}$ range found in the North Sea (+0.50 ‰ to -0.40 ‰ VSMOW, Harwood et al., 2008). This is well within the standard error of estimate of the original Grossman and Ku (1986) equation (1.37 °C).

To determine the timing of shell growth, the sub-annual $\delta^{18}O_{shell}$ results (first determined in an "increment percentage" scale) were wiggle-matched to the monthly $\delta^{18}O_{syn}$. We averaged the percentage-to-month alignment of every year to obtain an average growing season with a 10% increment resolution starting at 5%.

We obtained the growth rate by calculating the slope between each increment growth data point which we interpolated to monthly resolution. The monthly growth rate was compared to the diatom abundance data, used as a primary production proxy (Brzezinski et al., 1998; Irigoien et al., 2002), obtained from the Continuous Plankton Recorder (CPR) Survey, operated by the Sir Alister Hardy Foundation for Ocean Science (SAHFOS). The CPR is a near-surface (10 m) plankton sampler voluntarily towed each month behind merchant ships on their normal routes of passage. We used the annual maximum diatom count from the CPR standard area B2 (which covers the northern North Sea) for the years 1979 to 2003 (Johns, 2016).

4.3.5 Bottom water temperature reconstruction

To obtain water temperature from $\delta^{18}O_{aragonite}$ it is first necessary to subtract the water-mass effect on oxygen isotope values ($\delta^{18}O_{water}$) from those of the aragonite. We estimated $\delta^{18}O_{water}$ using the mixing line determined by Harwood et al. (2008). It is not possible to determine past salinities with the methods used in this study. However, since the average annual bottom water salinity amplitude of the North Sea for the 1950-2010 interval (0.16 ± 0.08 PSU, ICES, 2014) suggests that changes in water mass are rather small, we used a constant $\delta^{18}O_{water}$ (0.36 ± 0.003 ‰ VSMOW/-29.64 $\pm$ 0.003 ‰ VPDB; Brand et al., 2014; Coplen et al., 2002; Harwood et al., 2008) when applying Equation 1. This $\delta^{18}O_{water}$ value represents the average Feb-Oct water mass suggested by the average salinity from 1980-2010 (35.20 ± 0.006 PSU where the uncertainty represents the 95% upper and lower bootstrap bounds, ICES, 2014). The uncertainty in $\delta^{18}O_{water}$ produces a

change of 0.01 °C with a constant $\delta^{18}O_{aragonite}$ in Equation 1. As an alternative to Equation 1, we developed a calibration using the local sub-annual data but ultimately did not use it as we determined it was not significantly different to Equation 1 (Section 4.7.1).

We compared our BWT reconstruction with the BWT reconstruction from the Dogger Bank, central North Sea (Figure 3.1; Schöne et al., 2005c). The latter reconstruction is derived from 12 shells recovered from an approximate depth of 50 m. To facilitate a comparison with our reconstruction, the seasonal Dogger Bank reconstruction was resampled to annual resolution by treating the complete series as a single individual with varying temporal resolution and then averaging all the available data for a given year. The resulting annual series starts in 1866 and ends in 2001, with a hiatus between the years 1906 and 1947. We compared the linear trends from 1866 to 1900, from 1947 to 2001 and from 1880 to 2000 of both records with the F statistic of a one-way ANCOVA.

To better contextualise any trend observed between the 19th and 20th centuries, we calculated the linear trends in the 1551-2004 interval in 100-year sliding windows. Every window had an overlap of 90 years.

4.3.6   Comparison to NAO indices

We carried out an ordinary least squares (OLS) regression analysis between seasonal North Atlantic Oscillation indices (NAO; Luterbacher et al., 2001) and our BWT reconstruction for the 1700-2000 interval. We defined the indices as the average for winter (NAO_{DJF}), spring (NAO_{MAM}), summer (NAO_{JJA}) and for the growing season (Feb-Oct; NAO_{Gro}). To better account for uncertainties in our age model, we carried out the regression analysis in 50-year windows and examined the NAO/BWT relations within lags of ±5 years.

We also applied the methods of Petrie (2007) when carrying out an OLS regression analysis between seasonal NAO indices and our BWT reconstruction for the 1700-2000 interval: only the years when a given NAO index was in the same phase as during the two preceding years were selected, and these same-phase years were integrated into a three-year running sum ($\sum NAO_\tau = NAO_{\tau-2} + NAO_{\tau-1} + NAO_\tau$). As before, we carried out the regression analysis in 50-year windows and examined the $\sum NAO_\tau$ /BWT relations within lags of ±5 years. We compared the slopes of each 50-year window with the F statistic of a one-way ANCOVA.

Finally, we examined the effects of NAO_X (where X stands for the analysed season) on water column stratification by:

1. Organising the NAO_X into quintiles (Q). We ranked the most negative NAO_X years into Q1, the moderately negative years in Q2, the neutral years in Q3, the moderately positive years in Q4 and the most positive years in Q5.

2. Obtaining the gridded monthly sea surface temperature (SST) for the same 2° latitude by 2° longitude grid box defined in Section 4.3.4 (Figure 3.1; Rayner et al., 2003; obtained from the KNMI Climate Explorer climexp.knmi.nl) for years 1870-2004 and averaging them into the same seasons as NAO_X.

3. Calculating the year-to-year SST_X differences (ΔSST_X) and the year-to-year BWT differences (ΔBWT). This acts as a high-pass filter and reduces autocorrelation.

4. Performing OLS regression analyses between ΔBWT and ΔSST_X in Q 1-5 of every NAO_X.

Our hypothesis is that we will obtain a significant regression with a positive slope in the quintiles associated with prevalent wind stress over northern Europe. This would be indicative of the water column being mixed.

4.4 Results

4.4.1 Crossmatching testing

In their work Estrella-Martínez et al. (2019) added nine shells to the FGB chronology originally developed by Butler et al. (2009a) to extend it from its original coverage of 1755-2003 back to the 1540s. In general, the added interval is represented by fewer shells than the original which is reflected in their lower expressed population signal (EPS) values. This is also reflected in the lower correlations between pairs of shells involving those added by Estrella-Martínez et al. (2019) (italicised shell IDs in Table 1).

When testing the correlation between pairs of shells with a student-t test (Baillie and Pilcher, 1973), we found that the great majority of the correlations were significant at the $p<0.01$ level (boldface student-t values is Table 1). Two of the correlations were significant only at the $p<0.10$ level (underlined student-t values in Table 1) while five did not reach significance. The average temporal overlap between pairs of shells that passed the Baillie-Pilcher student-t test is 95 years while the average overlap for pairs that did not pass the test is 36 years.

Table 1. Pearson correlation coefficients between pairs of shells in their overlapping lifespans and the corresponding student-t test

		Pearson correlation coefficient													
		Shell ID: 040 …													
		1246	1254	1258	1260	1262	*0202*	*0237*	*0205*	*0249*	*0366*	*0246*	*0408*	*0419*	*0435*
Student-t statistic	1246		0.72	0.80	0.65	0.76	0.65	0.38	0.42	0.52	0.52	---	---	---	---
	1254	**15.6**		0.65	0.66	0.77	0.64	0.36	0.61	0.26	0.53	---	---	---	---
	1258	**20.65**	**13.28**		0.58	0.65	0.45	0.39	0.31	0.05	-0.01	---	---	---	---
	1260	**12.65**	**13.64**	**10.83**		0.64	0.60	0.64	0.40	0.48	0.61	0.29	0.08	---	---
	1262	**18.22**	**19.36**	**13.34**	**13.06**		0.60	0.36	0.51	0.33	0.57	---	---	---	---
	0202	**9.45**	**9.61**	**5.55**	**10.17**	**8.99**		0.45	0.60	0.37	0.59	0.25	---	---	---
	0237	**3.88**	**3.87**	**4.30**	**14.04**	**4.13**	**6.27**		0.31	0.47	0.56	0.33	0.54	---	---
	0205	**3.34**	**6.80**	**2.64**	**5.38**	**5.45**	**8.47**	**3.90**		0.22	0.31	0.08	---	---	---
	0249	**4.39**	**2.10**	0.34	**8.07**	**2.93**	**4.09**	**7.64**	**2.55**		0.58	0.32	0.11	---	---
	0366	<u>1.87</u>	**3.21**	-0.07	**10.7**	**4.25**	**6.55**	**9.15**	**3.35**	**10.18**		0.42	0.38	---	---
	0246	---	---	---	**3.39**	---	<u>1.37</u>	**3.72**	0.61	**3.84**	**5.60**		0.29	0.27	0.23
	0408	---	---	---	0.46	---	---	**3.75**	---	0.67	**2.85**	**4.07**		0.31	0.24
	0419	---	---	---	---	---	---	---	---	---	---	**2.88**	**3.66**		0.46
	0435	---	---	---	---	---	---	---	---	---	---	**2.34**	**2.58**	**7.48**	

Shells added by Estrella-Martínez et al. (2019) to the original Butler et al. (2009a) FGB chronology have their IDs italicised. Correlations that achieved significance at the p<0.01 level or better have their corresponding student-t statistic in boldface and those that achieved significance at the p<0.10 level have their corresponding student-t statistic underlined.

4.4.2 Sub-annual sampling and increment growth timing

We obtained a total of 225 sub-annual samples from one shell (shell ID 1247) covering the time interval of 1979 to 2002 (Figure 4.2A, Figure 4.2B). The average $\delta^{18}O_{shell}$ value of the sub-annual series, +2.96 ‰, shows an offset of -0.30 ‰ when compared to the instrumental-derived $\delta^{18}O_{syn}$, +3.26 ‰. As there is substantial evidence that *A. islandica* deposits its aragonitic shell in isotopic equilibrium with the ambient water (Marchitto et al., 2000; Weidman et al., 1994), we subtracted this offset manually (adjusted shell ID 1247*; Figure 4.2A-C).

We were able to wiggle-match the adjusted sub-annual oxygen isotope data of the shells to $\delta^{18}O_{syn}$ for every year except for 1990 and 1991 (Figure 4.2A-B), both of which showed seasonal cycles that differed from the instrumental series. For the successful years, an RMA regression shows a near 1:1 correspondence between shell 1247* and $\delta^{18}O_{syn}$ (Figure 4.2C). Using this alignment, we calculated an average growing season from early February to late October (Figure 4.2D) with maximum monthly growth rates ranging between 16.5 % per month and 19.4 % per month occurring in June and July (Figure 4.2E). The monthly-resolved

growth rate has the same general shape of the average diatom count for the CPR standard area B2 (Johns, 2016) but lags it by two months (Figure 4.2F).
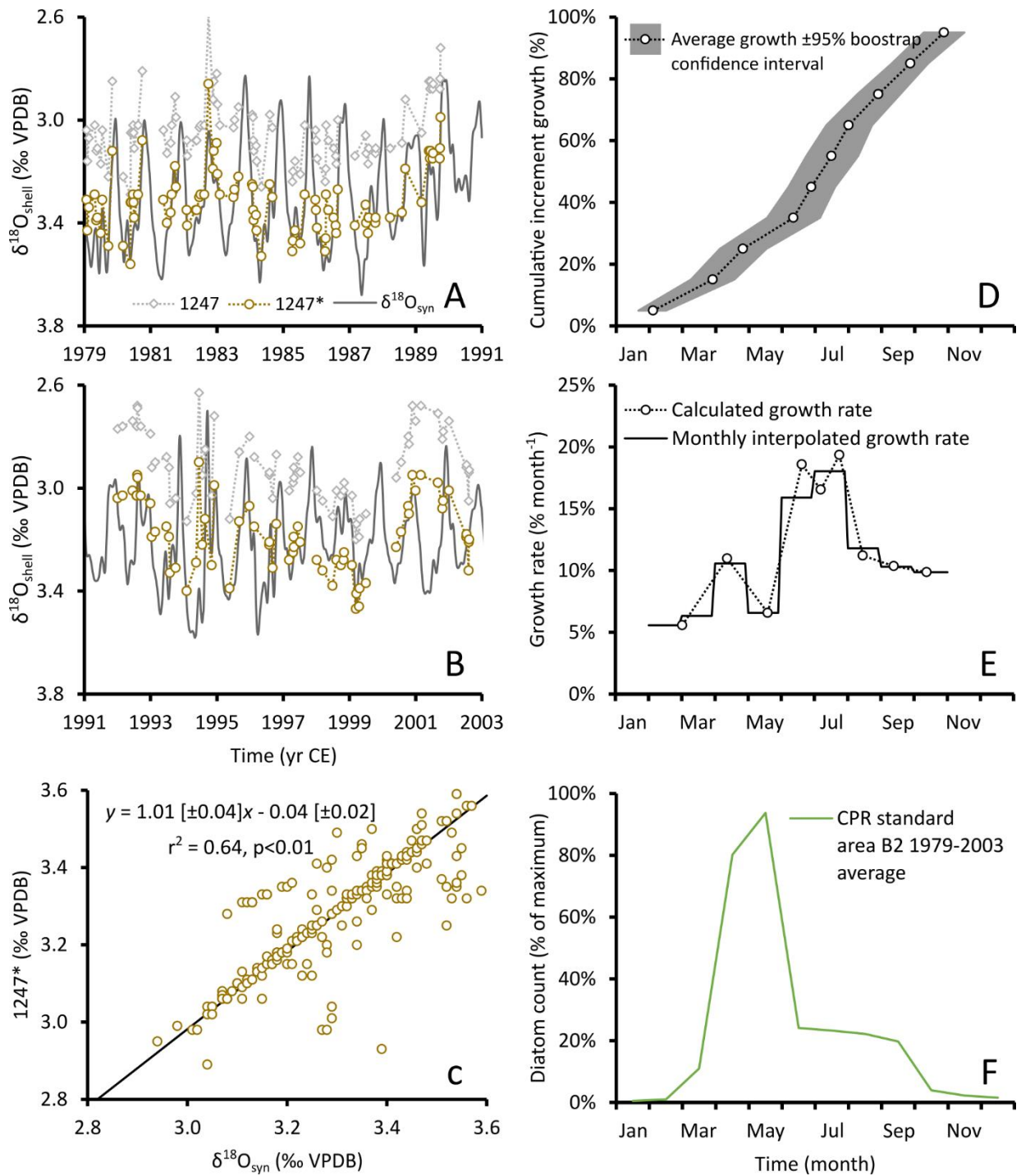
Figure 4.2 Results from sub-annual sampling time-matched to $\delta^{18}O_{syn}$.
Notice inverted vertical axis in A and B. $\delta^{18}O_{shell}$ from specimen 1247 shows a constant negative offset to $\delta^{18}O_{syn}$ (A and B). Once this offset is removed (1247*), the majority of the points fall on the unity line (C). The temporal alignment reveals the average shell growing season at the Fladen Ground and the average monthly growth rates (D and E). The growing season is out of phase with the average diatom bloom (F).

4.4.3 Annual δ¹⁸Oshell and bottom water temperature reconstruction

Following our convention to reject isotope data that came from samples with signal intensities significantly away from the calibration range and powder samples that were lost in the milling process, we obtained results for 418 out of the targeted 455 years of temporal coverage. The longest hiatuses occur in the 20th century in the intervals between 1939-1944 and 1955-1959. The average temporal overlap between specimens was nine years with a minimum of one year and a maximum of 26 years (Error! Reference source not found.A, **Error! Reference source not found.**B). The reason for our intended overlap not being obtained for every shell pair is that carbonate material extraction becomes more difficult in the narrower increments.

The composite (non-averaged) δ¹⁸O results fall within the range of +3.78 ‰ to +2.61 ‰, the former occurring in 1967 and the latter occurring in 1990. However, when compared to the instrumental Feb-Oct δ¹⁸O$_{syn}$ we observe an offset between shells 1246, 1266 and 1247 with respect to each other and with respect to δ¹⁸O$_{syn}$ (Error! Reference source not found.B). As the rest of the shell series do not display this offset pattern during the periods of overlap, we used the same reasoning as in Section 3.1 and manually added a constant to each anomalous shell to match the instrumental Feb-Oct δ¹⁸O$_{syn}$ average (i.e. each shell had its own offset constant). After these adjustments the δ¹⁸O results fall within the range of +3.76 ‰ to +2.81 ‰, the former occurring in 1560 and the latter occurring in 1781. We weight-averaged the results from the individual (adjusted) shells into a single series with an average value of +3.26 ‰, a 1σ standard deviation of 0.14 ‰ and no significant linear trend (Error! Reference source not found.C).

After the application of Equation 1 to our weight-averaged data we obtained a BWT series with a maximum of 9.16 °C (1781), a minimum of 5.03 °C (1560), an average of 7.20 °C and a standard deviation of 0.63 °C (Figure 4.4A). When comparing against the instrumental 75-135 m Feb-Oct average temperature (Figure 4.4B) we observe that our reconstruction lies within 0.5 °C of the real value 54% of the time between the years 1950 and 1996 (blue dashed line in Figure 4.4B) and within 1 °C 73% between the years 1950 and 1996 of the time (Figure 4.4C). If the years 1997-2004 are included, then the reconstruction lies within 0.5 °C of the real value 45% of the time and 1 °C 62% of the time. The correlation between the measured temperature and our reconstruction is 0.64 (p<0.01) for the years 1950-1996. Our reconstruction shows that there were four extended (≥4 yr, interrupted by ≤2 yr) episodes of high BWT, these being defined as values higher than the 1551-2004 average plus one standard deviation. These episodes occurred between 1675-1681, 1734-1740, 1818-1822, and 1848-1860. Similarly defined episodes of extended low BWT occurred between 1551-1554, 1558-1563, 1878-1897, 1908-1924, and 1965-1970.
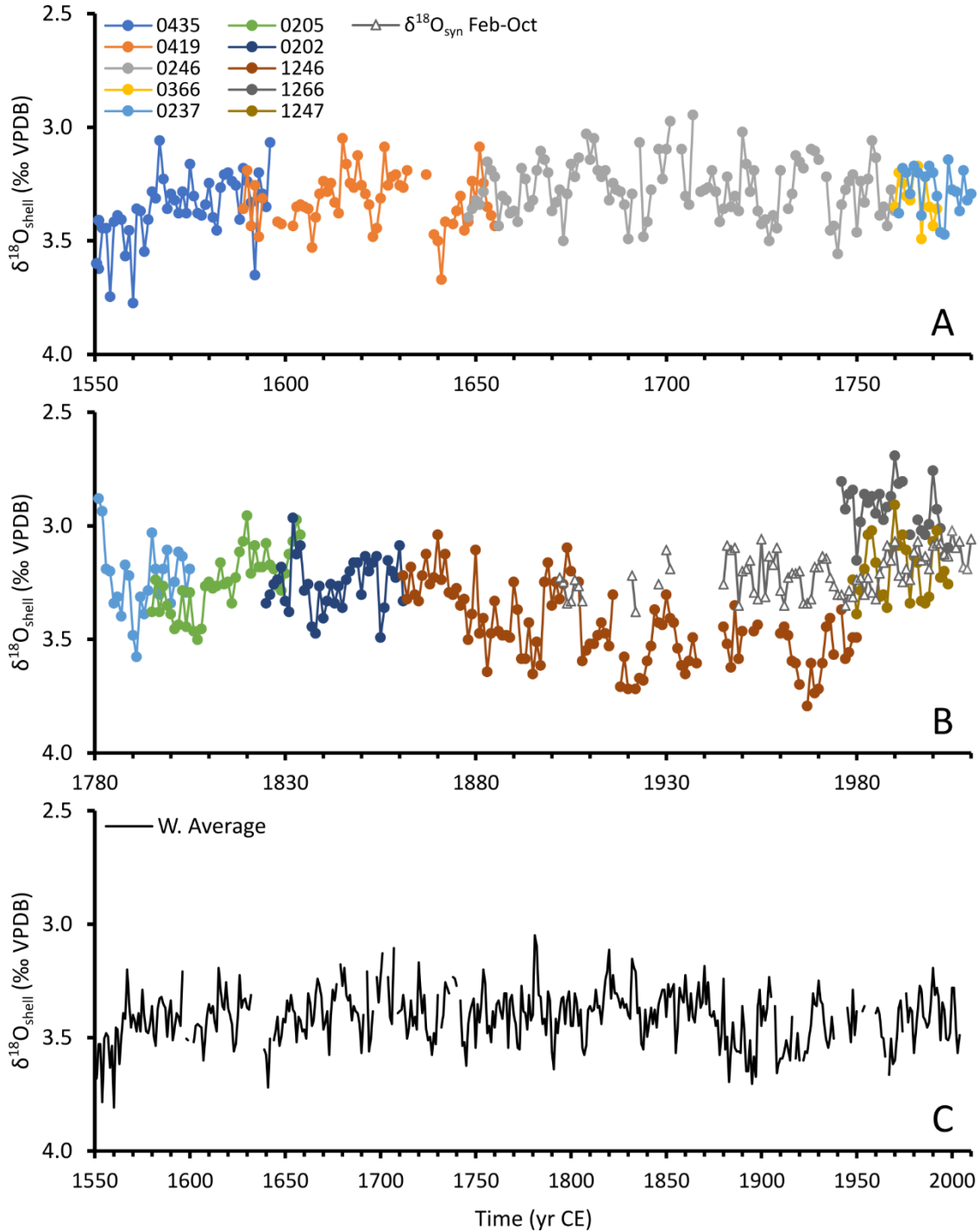
Figure 4.3 Annual $\delta^{18}O_{shell}$ results.
Notice the inverted vertical axis. The results were obtained from the increments of ten shells (A and B). Results from shells 1246, 1247 and 1266 show offsets when compared to $\delta^{18}O_{syn}$ and to each other (B). Once the offset was removed, we weight-averaged the results into a single series (C).

Our reconstruction shows the same general behaviour as that of the Dogger Bank BWT record (Schöne et al., 2005c) although it generally shows temperatures ~0.50 °C warmer. Our reconstruction shows a significant (p < 0.01) trend from 1866 to 1900 of -0.04 °C yr^{-1} while the Dogger Bank record shows a short-

of-significant (p = 0.06) trend of -0.02 °C yr^{-1} for the same time interval. A one-way ANCOVA suggests that there is no statistical difference in these trends (F = 1.33, p = 0.25). The correlation between the records for this time interval is not significant (r = 0.20, p = 0.25). For 1947 to 2001 both reconstructions show a non-significant near zero trend (0.01 °C yr^{-1}, p = 0.06 for the Fladen Ground; 0.00 °C yr^{-1}, p = 0.59 for the Dogger Bank; F = 0.75, p = 0.39). The correlation between the two records in this latter interval is similar to the 1866-1900 interval (r = 0.21) but it is also not significant (p = 0.13).
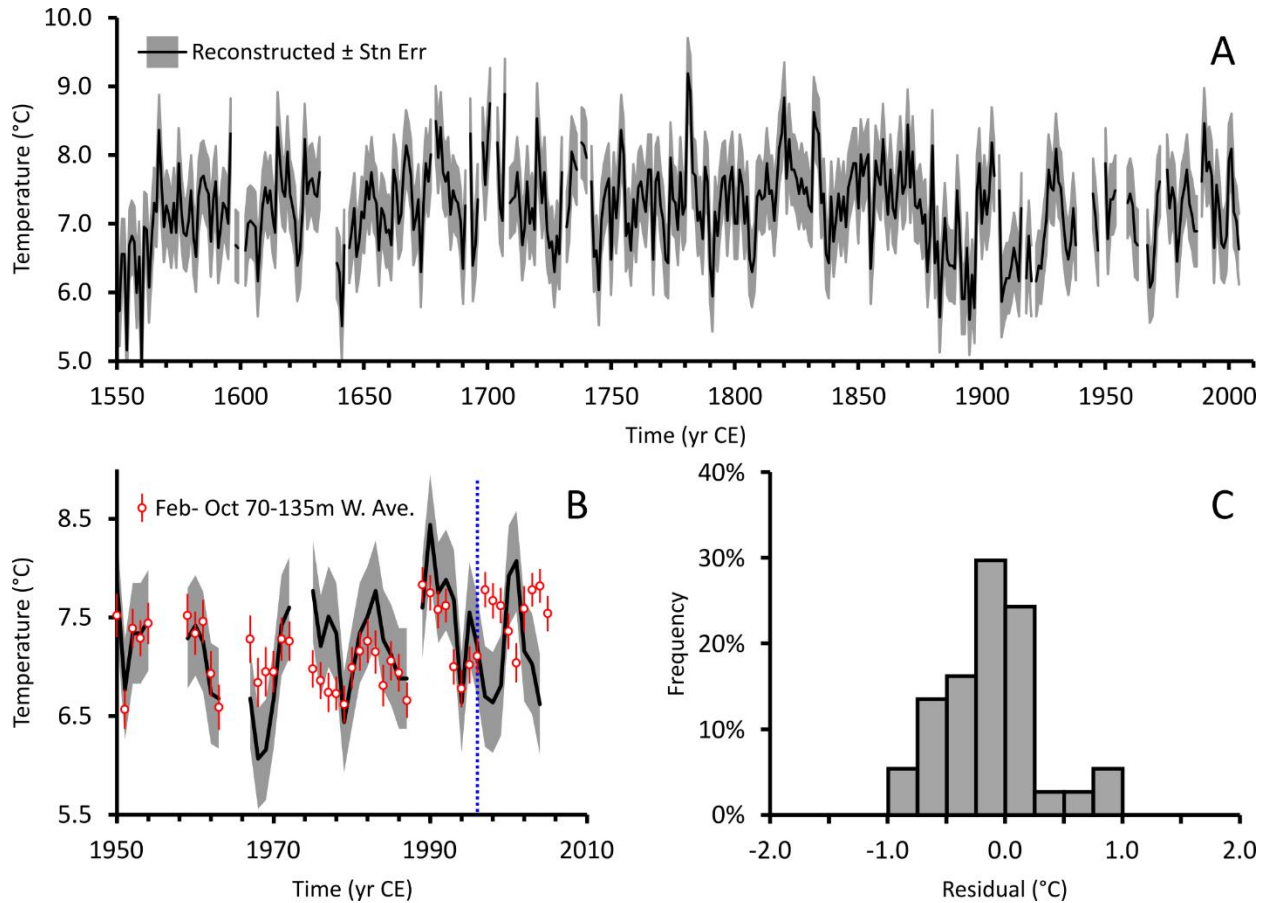
Figure 4.4 Bottom water temperature reconstruction obtained by applying Equation 1.
We used a constant δ^{18}O$_{water}$ of 0.36 ‰ VSMOW/-29.64 ‰ VPDB for the complete record (A). The reconstruction shows a high level of similarity to the instrumental Feb-Oct weighted average temperature until 1996 (B) and lies within 0.5 °C of the real value 54% of the time and within 1 °C 73% of the time for the years 1950-1996 (C).

In their work, Schöne et al. (2005c) determined a significant average BWT rise of 0.09 ± 0.02 °C decade^{-1} for the 1880-2001 interval, also observed in our recalculation of their data. Our BWT reconstruction shows a significant temperature trend of 0.06 ± 0.02 °C decade^{-1} for the same interval. A one-way ANCOVA determined that there is no significant difference between these two trends (F = 1.83, p = 0.18). The late 19th-late 20th century warming is not the only significant trend identified in our reconstruction. One additional significant warming trend is notable from 1640 to 1740 at a rate of 0.05 ± 0.02 °C decade^{-1}. We also observed

a significant cooling during all of the 19th century, with a maximum rate of -0.11 ± 0.02 °C decade^{-1} occurring between 1810 and 1910.

4.4.4 Relationship between bottom water temperature, stratification and NAO index

We did not find consistently significant regression lines between any of the seasonal NAO indices and BWT at any time lag during the time windows analysed (Tables S2-S5). We did, however, find consistent $\sum NAO_\tau$/BWT regression lines when comparing our reconstruction to NAO_{DJF} (Table 2). Some of these regressions were just-off significance at the α = 0.05 level except for the 1900-1949 window which showed a p-value of 0.47. With the exception of this window, the rest of the slopes are statistically undistinguishable from one another (one-way ANCOVA, F = 1.40, p = 0.25). We determined a $\sum NAO_\tau$/BWT common slope of 0.12 ± 0.03 °C per $\sum NAO_\tau$ unit for the time windows that showed regression with p-values 0.10 or lower.

Table 2. OLS regression analysis of our BWT reconstruction against winter $\sum NAO_\tau$.

Time interval	Slope ± Std Er. (°C per $\sum NAO_\tau$ unit)	Intercept ± Std Er. (°C)	r^2	p	n
1700-1749	0.17 ± 0.08	7.28 ± 0.16	0.21	0.06	18
1750-1799†	0.91 ± 0.34	9.39 ± 0.80	0.50	0.03	9
1800-1849	0.15 ± 0.06	7.55 ± 0.11	0.48	0.03	10
1850-1899	0.22 ± 0.10	6.91 ± 0.25	0.40	0.07	9
1900-1949‡	0.09 ± 0.11	6.76 ± 0.32	0.09	0.47	8
1950-2000	0.10 ± 0.03	7.19 ± 0.11	0.54	0.01	11
All p < 0.10	0.12 ± 0.03	7.33 ± 0.07	0.23	<0.01	57

† +1 yr lag, NAO leads
‡ +4 yr lag, NAO leads

The results from our $\Delta BWT/\Delta SST_X$ analyses are summarised in Table 3 while the years representing each quintile are presented in Section 1.1.1 (Table S6). We found significant positive $\Delta BWT/\Delta SST_X$ slopes for the NAO_{DJF} years in Q5, the NAO_{MAM} years in Q4 and the NAO_{Gro} years in Q1. On the other hand, we found a significant negative $\Delta BWT/\Delta SST_X$ slope for the NAO_{JJA} years in Q2.

Table 3. OLS regression analyses between our BWT reconstruction and gridded SST during the 1870-2004 interval according to NAO phase and magnitude going from the most negative (Q1) to the most positive values (Q5). Note that the years represented in each quintile are different for every season. Trends in **boldface** are significant at the α = 0.05 level.

	NAO quintile	Q1	Q2	Q3	Q4	Q5
ΔSST_{DJF}[†] vs. ΔBWT	Slope ± Std Er.[‡]	0.25 ± 0.36	0.40 ± 0.22	-0.37 ± 0.29	0.07 ± 0.35	**0.89 ± 0.29**
	r^2	0.03	0.15	0.08	0.00	**0.35**
	p	0.49	0.09	0.22	0.85	**<0.01**
ΔSST_{MAM}[†] vs. ΔBWT	Slope ± Std Er.[‡]	-0.15 ± 0.27	0.01 ± 0.44	0.19 ± 0.26	**0.66 ± 0.28**	0.46 ± 0.35
	r^2	0.01	0.00	0.03	**0.22**	0.09
	p	0.60	0.98	0.48	**0.03**	0.20
ΔSST_{JJA}[†] vs. ΔBWT	Slope ± Std Er.[‡]	0.15 ± 0.26	**-0.55 ± 0.24**	0.02 ± 0.21	0.07 ± 0.23	-0.06 ± 0.23
	r^2	0.02	**0.21**	0.00	0.00	0.00
	p	0.58	**0.04**	0.92	0.77	0.81
ΔSST_{Gro}[†] vs. ΔBWT	Slope ± Std Er.[‡]	**0.69 ± 0.30**	-0.24 ± 0.43	-0.07 ± 0.47	0.04 ± 0.34	-0.72 ± 0.56
	r^2	**0.22**	0.02	0.00	0.00	0.09
	p	**0.03**	0.58	0.89	0.90	0.13

[†]NAO averaged for the same months as SST

[‡]Units: °C per NAO unit

4.5 DISCUSSION

4.5.1 Crossmatching confidence

The lower EPS values in the extension of the FGB chronology carried out by Estrella-Martínez et al. (2019) leave something to be desired. Normally, the EPS scores of a given chronology need to reach a threshold value of 0.85 in order to say that chronology confidently represents the environmental signal that is forcing the relative growth of the complete bivalve community (Buras, 2017; Wigley et al., 1984). The EPS (and its closely associated score, the subsample signal strength) is also used to evaluate the fidelity with which a given chronology is capable of representing the higher frequencies the environmental forcings (Black et al., 2016). However, the crossmatching exercise is not always explicitly tested.

In the Baillie-Pilcher student-t test (Baillie and Pilcher, 1973), a t statistic of around 2.33 would be expected to occur once in 100 times by chance. In our tests this is confirmed, as the majority of the correlations deemed significant at the p<0.01 had a t statistic of 2.33 or greater. Baillie and Pilcher (1973)

arbitrarily suggested that the t statistics should reach a threshold of 3.50 for the pairs of shells being considered crossmatched with a high degree of certainty. Although the majority of the correlation exercise we carried out gave us significant results, we did not always reach the t value of 3.5. This is further evidence for the temporal uncertainty estimate proposed by Estrella-Martínez et al. (2019) of 5%.

4.5.2 Isotope offsets in shells 1246, 1266 and 1247

The observed offset between the $\delta^{18}O_{shell}$ values of shells 1246, 1266 and 1247 and $\delta^{18}O_{syn}$ and among each other is highly inconsistent with the published data that *A. islandica* deposits its aragonitic shell in isotopic equilibrium with the ambient water. The sub-annual results of shell 1247 are, on average, 0.17 ‰ more negative than the annual results from the same shell. Similarly, the annual results from shell 1266 are 0.28 ‰ more negative than the annual results from shell 1247. Assuming a constant $\delta^{18}O_{water}$ value, these offsets would be equivalent to water temperature changes of +0.82 °C and +1.17 °C, respectively, across the entire lifetime of the specimens. Given that the specimens were collected from close proximity, these persistent temperature fluctuations seem unlikely. It is similarly unlikely that water masses with different $\delta^{18}O_{water}$ would differentially affect the specimens for extended times.

A possible cause for the observed offset is a difference in $\delta^{18}O$ from different regions within the outer shell layer. The milling protocol that we employed called for the sampling of the entire area of every increment (Section 2.3). However, a study based on four North Sea *A. islandica* shells by Trofimova et al., (2018) found that regions within the outer shell layer defined by their crystal structure may show different stable oxygen isotope compositions. Trofimova et al. (2018) found that the innermost region (IMR) of the outer shell layer showed a higher proportion of ^{18}O (i.e. more positive $\delta^{18}O$ values) than the outermost region (OMR) of the outer shell layer. The results from Trofimova et al. (2018) suggest that IMR $\delta^{18}O$ values would also have a positive offset from an in-situ $\delta^{18}O_{syn}$. In contrast, the $\delta^{18}O$ results suggested that the OMR was deposited closer to isotopic equilibrium with the ambient water. Nevertheless, the $\delta^{18}O$ differences between the IMR and OMR were inconsistent and often fell within the uncertainty ranges of each other. Given that the IMR makes up, on average, ~75% of the outer shell layer (Trofimova et al., 2018) we would expect our results to show an inconsistent positive offset from $\delta^{18}O_{syn}$. This is not the case for any of our anomalous shells (Figure 4.2A, Figure 4.2B, and Figure 4.3B).

A more plausible cause for these offsets is the inappropriate storage of $CaCO_3$ powder extracted from the anomalous shells. Oxygen isotopes in fine carbonate powder are prone to exchange with meteoric water when continuously exposed to high relative humidity (Hut, 1987; Nishida and Ishimura, 2017; Paul and Skrzypek, 2006; Rahaman et al., 2008). The exchange happens via the hydroxyl group in the reactions

$$HOH^* + CO_2 \rightleftharpoons HCO_2OH^* \tag{2}$$

$$HCO_2OH^* \rightleftharpoons CO_2OH^{*-} + H^+ \tag{3}$$

$$CO_2OH^{*-} + H^+ + CaCO_3 \rightleftharpoons Ca^{2+} + HCO_3^- + CO_2OH^{*-} \tag{4}$$

$$Ca^{2+} + HCO_3^- + CO_2OH^{*-} \rightleftharpoons CaCO_3^* + H_2O + CO_2 \tag{5}$$
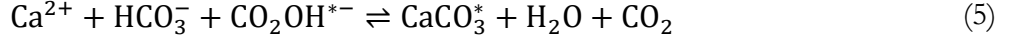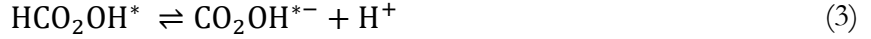
In the course of developing this investigation, shell 1266 was sampled before the sub-annual sampling of shell 1247 which itself occurred before annual resolution sampling of shells 1247 and 1246. The powder extracted from these specimens was stored in a low-adsorption weighting paper envelope inside plastic centrifuge vials which were kept in plastic bags with no desiccant for 54-78 days before being hermetically sealed in a vastly reduced volume metallic vial prior to transport to Germany for isotopic characterisation. Powder samples from the rest of the shells examined, on the other hand, were stored alongside silica desiccant.

4.5.3   Shell growing season in the Fladen Ground

Examination of the sub-annual 1247* $\delta^{18}O_{shell}$ results relative to the instrumental $\delta^{18}O_{syn}$ indicate an *A. islandica* shell growing season in the Fladen Ground lasts from early February until late October. This is in close agreement with results from near-surface shells from the Dogger Bank that were found to carry out most of their increment growth from February to September (Schöne et al., 2005b). We did not observe an equivalent secondary growing season from mid-November to mid-December as reported for the Dogger Bank (Schöne et al., 2005b) but the 95% bootstrap confidence intervals determined from our data would partially contain this secondary growth (Figure 4.2D).

The calculated average *A. islandica* growth rate has a similar trend to that of the diatom count for the CPR standard area B2 (Johns, 2016) but the two curves are out of phase by about two months (Figure 2E and 2F). This can be explained by the local hydrography in the northern North Sea. Our results suggest that the bivalves have an initial growth spurt in April, coinciding with the near-maximum diatom count during the spring bloom (Johns, 2016) and, hence, greater food availability. This initial growth diminishes in May, roughly the same time as the onset of thermal stratification in the northern North Sea (ICES, 2014; Otto et al., 1990; Sprintall and Cronin, 2001). As the thermocline develops, the *A. islandica* community at the Fladen Ground is disconnected from the phytoplankton bloom and their growth slows down. The growth rates increase again over the summer with the downward nutrient transportation in the form of fish/copepod faecal pellets and residual nutrients from the previous phytoplankton bloom (Estrella-Martínez et al., 2019).

A question that remains from our wiggle-matching exercise is why were we unsuccessful in aligning our $\delta^{18}O_{shell}$ results to the instrumental $\delta^{18}O_{syn}$ in the years 1991 and 1992. A plausible explanation lies in the development of the Saltire, Scott, Miller and Tiffany oil fields, all developed between 1991 and 1992 and all in close proximity to our collection site. The development of these oil fields might have disturbed the ambient water temperature enough to be recorded in the *A. islandica* shells (Cordes et al., 2016; Peterson et al., 1996), but this disturbance would have otherwise been averaged out in our temperature and salinity calculation for the wider 2° latitude by 2° longitude grid box centred at the collection site (Figure 4.1).

4.5.4 Long-term bottom water temperature trends

The comparison of our reconstruction to the Dogger Bank record (Schöne et al., 2005c) alongside the ~0.50 °C temperature difference between them, is consistent with the results for the last 30 years of the 20th century from the North Sea. In their study, Berx and Hughes (2009) found a zonal temperature pattern in the bottom waters of the central and northern North Sea with the waters in the Dogger Bank being slightly colder than those at the Fladen Ground. This suggests that the manual $\delta^{18}O_{syn}$-based adjustment made to our data is accurate and gives us confidence in the rest of our reconstruction and permits examination of the 1880-2001 Dogger Bank warming in a longer context.

With the additional coverage of years 1907-1946 compared to the Schöne et al. (2005c) reconstruction, we can suggest a minor revision to the warming rate to 0.08 ± 0.02 °C decade^{-1} (weighted average) for the 1880-2001 interval. Our reconstruction suggests that another warming occurred during the 1640-1740 interval and a rapid cooling occurred during the 19th century. These centennial trends do not seem to correspond to centennial trends in North Atlantic SST (Gray et al., 2004; Mann et al., 2009) or any of the NAO indices defined for this study (Luterbacher et al., 2001).

4.5.5 Persistent NAO phase as driver of average BWT

In their work Schöne et al. (2005c) found that minimum BWT in the North Sea share between 28 and 50 % of their variability with NAO_{DJF}. As they commented, this is not surprising as northern European winter temperatures are mainly controlled by the winter atmospheric pressure gradient (Hurrell et al., 2003). The Dogger Bank BWT reconstruction can thus be seen as evidence of NAO_{DJF} seasonal temperature control of bottom waters. The particular issue, however, is determining the controls on *average* BWT. Our results suggest it is the persistence of the NAO_{DJF} rather than the high frequency variability that has influence on the BWT of the North Sea.

The same result has been observed for the second half of the 20th century in the Labrador Sea (Petrie, 2007), the northern Pacific and northern Atlantic (Alexander and Deser, 1995) and in mid-latitude waters (Curry and McCartney, 2001). Due to the enhanced mixing in winter, NAO_{DJF} in a given year is able to generate anomalies in BWT. As the water column stratifies, the BWT is less susceptible to atmospheric changes at the surface. Due to the high thermal inertia of water, the BWT anomalies can be reinforced if the NAO_{DJF} stays in the same phase for several years. Our results suggest that the winter NAO, integrated over three years ($\sum NAO_5$; see Section 4.3.6, Table 2) shares between 9 and 54 % variability with the BWT, well in line with the results from the Dogger Bank (Schöne et al., 2005c).

4.5.6 NAO modulation of water column mixing

The general pattern of all of the $\Delta BWT/\Delta SST_X$ regression analyses is consistent with our mixed water column hypothesis: We observed significant regression with a positive slope in the quintiles associated with prevalent wind stress over northern Europe, indicative of a well-mixed water column. As the water column in the northern North Sea is mixed during the winter months, finding the strongest $\Delta BWT/\Delta SST_X$ relation in the years dominated by predominantly positive NAO_{DJF} (Q5) is not surprising, as the positive phase of the NAO_{DJF} is associated with increased storminess and wind stress over the north-eastern Atlantic and north-western North Sea (Burningham and French, 2013; Hurrell et al., 2003), which enhances water column mixing. That this relation does not hold for the years with moderately positive NAO_{DJF} (Q4) was unexpected. An explanation for this disagreement is provided in a study by Burningham and French (2013). They found that only extreme wind speed in the north-western North Sea is correlated to NAO_{DJF} while mean wind strength shows a weak correlation. This suggests that the water column at the northern North Sea may not mix completely in less severe winters.

The same explanation applies to years with moderately positive NAO_{MAM} (Q4), although the relationship is not as strong as in the winter (Table 3). Years with positive NAO_{MAM} are associated with increased storminess and wind stress over the north-eastern Atlantic and North Sea (Wang et al., 2009). The absent $\Delta BWT/\Delta SST_X$ relationship in Q5 is likely due to the storm track being more in the Norwegian Sea than in the North Sea (Wang et al., 2009), while the weak $\Delta BWT/\Delta SST_X$ relationship in Q4 is likely due to the lower shell growth rate in the spring months (Figure 4.2E), limiting their temperature representation in our BWT reconstruction.

The lack of significant $\Delta BWT/\Delta SST_X$ correlations in the years corresponding to neutral phases of every NAO index defined can be interpreted as representing stable, stratified conditions. Depending on the season, deviations from neutral NAO indices are associated with increased frequency and increased

magnitude of extreme rainfall over northern Great Britain (Guimares Nobre et al., 2017). As these extreme rainfall events are often accompanied by increased winds, we can deduce that the climate in the vicinity of the Fladen Ground during years dominated by neutral NAO in any season is relatively calm. The reduced wind stress would, therefore, not be enough to induce water column mixing and the temperatures at the bottom and surface waters would be independent from one another.

The inverted (absent) $\Delta BWT/\Delta SST_X$ relationship during the years in Q2 (Q1) of NAO_{JJA} works against our hypothesis, as years with negative NAO_{JJA} are associated with increased Northern Europe storminess (Dong et al., 2013; Folland et al., 2009; Linderholm and Folland, 2017). However, the storm track in Q1 years of NAO_{JJA} is concentrated over the central and southern North Sea and the European continent (Dong et al., 2013; Folland et al., 2009). This suggests that the summer thermal stratification in the northern North Sea is sufficiently resilient to summer storms to impede water column mixing to the seabed, especially if the majority of the storm tracks are routed further south. The findings by Dong et al. (2013) and Folland et al. (2009) indicate that this might not be the case for the Dogger Bank sector.

The results of the regression analysis for NAO_{Gro} are in contrast to those for NAO_{JJA}. Here we found that the years dominated by predominantly negative NAO_{Gro} (Q1) show a significant $\Delta BWT/\Delta SST$ positive slope. A possible solution to these conflicting results is the spatial shift of the NAO poles from winter into summer, with the low pressure pole of the NAO shifting westward from Iceland towards Greenland and the high pressure pole shifting north-eastward from the Azores over to the Iberian Peninsula and the British Isles (Feldstein, 2007). It is possible that during the seasonal NAO pole motion the average storm track associated with NAO_{Gro} (Gro = Feb-Oct) lies further north than during NAO_{JJA}. This would suggest an amplified disturbance of the water column which would delay stratification beyond normal mid-spring onset (ICES, 2014; Otto et al., 1990; Sprintall and Cronin, 2001).

4.6 CONCLUSIONS

We have developed an absolutely-dated 455-year long oxygen stable isotope series from the shells of the bivalve *A. islandica*, currently the longest chronology for the North Sea region. We determined that the annual $\delta^{18}O_{shell}$ data mainly reflects the water temperature variability from February to October. Our reconstruction indicates that the average temperature at the bottom of the northern North Sea has remained stable at 7.20 °C (σ = 0.63 °C) for the past c. 500 years and shows significant centennial warming trends of 0.05 $\pm$ 0.02 °C decade^{-1} between the years 1540-1740 and 0.08 $\pm$ 0.02 °C decade^{-1} for the years 1880-2000, with a significant cooling at a rate of -0.11 $\pm$ 0.02 °C decade^{-1} occurring between 1810 and 1910. These trends do not correspond to wider North Atlantic SST.

Our analysis indicates that only persistent NAO$_{DJF}$ conditions affect the average BWT at the Fladen Ground while higher frequency variability does not show a consistent effect. BWT anomalies are reinforced when the NAO$_{DJF}$ stays in the same phase for at least three consecutive years. Between 9 and 54 % variability in average BWT can be explained by these low frequency NAO$_{DJF}$ changes, a similar result to the minimum sub-annual BWT at the Dogger Bank.

Finally, our regression analysis suggests that the thermal stratification in the northern sectors of the North Sea is not resilient to storms passing through these sectors. However, the storms need to be strong and frequent to completely mix the water column in any given season. Storms moving through the central and southern sectors in the North Sea do not seem to be sufficiently strong or close to mix the water column in the northern North Sea.

Our work provides data necessary for the testing and verification of climate models hindcasting to the 16th century. However, robust, annually resolved SST reconstructions would be required to further test our water column mixing hypothesis beyond the 1870s. Understanding the historical variability of the water column mixing would help to determine the forcing of the mid-17th century warming and the 19th century cooling in the depths of the North Sea.

4.7 SUPPLEMENTARY MATERIAL

4.7.1 δ^{18}O$_{shell}$ to water temperature calibration

We used a piecewise cubic Hermite interpolation to reduce the wiggle-matched δ^{18}O$_{shell}$ data into monthly resolution and subtracted the instrumental monthly δ^{18}O$_{water}$ (‰ VPDB; Brand et al., 2014; Harwood et al., 2008). We used the result to carry out a reduced major axis (RMA) regression against the instrumental monthly temperature. The resulting regression line was compared to the "all data" and "mollusc" regression lines determined by Grossman and Ku (1986), corrected for the updated VPDB-SMOW conversion (Brand et al., 2014). Statistical differences in slopes were assessed in PAST v 3.19 (Hammer et al., 2001) with a likelihood-ratio test and compared to the χ[2] distribution following the methods of Warton et al. (2006). A p-value >0.05 would mean that the slopes of the lines are statistically equivalent.
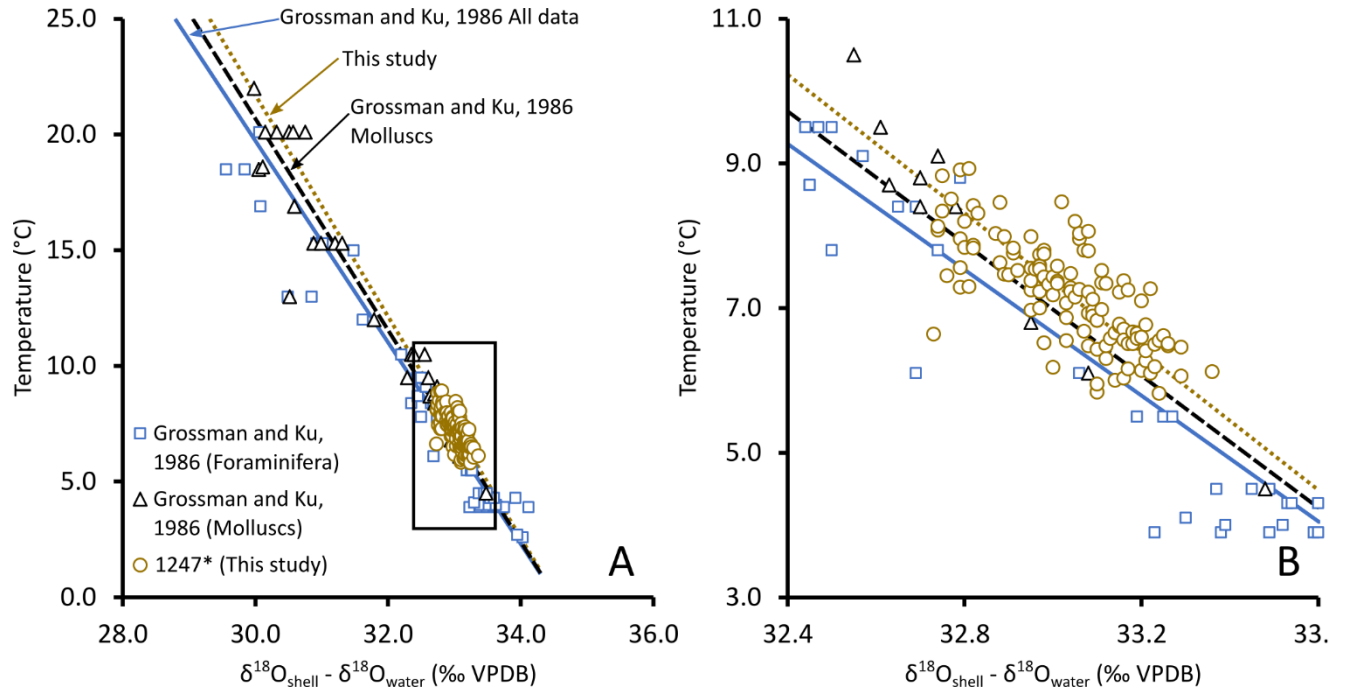
Figure 4.5 Regression of our $\delta^{18}O_{shell}$ - $\delta^{18}O_{water}$ against water temperature.
The regression line determined in our study is statistically equivalent to the 'mollusc' and 'all data' lines developed by Grossman and Ku (1986). Panel B shows a zoomed view of the black rectangle in panel A.

By using piecewise cubic Hermite interpolation we were able to reduce the wiggle-matched sub-annual data to monthly resolution. This allowed us to perform an RMA regression against the monthly 70-135 m water temperature after removing salinity effects (Figure 4.5A, Figure 4.5B). The resulting equation,

$$T = 165.14 \, [\pm\, 9.68] - 4.78 \, [\pm\, 0.29] \, (\delta^{18}O_{aragonite} - \delta^{18}O_{water}) \qquad \text{(SM1)}$$

has a slope that is statistically indistinguishable from that of Equation 1 (common slope = -4.36 °C ‰$^{-1}$, χ^2 = 2.22, p = 0.14) and "mollusc" (common slope = -4.59 °C ‰$^{-1}$, χ^2 = 0.46, p = 0.50) regression line determined by Grossman and Ku (1986). The quantities in square brackets in Equation SM1 represent the standard error and isotope values represent deviations from the VPDB standard.

Table S1 summarises the statistics for Equation SM1 and the "all data" (Equation 1 in the main manuscript) and "mollusc" lines from Grossman and Ku (1986). Equation SM1 shows the lowest standard error of estimate, but its residuals show some heteroscedasticity, given by the Breusch-Pagan score, meaning that the variability of the residuals grows at the at some point in the predictive range of the equation (in the case of Equation SM1, the residual variability grows at the higher temperatures). The Grossman and Ku (1986) "all data" line has a higher standard error of estimate and higher levels of heteroscedasticity but also

shows the highest coefficient of determination. Given this coefficient and the test on common slopes, we applied the Grossman and Ku (1986) "all data" equation in the rest of our analysis.

Table S1. Regression line statistics.

Equation	n	r^2	p_{Eq}	Standard error of estimate (°C)	Breusch-Pagan test on residuals	p_{BP}
1[†]	80	0.94	<0.01	1.37	17.55	<0.01
SM1	122	0.55	<0.01	0.51	4.60	0.03
Mollusc[†]	28	0.92	<0.01	1.49	3.18	0.07

[†]Grossman and Ku (1986)

4.7.2 NAO/BWT regressions

Table S2. Results from OLS regressions between NAO_{DJF} and BWT

	NAO before BWT										NAO and BWT on same year			NAO after BWT												
	Lag -5			Lag -4			Lag -3			Lag -2			Lag -1			Lag 0			Lag +1			Lag +2			Lag +3			Lag +4			Lag +5		
Interval	Slope ±Std Er.	r^2	p	Slope ±Std Er.	r^2	p	Slope ±Std Er.	r^2	p	Slope ±Std Er.	r^2	p	Slope ±Std Er.	r^2	p	Slope ±Std Er.	r^2	p	Slope ±Std Er.	r^2	p	Slope ±Std Er.	r^2	p	Slope ±Std Er.	r^2	p	Slope ±Std Er.	r^2	p	Slope ±Std Er.	r^2	p
1659-1699	0.14 ±0.1	0.05	0.19	0.11 ±0.1	0.03	0.30	0.04 ±0.1	0.01	0.67	-0.03 ±0.1	0.00	0.79	-0.05 ±0.09	0.01	0.59	0.07 ±0.09	0.02	0.44	0.05 ±0.09	0.01	0.60	0.06 ±0.09	0.01	0.53	-0.06 ±0.09	0.01	0.57	-0.01 ±0.09	0.00	0.88	0 ±0.11	0.00	1.00
1700-1749	-0.18 ±0.15	0.04	0.22	-0.17 ±0.14	0.03	0.25	0.12 ±0.15	0.01	0.44	0.27 ±0.15	0.07	0.09	0.26 ±0.14	0.08	0.07	**0.34 ±0.13**	**0.14**	**0.01**	0.23 ±0.15	0.06	0.12	0.22 ±0.14	0.06	0.11	-0.1 ±0.14	0.01	0.48	-0.18 ±0.14	0.04	0.20	-0.11 ±0.12	0.02	0.36
1750-1799	-0.23 ±0.11	0.08	0.04	-0.14 ±0.11	0.03	0.23	-0.14 ±0.11	0.03	0.21	-0.2 ±0.11	0.07	0.06	0.05 ±0.11	0.00	0.67	0.06 ±0.11	0.01	0.59	-0.18 ±0.11	0.06	0.09	-0.12 ±0.11	0.03	0.26	-0.03 ±0.11	0.00	0.78	-0.06 ±0.11	0.01	0.61	0.09 ±0.11	0.01	0.41
1800-1849	-0.02 ±0.1	0.00	0.86	-0.04 ±0.1	0.00	0.68	-0.02 ±0.1	0.00	0.80	-0.07 ±0.1	0.01	0.47	-0.01 ±0.1	0.00	0.92	-0.08 ±0.1	0.01	0.43	0.07 ±0.1	0.01	0.45	0.02 ±0.1	0.00	0.81	0.03 ±0.1	0.00	0.76	0.02 ±0.1	0.00	0.86	-0.04 ±0.1	0.00	0.69
1850-1899	0.11 ±0.11	0.02	0.32	0.07 ±0.11	0.01	0.53	0.02 ±0.11	0.00	0.86	0.13 ±0.11	0.03	0.27	0.14 ±0.12	0.03	0.22	-0.07 ±0.12	0.01	0.55	0.2 ±0.11	0.06	0.09	0.12 ±0.12	0.02	0.31	0.15 ±0.11	0.03	0.20	0.07 ±0.11	0.01	0.52	0.11 ±0.12	0.02	0.34
1900-1949	0.11 ±0.1	0.03	0.31	0.03 ±0.11	0.00	0.75	0.07 ±0.1	0.01	0.47	0.05 ±0.1	0.01	0.66	-0.11 ±0.1	0.03	0.25	-0.1 ±0.11	0.02	0.35	-0.13 ±0.11	0.04	0.23	-0.1 ±0.11	0.02	0.35	-0.13 ±0.1	0.04	0.22	-0.12 ±0.11	0.03	0.27	**-0.25 ±0.1**	**0.14**	**0.02**
1950-2000	-0.03 ±0.08	0.00	0.75	0.01 ±0.08	0.00	0.94	0.01 ±0.08	0.00	0.86	-0.05 ±0.07	0.01	0.52	0.07 ±0.07	0.02	0.36	0.07 ±0.07	0.02	0.32	**0.17 ±0.07**	**0.15**	**0.01**	**0.27 ±0.06**	**0.33**	**<0.01**	**0.21 ±0.07**	**0.18**	**<0.01**	0.11 ±0.08	0.05	0.15	0.03 ±0.07	0.01	0.64

Slope units: °C per NAO unit

Table S3. As Table S2 but for NAO$_{MAM}$

Interval	NAO before BWT															NAO and BWT on same year			NAO after BWT																
	Lag -5			Lag -4			Lag -3			Lag -2			Lag -1			Lag 0			Lag +1			Lag +2			Lag +3			Lag +4			Lag +5		
	Slope ±Std Er.	r²	p	Slope ±Std Er.	r²	p	Slope ±Std Er.	r²	p	Slope ±Std Er.	r²	p	Slope ±Std Er.	r²	p	Slope ±Std Er.	r²	p	Slope ±Std Er.	r²	p	Slope ±Std Er.	r²	p	Slope ±Std Er.	r²	p	Slope ±Std Er.	r²	p	Slope ±Std Er.	r²	p
1659-1699	0.19 ±0.21	0.03	0.37	**0.48 ±0.22**	**0.13**	**0.03**	0.26 ±0.21	0.04	0.24	0.41 ±0.22	0.09	0.07	0.09 ±0.3	0.00	0.76	**0.42 ±0.2**	**0.10**	**0.05**	-0.03 ±0.23	0.00	0.88	0.09 ±0.22	0.00	0.70	-0.1 ±0.25	0.01	0.68	-0.19 ±0.23	0.02	0.42	-0.04 ±0.25	0.00	0.87
1700-1749	-0.35 ±0.18	0.09	0.06	-0.07 ±0.19	0.00	0.72	0.11 ±0.2	0.01	0.60	0.07 ±0.2	0.00	0.72	0.27 ±0.18	0.05	0.14	-0.22 ±0.2	0.03	0.27	-0.1 ±0.2	0.01	0.59	0.15 ±0.18	0.01	0.43	0.1 ±0.2	0.01	0.61	0.1 ±0.19	0.01	0.60	0.1 ±0.18	0.01	0.57
1750-1799	-0.09 ±0.11	0.01	0.42	-0.1 ±0.1	0.02	0.37	-0.09 ±0.1	0.02	0.36	-0.12 ±0.1	0.03	0.25	-0.04 ±0.1	0.00	0.68	-0.15 ±0.1	0.05	0.14	-0.06 ±0.1	0.01	0.54	**0.24 ±0.1**	**0.11**	**0.02**	**0.28 ±0.1**	**0.15**	**<0.01**	0.18 ±0.1	0.06	0.09	0.23 ±0.1	0.10	0.03
1800-1849	0.05 ±0.08	0.01	0.54	0 ±0.08	0.00	0.97	-0.01 ±0.08	0.00	0.91	0.04 ±0.08	0.00	0.63	**0.16 ±0.08**	**0.08**	**0.05**	0.04 ±0.08	0.01	0.61	0.14 ±0.08	0.06	0.09	0.08 ±0.08	0.02	0.36	0.05 ±0.08	0.01	0.56	-0.1 ±0.08	0.03	0.22	-0.12 ±0.08	0.04	0.16
1850-1899	-0.05 ±0.11	0.00	0.65	-0.01 ±0.11	0.00	0.94	-0.06 ±0.11	0.01	0.61	-0.12 ±0.12	0.02	0.32	-0.11 ±0.12	0.02	0.34	-0.19 ±0.12	0.05	0.11	0.05 ±0.12	0.00	0.67	-0.02 ±0.12	0.00	0.85	0.05 ±0.12	0.00	0.69	-0.02 ±0.12	0.00	0.86	0.07 ±0.12	0.01	0.58
1900-1949	0.08 ±0.1	0.02	0.42	-0.04 ±0.1	0.00	0.72	0.01 ±0.1	0.00	0.95	-0.08 ±0.1	0.02	0.44	-0.12 ±0.09	0.04	0.19	-0.08 ±0.1	0.02	0.41	-0.03 ±0.1	0.00	0.80	-0.1 ±0.1	0.03	0.31	-0.06 ±0.1	0.01	0.55	-0.02 ±0.1	0.00	0.83	**-0.2 ±0.1**	**0.09**	**0.05**
1950-2000	0 ±0.1	0.00	1.00	-0.12 ±0.09	0.04	0.22	0.06 ±0.1	0.01	0.55	0.02 ±0.09	0.00	0.82	0.04 ±0.09	0.01	0.63	-0.03 ±0.1	0.00	0.74	0.02 ±0.09	0.00	0.87	0.12 ±0.09	0.04	0.20	-0.04 ±0.09	0.01	0.66	-0.06 ±0.1	0.01	0.53	-0.06 ±0.1	0.01	0.59

Slope units: °C per NAO unit

Interval	NAO before BWT															NAO and BWT on same year			NAO after BWT															
	Lag -5			Lag -4			Lag -3			Lag -2			Lag -1			Lag 0			Lag +1			Lag +2			Lag +3			Lag +4			Lag +5		
	Slope ±Std Er.	r²	p	Slope ±Std Er.	r²	p	Slope ±Std Er.	r²	p	Slope ±Std Er.	r²	p	Slope ±Std Er.	r²	p	Slope ±Std Er.	r²	p	Slope ±Std Er.	r²	p	Slope ±Std Er.	r²	p	Slope ±Std Er.	r²	p	Slope ±Std Er.	r²	p	Slope ±Std Er.	r²	p
1659-1699	0.29 ±0.29	0.03	0.33	0.41 ±0.3	0.05	0.19	0.06 ±0.31	0.00	0.84	0.27 ±0.46	0.01	0.56	-0.35 ±0.3	0.04	0.25	**0.62 ±0.29**	**0.12**	**0.04**	0.39 ±0.31	0.04	0.22	0.36 ±0.32	0.04	0.26	-0.03 ±0.49	0.00	0.95	0 ±0.31	0.00	0.99	0.19 ±0.55	0.00	0.73
1700-1749	0.04 ±0.2	0.00	0.85	0 ±0.19	0.00	0.99	0.01 ±0.19	0.00	0.94	-0.2 ±0.19	0.03	0.30	0.27 ±0.18	0.05	0.14	-0.19 ±0.2	0.02	0.35	-0.09 ±0.19	0.01	0.63	0.1 ±0.19	0.01	0.59	0.11 ±0.19	0.01	0.57	0.06 ±0.21	0.00	0.76	0.04 ±0.18	0.00	0.83
1750-1799	0.01 ±0.1	0.00	0.91	-0.08 ±0.1	0.01	0.40	-0.13 ±0.09	0.04	0.17	-0.17 ±0.09	0.06	0.08	-0.06 ±0.1	0.01	0.56	0.07 ±0.1	0.01	0.44	0.09 ±0.1	0.01	0.35	-0.04 ±0.1	0.00	0.72	-0.02 ±0.1	0.00	0.82	-0.1 ±0.11	0.02	0.35	-0.09 ±0.11	0.02	0.40
1800-1849	0 ±0.07	0.00	0.96	-0.15 ±0.07	0.10	0.03	**-0.13 ±0.07**	**0.08**	**0.05**	**-0.18 ±0.06**	**0.14**	**<0.01**	**-0.18 ±0.06**	**0.14**	**<0.01**	**-0.16 ±0.07**	**0.11**	**0.02**	-0.09 ±0.07	0.03	0.20	-0.06 ±0.07	0.02	0.33	-0.05 ±0.07	0.01	0.44	-0.01 ±0.06	0.00	0.86	-0.03 ±0.06	0.00	0.63
1850-1899	0.12 ±0.09	0.04	0.17	0.07 ±0.09	0.01	0.42	**0.2 ±0.09**	**0.08**	**0.04**	0.03 ±0.1	0.00	0.74	**0.22 ±0.1**	**0.09**	**0.03**	**0.24 ±0.1**	**0.11**	**0.02**	0.04 ±0.1	0.00	0.67	0.12 ±0.1	0.03	0.23	0.05 ±0.1	0.01	0.61	0.03 ±0.1	0.00	0.78	**0.28 ±0.09**	**0.17**	**<0.01**
1900-1949	0.15 ±0.09	0.06	0.13	0.09 ±0.1	0.02	0.40	-0.09 ±0.09	0.02	0.34	-0.06 ±0.09	0.01	0.55	-0.07 ±0.09	0.02	0.44	-0.13 ±0.09	0.06	0.12	-0.15 ±0.09	0.08	0.08	**-0.22 ±0.08**	**0.17**	**<0.01**	-0.07 ±0.09	0.01	0.47	0.02 ±0.09	0.00	0.86	0.1 ±0.1	0.02	0.32
1950-2000	0.11 ±0.09	0.03	0.24	-0.03 ±0.09	0.00	0.72	-0.14 ±0.09	0.06	0.12	-0.15 ±0.09	0.06	0.12	-0.08 ±0.1	0.01	0.46	0.19 ±0.09	0.09	0.05	0.08 ±0.09	0.02	0.37	0.12 ±0.09	0.04	0.18	0.06 ±0.1	0.01	0.55	0 ±0.09	0.00	0.99	0.01 ±0.08	0.00	0.90

Slope units: °C per NAO unit

Table S5. As Table S2 but for NAO$_{Gro}$

Interval	NAO before BWT															NAO and BWT on same year			NAO after BWT															
	Lag -5			Lag -4			Lag -3			Lag -2			Lag -1			Lag 0			Lag +1			Lag +2			Lag +3			Lag +4			Lag +5		
	Slope ±Std Er.	r²	p	Slope ±Std Er.	r²	p	Slope ±Std Er.	r²	p	Slope ±Std Er.	r²	p	Slope ±Std Er.	r²	p	Slope ±Std Er.	r²	p	Slope ±Std Er.	r²	p	Slope ±Std Er.	r²	p	Slope ±Std Er.	r²	p	Slope ±Std Er.	r²	p	Slope ±Std Er.	r²	p
1659-1699	0.2 ±0.26	0.02	0.46	0.46 ±0.27	0.08	0.09	0.26 ±0.27	0.03	0.35	0.4 ±0.32	0.04	0.22	-0.03 ±0.31	0.00	0.93	**0.69 ±0.24**	**0.19**	**<0.01**	0.34 ±0.28	0.04	0.23	0.32 ±0.27	0.04	0.24	0 ±0.34	0.00	0.99	-0.06 ±0.27	0.00	0.82	-0.15 ±0.36	0.01	0.69
1700-1749	-0.24 ±0.29	0.02	0.41	-0.16 ±0.27	0.01	0.56	0.03 ±0.28	0.00	0.92	0.04 ±0.29	0.00	0.90	0.43 ±0.27	0.05	0.13	-0.32 ±0.33	0.02	0.33	-0.07 ±0.28	0.00	0.82	0.43 ±0.27	0.06	0.11	0.08 ±0.27	0.00	0.78	0.07 ±0.29	0.00	0.80	0.03 ±0.25	0.00	0.89
1750-1799	-0.06 ±0.17	0.00	0.71	-0.02 ±0.17	0.00	0.91	**-0.32 ±0.15**	**0.09**	**0.04**	**-0.55 ±0.14**	**0.25**	**<0.01**	-0.13 ±0.16	0.01	0.40	0.01 ±0.16	0.00	0.97	-0.09 ±0.16	0.01	0.56	0.19 ±0.16	0.03	0.25	0.28 ±0.17	0.06	0.10	0.07 ±0.17	0.00	0.70	0.01 ±0.17	0.00	0.96
1800-1849	0.13 ±0.15	0.02	0.39	-0.18 ±0.15	0.03	0.24	-0.21 ±0.15	0.04	0.18	-0.11 ±0.15	0.01	0.48	-0.1 ±0.15	0.01	0.50	-0.19 ±0.15	0.03	0.21	0.01 ±0.15	0.00	0.93	0.03 ±0.14	0.00	0.85	0.01 ±0.14	0.00	0.95	-0.14 ±0.14	0.02	0.34	-0.19 ±0.14	0.04	0.18
1850-1899	0.19 ±0.15	0.03	0.21	0.11 ±0.15	0.01	0.49	0.17 ±0.16	0.02	0.30	0.11 ±0.17	0.01	0.52	0.31 ±0.17	0.07	0.07	0.11 ±0.17	0.01	0.53	0.21 ±0.17	0.03	0.23	0.25 ±0.17	0.04	0.14	0.15 ±0.17	0.02	0.39	0.11 ±0.17	0.01	0.51	0.27 ±0.17	0.05	0.11
1900-1949	0.25 ±0.18	0.05	0.16	0.1 ±0.18	0.01	0.59	-0.08 ±0.18	0.00	0.67	-0.21 ±0.17	0.03	0.24	-0.22 ±0.17	0.04	0.20	-0.32 ±0.17	0.08	0.07	**-0.32 ±0.16**	**0.09**	**0.05**	**-0.48 ±0.16**	**0.19**	**<0.01**	-0.23 ±0.17	0.04	0.19	-0.05 ±0.18	0.00	0.77	-0.33 ±0.18	0.08	0.07
1950-2000	0.23 ±0.16	0.05	0.16	-0.02 ±0.16	0.00	0.92	-0.13 ±0.16	0.02	0.43	-0.18 ±0.17	0.03	0.30	-0.06 ±0.18	0.00	0.75	0.24 ±0.16	0.05	0.14	0.18 ±0.16	0.03	0.25	**0.45 ±0.15**	**0.18**	**<0.01**	0.14 ±0.16	0.02	0.38	0.08 ±0.16	0.01	0.61	-0.02 ±0.16	0.00	0.89

Slope units: °C per NAO unit

4.7.3 Years in each quintile

Table S6. Years represented in each NAO quintile analysed.

NAO season	NAO quintile					NAO season	NAO quintile				
	Q1	Q2	Q3	Q4	Q5		Q1	Q2	Q3	Q4	Q5
NAO_{DJF}	1879	1875	1873	1872	1882	NAO_{JJA}	1872	1871	1875	1874	1873
	1881	1876	1877	1874	1894		1877	1883	1879	1881	1876
	1888	1880	1884	1878	1904		1878	1884	1892	1889	1882
	1895	1886	1885	1883	1915		1880	1887	1895	1894	1886
	1900	1891	1892	1887	1920		1885	1897	1896	1913	1890
	1902	1893	1897	1889	1923		1888	1898	1900	1925	1909
	1929	1896	1903	1890	1925		1891	1908	1901	1927	1914
	1932	1899	1905	1898	1930		1893	1910	1905	1930	1919
	1936	1901	1911	1908	1931		1899	1911	1920	1936	1923
	1963	1912	1914	1909	1961		1902	1912	1926	1950	1924
	1964	1919	1924	1910	1973		1903	1929	1932	1965	1933
	1965	1926	1927	1913	1974		1904	1931	1934	1969	1935
	1968	1933	1928	1916	1983		1915	1937	1962	1972	1938
	1969	1947	1934	1937	1984		1916	1947	1970	1974	1946
	1977	1948	1935	1949	1989		1928	1948	1971	1979	1954
	1978	1962	1938	1950	1994		1949	1963	1977	1983	1961
	1979	1971	1946	1954	1995		1968	1964	1981	1985	1973
	1985	1982	1970	1981	1999		1986	1978	1982	1989	1988
	1987	1986	1972	1990	2000		1987	1980	1984	1994	1990
	1996	1992	1980	1991			1995	1997	1991	1996	1992
	1997	1998	1988	1993			1999	2000	1993	1998	
NAO_{MAM}	1871	1873	1872	1874	1885	NAO_{Gro}	1871	1872	1884	1876	1873
	1877	1875	1879	1876	1890		1877	1875	1885	1879	1874
	1881	1878	1880	1882	1894		1878	1883	1894	1886	1882
	1883	1884	1900	1889	1896		1880	1891	1901	1889	1890
	1886	1888	1902	1895	1897		1881	1892	1905	1896	1913
	1887	1891	1919	1898	1903		1887	1898	1908	1897	1914
	1892	1901	1923	1905	1904		1888	1911	1909	1903	1920
	1893	1916	1926	1908	1912		1893	1912	1910	1904	1923
	1899	1932	1927	1910	1913		1895	1916	1919	1924	1934
	1909	1933	1937	1911	1914		1899	1929	1927	1925	1935
	1915	1936	1938	1930	1920		1900	1932	1930	1946	1938
	1924	1961	1946	1934	1925		1902	1933	1937	1948	1950
	1928	1968	1950	1947	1949		1915	1936	1964	1970	1954
	1929	1969	1954	1948	1963		1926	1947	1971	1972	1961
	1931	1974	1965	1964	1972		1928	1949	1973	1974	1963
	1935	1981	1970	1971	1982		1931	1962	1977	1979	1982
	1962	1984	1977	1978	1986		1968	1965	1981	1983	1989
	1973	1987	1985	1979	1989		1987	1969	1984	1988	1990
	1980	1988	1993	1983	1992		1993	1978	1985	1991	1992
	1996	1995	1998	1990	1994		1995	1980	1986	1998	1994
	1997	2000	1999	1991			1997	1996	1999	2000	

5. 8.2 KA EVENT NORTH SEA HYDROGRAPHY DETERMINED BY BIVALVE SHELL STABLE ISOTOPE GEOCHEMISTRY

Juan Estrella-Martínez[1], Philippa L. Ascough[2], Bernd R. Schöne[3], James D. Scourse[4], and Paul G. Butler[4]

[1]School of Ocean Sciences, Bangor University, Bangor, Wales, UK.

[2]NERC Radiocarbon Facility, Scottish Universities Environmental Research Centre, East Kilbride, Scotland, UK.

[3]Institute of Geosciences, Johannes Guttenberg University, Mainz, Germany.

[4]College of Life and Environmental Sciences, University of Exeter, Penryn, Cornwall, UK.

5.1 Abstract

The abrupt 8.2 ka cold event has been widely described from Greenland and North Atlantic records. However, its expression in shelf seas is poorly documented, and the temporal resolution of most marine records is inadequate to precisely determine the chronology of major events. A robust hydrographical reconstruction can provide an insight on climatic reaction times to perturbations to the Atlantic Meridional Overturning Circulation. Here we present an annually-resolved temperature and water column stratification reconstruction based on stable isotope geochemistry of *Arctica islandica* shells from the Fladen Ground (northern North Sea) temporally coherent with Greenland ice core records. Our age model is based on a growth increment chronology obtained from four radiometrically-dated shells covering the 8290-8100 cal BP interval. Our results indicate that a sudden sea level rise (SSLR) event-driven column stratification occurred between ages 8320-8220 cal BP. Thirty years later, cold conditions inhibited water column stratification but an eventual incursion of sub-Arctic waters into the North Sea re-established density-driven stratification. The water temperatures reached their minimum of ~3.8 °C 55 years after the SSLR. Intermittently-mixed conditions were later established when the sub-Arctic waters receded.

5.2 Introduction

The 8.2 ka (before 1950 CE) cold event is usually defined by lower stable oxygen isotope values and a reduced ice accumulation rate in Greenland ice cores (Rasmussen et al., 2007). Although this event has been extensively described in the context of the Greenland ice cores and across the wider North Atlantic (Came et al., 2007; Ellison et al., 2006; Rasmussen et al., 2007; Thomas et al., 2007; Thornalley et al., 2009), its expression in the Atlantic shelf seas is less well documented (Herrle et al., 2018; Klitgaard-Kristensen et al., 1998). Here we present an annually-resolved reconstruction of the environmental conditions prevalent in the northern North Sea (Figure 5.1) based on stable isotope geochemistry from radiocarbon-dated ocean quahog (*Arctica islandica*) shells centred around the 8.2 ka event.

The shell of the bivalve mollusc *A. islandica* is a key annually-resolved marine climatological archive for the North Atlantic margins (Reynolds et al., 2016). The shells of *A. islandica* are common in the fossil record and readily dated by radiocarbon. The stable oxygen isotope composition (δ^{18}O) of the shell reflects the δ^{18}O of the water where the animal lived (Weidman et al., 1994) while the stable carbon isotope composition (δ^{13}C) of the shell shows a consistent offset from the δ^{13}C of the dissolved inorganic carbon of the water column (Beirne et al., 2012; Schöne et al., 2011a). Robust growth increment chronologies can be built from the annual increments in the *A. islandica* shell (Butler et al., 2009a; Estrella-Martínez et al., 2019;

Schöne et al., 2003; Scourse et al., 2006a), providing an accurate and annually-resolved chronological template for stable isotope data.

With this study we aim to determine the timing and causes of water column stratification in the North Sea in and around the 8.2 ka event, to reconstruct water temperatures during the 8.2 ka event and to establish an order of events registered in the North Sea in and around the 8.2 ka event. By comparing our reconstruction against Greenland ice core records we will also provide evidence against the hypothesis of a large asynchrony between the International Radiocarbon Calibration Curve (IntCal13) and the Greenland Ice Core Chronology 2005 (GICC05) proposed by Torbenson et al. (2015). As the first attempt to apply high resolution molluscan sclerochronological techniques to determine early Holocene environmental conditions this contribution constitutes a novel application of *A. islandica* sclerochronology.
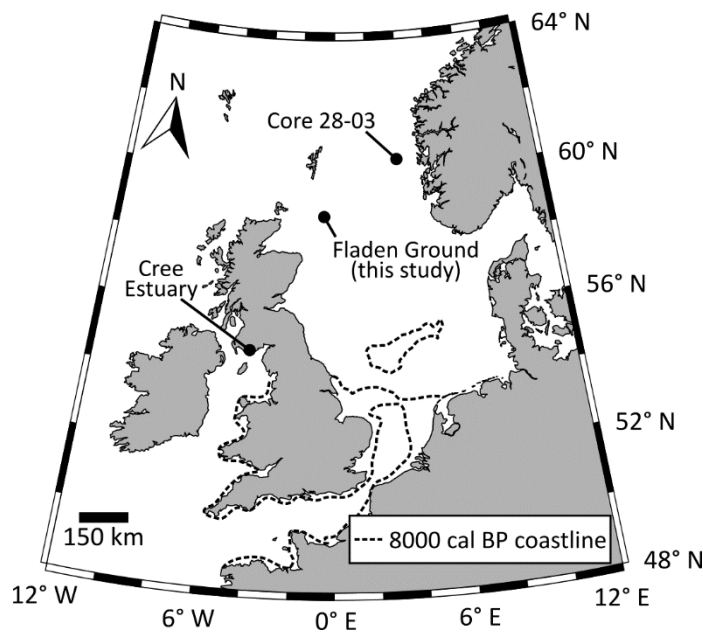
Figure 5.1 Approximate location of the sites mentioned in this work.
The dashed line represents the approximate location of the coastline in 8000 cal BP (Sturt et al., 2013).

5.3 METHODS

The *A. islandica* shells used in this study were collected from the Fladen Ground in the northern North Sea at 58.831° N, -0.356° E at a depth of 115 m. The collection was acquired by the RV *Scotia* as part of the EU HOLSMEER (Scourse et al., 2006b) project in 2001. A total of ten shells with heights >70.0 mm and taphonomic characteristics that suggested the specimens were ancient (Nielsen, 2004) were selected. These were sectioned using standard sclerochronological procedures (Butler et al., 2009a; Scourse et al., 2006a). Polished shell sections were viewed under reflected light, and the imaging software package ImagePro

Premier 9.1 was used to identify and measure the growth increments in the outer layer of the ventral margin of the shell.

Radiocarbon dating was carried out on the edge of the ventral shell portion (deposited in late ontogeny) of the ten shells. To achieve the optimal carbonate mass required for accelerator mass spectrometry dating, it was necessary to cut samples that integrate the final years of growth. Precisely determining the number of years integrated in each sample was not possible since the age and length are related by a non-linear function (Murawski et al., 1982). We used a working approximation of 30 years. The material was submitted for preparation and measurement to the Natural Environment Research Council Radiocarbon Laboratory at East Kilbride, United Kingdom, where it was processed using the methods described by Butler et al. (2009b) prior to ^{14}C analysis.

Calibration of radiocarbon ages was achieved with OxCal 4.3 (Bronk Ramsey, 2009). We used the Marine13 calibration curve (Reimer et al., 2013) which provides a time-dependant offset from the atmospheric IntCal13 curve for the global ocean, and applied a local correction (ΔR) of 64 $\pm$ 41 ^{14}C yr (Ascough et al., 2017). The dated specimens were put in relative stratigraphic order and crossmatched with each other following the methods described by Butler et al. (2009a), Estrella-Martínez et al. (2019) and Scourse et al. (2006a). Two growth increment chronologies (GIC) were built using ARSTAN (Cook and Krusic, 2014) also following the methods described by Butler et al. (2009a), Estrella-Martínez et al. (2019) and Scourse et al. (2006a). Once crossmatched, the calibrated age range was constrained using the tree ring sequence built into OxCal 4.3 (Bronk Ramsey et al., 2001). The chronologies developed here only function as a stratigraphic template on which to base the stable isotope geochemical results and are not examined in their own right.

The strength of the chronologies was analysed with the standard dendrochronology and sclerochronology statistic EPS which measures the variance explained by a finite subsample of a population chronology (Wigley et al., 1984). The EPS is a function of the number of shells contributing to the chronology (sample depth) and the average correlation between shell pairs. A high EPS is usually interpreted as indicating the presence of a strong common environmental signal in the growth increment series of the sampled shell population. An EPS of 0.85 is commonly used as a threshold to indicate that a chronology is reasonably representative of the whole population (Buras, 2017; Wigley et al., 1984). In this case the EPS was calculated in a 30-year sliding window.

Three of the four shells belonging to the most recent chronology were selected for isotopic analysis at annual resolution. The selection was based on temporal coverage of the individual shells and their taphonomic state, with preference given to the shells that showed the least erosion, the broadest increments and those that provided at least 10 years of temporal overlap between shell pairs. Milling was carried out on the ventral margin on the outer layer of each shell at the School of Ocean Sciences, Bangor University, using a computerised New Wave/Elemental Scientific micromill system fitted with a spherical tungsten carbide dental burr with a diameter of 300 μm at the tip. Rotation speed was limited to 12% (4,450 rpm) to minimise $CaCO_3$ polymorph transformation (Foster et al., 2008). The entirety of the outer layer in each annual increment was milled between the growth lines to an average depth of 100 μm.

All the powder extracted from a given increment was thoroughly homogenized before an aliquot of the sample was isotopically characterised at the Institute of Geosciences, University of Mainz (Germany) following the methods described by Colonese et al. (2017). Isotope data showed a 1σ external reproducibility (accuracy based on 421 NBS-19 samples) better than 0.04 ‰ for $\delta^{18}O$ and 0.03 ‰ for $\delta^{13}C$ and average internal precision of 0.09 ‰ for $\delta^{18}O$ and 0.04 ‰ for $\delta^{13}C$. Both isotope values were reported as per mil deviations relative to the Vienna Pee Dee Belemnite (VPDB) standard. No correction for different acid fractionation factors of shells samples (aragonite) and the reference material (calcite) was applied (Füllenbach et al., 2015).

We inspected the results against the average peak intensity given by the mass spectrometer and rejected those that showed abnormally high/low isotope values and those with intensities falling significantly outside the range of the reference materials that were not paired with a higher intensity sample. The $\delta^{18}O$ and $\delta^{13}C$ results were weight-averaged into single series before further analysis. The weights were given by $1/\sigma^2$ where σ represents the internal precision for each sample which is affected by the peak intensity.

$\delta^{18}O$ and $\delta^{13}C$ values in intervals where an extended (>10 yr) noticeable change in average occurred were checked for normality using the Shapiro-Wilk W score (Adefisoye et al., 2016). The average values in these intervals were compared using a two-tailed t-test and the variance was compared using an F-test. We also assessed the significance of linear trends in these intervals.

We approximated the long-term variability in $\delta^{13}C$ using a weighted Fourier regression consisting of the largest two coefficients. The weights were given by $1/\sigma^2$ where σ represents the internal precision for each sample. To emphasise the high frequency variability in $\delta^{13}C$, we subtracted the Fourier regression from the weight-averaged results.

We compared our data to the *N. pachyderma* (s) abundance record developed by Klitgaard-Kristensen et al. (1998) from sediment core 28-03 (60.867° N, 3.733° E) which covers the 8.2 ka event in the northern North Sea with an average temporal resolution of 7 years. The age model for this core was updated using the Marine13 calibration curve (Reimer et al., 2013) with a local ΔR correction of 64 ± 41 ^{14}C yr (Ascough et al., 2017). We arbitrarily used the median of each re-calibrated age range and converted core depth by linearly interpolating the dates. We also compared our results to the sudden relative sea level rise (SSLR) data derived from terrestrial cores from the Cree Estuary, south west Scotland (Lawrence et al., 2016).

5.4 RESULTS

5.4.1 Radiocarbon Calibration and Chronologies

The 2σ calibrated radiocarbon ages of our samples place the age of death of the bivalves into two temporal ranges: 8960-8540 cal BP and 8350-7990 cal BP (Table 1). For ease of analysis, we arbitrarily selected the median calibrated age for each shell as a reference point upon which to base the results and discussion. The reader is cautioned, however, that the calibration ranges are not necessarily normally distributed. Based on this assumption, our chronologies cover the intervals of 8860-8690 cal BP with possible range of ±164 years (8.7 ka chronology) and 8290-8080 cal BP (sclero ages 1-207) with possible range of ±106 years (8.2 ka chronology, "8.2kC", Figure 5.2a). The ±106 yr age range is applicable to all further references to dates derived from 8.2kC. The temporal uncertainty of the calibrated ranges rules out the possibility of merging the two floating chronologies into a single one. We thus made the choice of concentrating this investigation on 8.2kC. The 8.7 ka chronology and statistics can be found in Section 5.7.
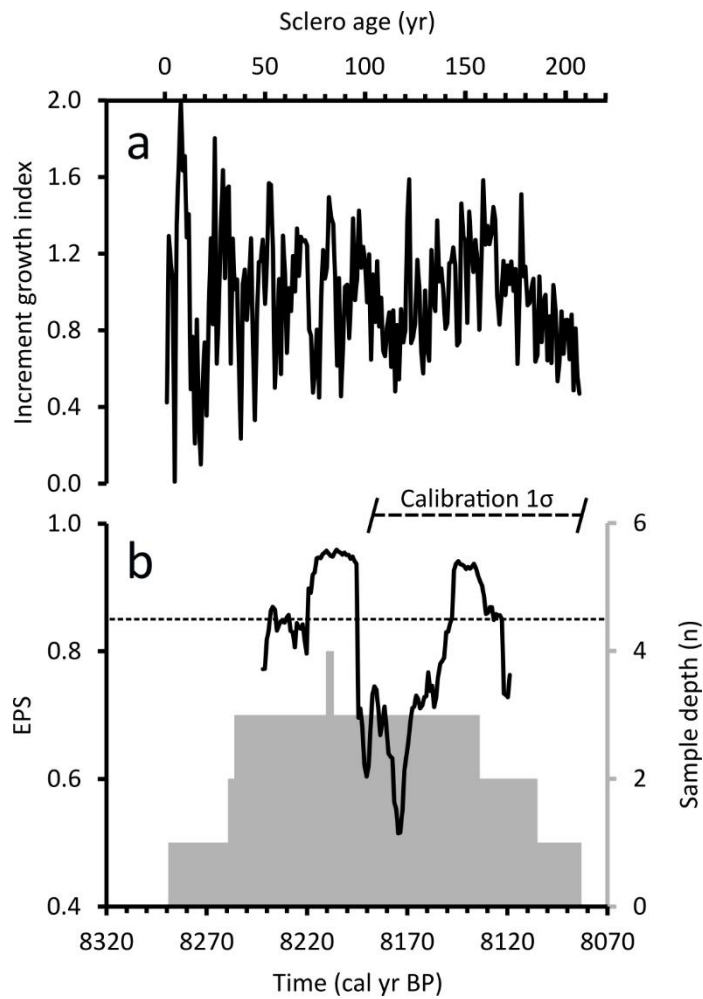
Figure 5.2 8.2kC and associated statistics. Growth increment chronology produced from the shells collected at the Fladen Ground (a). The chronology has a total sample depth of four shells and an average EPS of 0.81 (b).

The average expressed population signal (EPS; Wigley et al., 1984) score of 8.2kC is 0.81 and the 30-yr running EPS lies above the 0.85 threshold in sclero ages 52-61, 71-95, and 143-168 for a total of 49% of the calculated window (Figure 5.2b). The lowest EPS score occurred when multiple specimens settled within a short time span combined with times of extended lower than average increment growth in other shells already contained in the chronology.

Table 1. Radiocarbon dating results and calibration.

Laboratory ID	Shell ID (010…)	Radiocarbon age ± 1σ (^{14}C yr BP)	Time gap (yr)	2σ calibrated range (cal yr BP)	Bayesian range (cal yr BP)
SUERC-8459	705	8356 ± 28	9	8990 - 8650	8960 - 8640
SUERC-8314	711	8332 ± 28	15	8970 - 8630	8950 - 8630
SUERC-8056	653	8306 ± 29	58	8950 - 8600	8940 - 8610
SUERC-8060	655	8275 ± 28	6	8930 - 8570	8880 - 8550
SUERC-8277	671	8247 ± 27	9	8880 - 8540	8880 - 8550
SUERC-8272	669	8231 ± 29	-	8860 - 8510	8870 - 8540
SUERC-8290	682	7794 ± 24	78	8320 - 8060	8350 - 8140
SUERC-8063	658	7810 ± 25	24	8340 - 8100	8270 - 8060
SUERC-8065	660	7801 ± 29	22	8330 - 8070	8250 - 8040
SUERC-8292	684	7752 ± 23	-	8280 - 8020	8200 - 7990

5.4.2   Annual stable isotope geochemistry

We obtained annual δ^{18}O and δ^{13}C results from three shells in 8.2kC covering sclero ages 5-186, equivalent to the interval 8286 – 8105 cal BP (Figure 5.3a, Figure 5.3b). We achieved a temporal overlap of 13 years between the first and second shell and an overlap of 21 years between the second and third shell. We were not able to extend the isotopic series to cover the entirety of the chronology as single-increment sampling becomes increasingly difficult in later ontogeny. Following our sample-rejection convention, we obtained 175 out 182 years sampled for δ^{18}O but complete temporal coverage for δ^{13}C. The composite (non-averaged) δ^{18}O results fall within the range of 3.87 ‰ to 2.23 ‰, the former occurring in sclero age 107 and the latter in sclero age 152. Similarly, the composite δ^{13}C results fall within the range of 3.08 ‰ to 1.15 ‰, the former occurring in sclero age 52 and the latter in sclero age 106.

The weight-averaged δ^{18}O results (Figure 5.3A) can be divided into three intervals that show distinct average values and variance: sclero ages 5-50 (i1), 51-90 (i2), and 91-186 (i3). i1 has an average of 3.07 ‰, a variance of 0.03 ‰^{2} and shows a small but significant positive trend of 0.04 ‰ decade^{-1}. i2 shows an average of 3.34 ‰ and a variance of 0.03 ‰^{2}. Finally, i3 has an average δ^{18}O value of 3.04 ‰ and a variance of 0.05 ‰^{2}. The δ^{18}O values in all three intervals are normally distributed after the removal of one extreme value in each: the maximum value in i1 (W = 0.94, p = 0.05), the three maxima in i2 (W = 0.94, p = 0.05) and the

minimum in i3 (W = 0.98, p = 0.09). A two-tailed t-test on the modified values shows that the i1-i2 and i2-i3 changes in average are significant but the changes in variance are not (F-test).
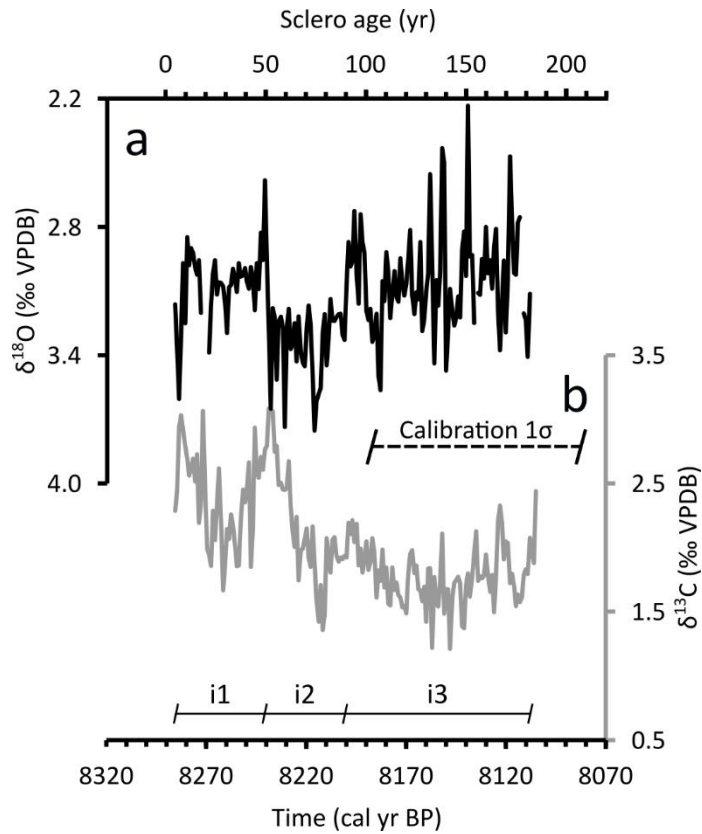
Figure 5.3 Stable isotope geochemistry. Annual weight-averaged $\delta^{18}O$ (**a**) and $\delta^{13}C$ (**b**) results. Notice inverted axis in **a**. Values in **a** can be divided into three intervals that show distinct average values and variance: Sclero ages 5-50 (i1), 51-90 (i2), and 91-186 (i3).

Using the same interval definitions, the weight-averaged $\delta^{13}C$ results (Figure 5.3B) also show distinct average values and variance. i1 has an average of 2.39 ‰ and variance of 0.13 ‰^{2}. i2 shows an average of 2.17 ‰, a variance of 0.21 ‰^{2} and a significant linear trend of -0.03 ‰ yr^{-1}. Finally, i3 has an average $\delta^{13}C$ value of 1.79 ‰, a variance of 0.05 ‰^{2} and no significant linear trend. The $\delta^{13}C$ values in all three intervals are normally distributed without alteration and a two-tailed t-test shows that the i1-i2 and i2-i3 changes in average are significant but only the i2-i3 change in variance is significant (F-test).

The Fourier $\delta^{13}C$ residuals (Figure 5.4) show distinct average properties in the defined intervals as well. i1 has an average of -0.05 ‰ and variance of 0.12 ‰^{2}. i2 shows an average of -0.06 ‰ and a variance of 0.14 ‰^{2}. Finally, the residuals show an average value of 0.04 ‰ and a variance of 0.04 ‰^{2} in i3. The residuals are normally distributed in all three intervals without alteration. The two-tailed t-test shows no significant in change in average and an F-test shows only the i2-i3 change in variance to be significant.

The calibrated age of interval i1 overlaps with a SSLR event identified at the Cree Estuary (black diamond and whiskers in Figure 5.4; Lawrence et al., 2016). The possible age range for the SSLR event also overlaps with the calibrated age of i2 which coincides with a sudden *Neogloboquadrina pachyderma* (sinistral coiled, "s") abundance increase in the far-north North Sea which is identified as the 8.2 ka event (average re-calibrated 2σ temporal range: ±158 years, Figure 5.4; Klitgaard-Kristensen et al., 1998). During i2, the maximum (minimum) δ^{18}O (δ^{13}C) correspond with the maximum *N. pachyderma* (s) abundance in the core 28-03 (Klitgaard-Kristensen et al., 1998). By the start of i3 the *N. pachyderma* (s) levels in the North Sea had already returned to their background levels.

5.5 DISCUSSION

The EPS in the newly developed chronologies does not generally achieve the recommended threshold of 0.85(Wigley et al., 1984). The low EPS values shown in 8.2kC are likely due to the erratic juvenile growth of two specimens that make up its mid-section combined with lower than average shell growth in the other specimens. One way to avoid this problem is to disregard the first 20-30 years of growth when constructing *A. islandica* chronologies(Butler et al., 2009b) but the exclusion of juvenile years in this study would have meant a shorter chronology and a rather extended initial interval where the chronology would have been represented by only one shell.

Another possible explanation of the lower EPS values is growth increment counting errors where the sample depth is low. It has been shown that a 1% counting error rate can induce high EPS variability while a 5% error rate induces a continuous decrease in EPS for the entirety of the series (Black et al., 2016). Given the relatively high average EPS values for 8.2kC and the fact we observe EPS recoveries through our record, we estimate our counting error rate to be between 1 and 5%. This allows us to confidently base our stable isotopic results on the age model provided by the growth increment chronology.

When interpreting *A. islandica* stable isotope data we must consider the possibility that the organism is actively controlling the isotope composition of its shell ("vital effect"). There is unambiguous evidence that this is not the case for δ^{18}O (Schöne et al., 2005a; Weidman et al., 1994). The evidence is less clear in the case of δ^{13}C. Two studies arrived at conflicting results when examining the *A. islandica* vital effects on δ^{13}C (Butler et al., 2011; Schöne et al., 2005a). However, an analysis of 21 shells from Iceland found that vital effects represent only a small component of the δ^{13}C variability in the first 30 years of the animal's life (Reynolds et al., 2017a). We can therefore make palaeoenvironmental interpretations using both δ^{18}O and δ^{13}C data.

The greater temporal resolution provided by 8.2kC allows the close examination of the environmental conditions in and around the 8.2 ka event in the North Sea. During i1 we observe relatively stable $\delta^{18}O$ values that become slightly higher near sclero age 20, equivalent to 8270 cal BP (Figure 5.3a). The change is easier to observe in $\delta^{13}C$ and in the Fourier $\delta^{13}C$ residuals (Figure 5.4) which show relatively large ^{13}C depletions during the same sclero ages. The slight positive $\delta^{18}O$ deviation can be interpreted either as a modest cooling, a change in $\delta^{18}O_{water}$ or both. This is difficult to assess since there are no quantitative water-mass-independent temperature reconstructions for the North Sea with comparable temporal resolution for the temporal interval in question.

The changes in stable carbon isotope composition starting in i1, however, can be interpreted as the onset of stratification in the northern North Sea. This is because the *A. islandica* data represents a benthic record. During stratified conditions, limited vertical mixing results in a poorly ventilated deeper layer. Because primary production is limited to the shallow photic zone, the deeper layer is enriched in ^{12}C. Shell carbonate precipitated under such conditions would, hence, have a lower $\delta^{13}C$ value (Austin and Scourse, 1997; Purton and Brasier, 1997; Scourse et al., 2002). Large and consistent deviations in the Fourier $\delta^{13}C$ residuals emphasise the higher frequency (sudden) changes in water stratification that can otherwise be masked by the gradual increase in sea level during the early Holocene.

The sudden North Sea water stratification was likely caused by the SSLR identified at the Cree Estuary. This SSLR event, attributed to the second drainage of the Lake Agassiz-Ojibway, had an estimated 0.4 m magnitude at the Cree Estuary (Lawrence et al., 2016). The SSLR date range (8270 ± 53 cal BP, 3σ, Figure 5.4) overlaps with the calibrated date when the Fourier $\delta^{13}C$ residuals suggest stratified conditions initiated at the Fladen Ground during i1 (8270 cal BP, Figure 5.3b). Given modern flushing times, northward Irish/Hebridean Sea currents (Burrows and Thorpe, 1999; Ellett and Edwards, 1983) and the trajectory of the meltwater pulse suggested by Lawrence et al. (2016), it is highly likely that these two events are coeval or that they occurred within a year of each other. Synchronising these two events on the same age has the effect of reducing the 8.2kC dating range to ± 53 years.

The sudden stratification event of our SSLR-synchronised Fourier $\delta^{13}C$ residuals during i2 can be put in context when we compare our record to the North Sea age-recalibrated *N. pachyderma* (s) series (Klitgaard-Kristensen et al., 1998). The authors of that study determined that a brief incursion of sub-Arctic waters pushed the 20% abundance *N. pachyderma* (s) isoline towards the North Sea, extending to the Norwegian west coast. Background conditions broadly similar to modern day were established upon the retreat of the sub-Arctic waters (Klitgaard-Kristensen et al., 1998). We can use this water advection/retreat and

temperature drop assumptions to partially disentangle the temperature and water mass components of the $\delta^{18}O$ proxy in our *A. islandica* shells. Using an updated version of the classical palaeotemperature equation (Section 4.3.4; Grossman and Ku, 1986) with the modern North Sea average (Harwood et al., 2008) $\delta^{18}O_{water}$ value (0.26 ‰ SMOW) we can determine the i3 water temperature. We can then use the estimated 2 °C lower temperatures during the incursion of sub-Arctic waters to determine the average $\delta^{18}O_{water}$ during that interval and repeat the procedure to determine the temperature and $\delta^{18}O_{water}$ prior to the sub-Arctic water incursion (Figure 5.4). Our estimated average $\delta^{18}O_{water}$ (0.03 ‰ SMOW) during the sub-Arctic water incursion into the North Sea suggests that the 20% abundance *N. pachyderma* (s) isoline laid on fresher waters than on present day. This is in agreement with fresher waters being prevalent in higher latitudes during the 8.2 ka event (Quillmann et al., 2012) which, in turn, point to a weakened Atlantic Meridional Overturning Circulation (Ellison et al., 2006; Kleiven et al., 2008).
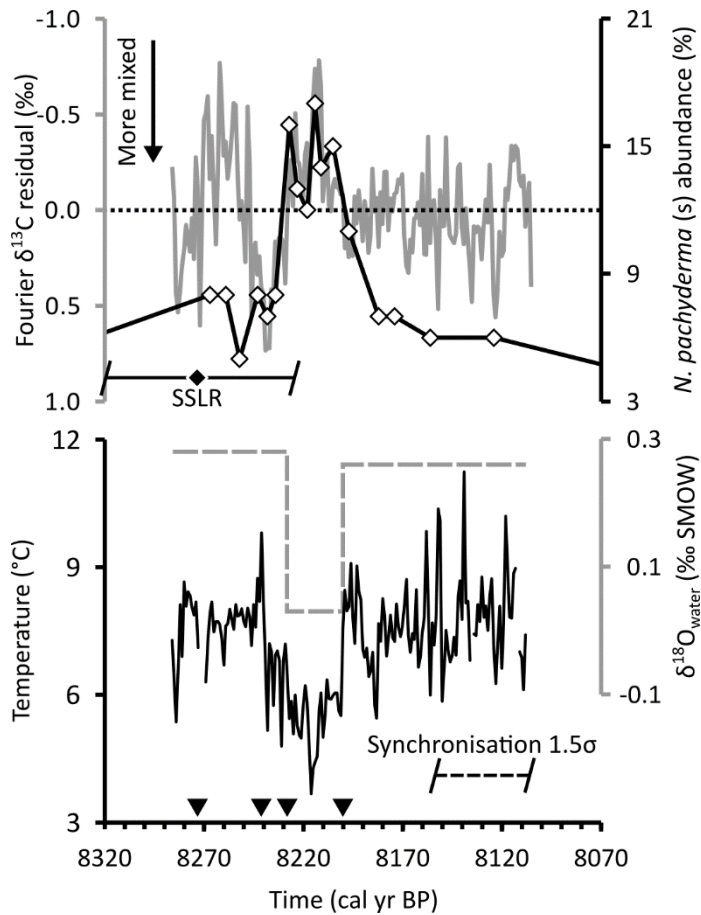
Figure 5.4 Fourier $\delta^{13}C$ residuals (solid grey line, inverted axis) compared with the *N. pachyderma* (s) abundance record from core 28-03 (white diamonds connected by black line, Klitgaard-Kristensen et al., 1998), $\delta^{18}O_{water}$ and temperature reconstruction. The residuals can be interpreted as a relative measure of water column stratification and show to be receptive to sudden sea level rise (black diamond and whiskers, Lawrence et al., 2016) and changes in $\delta^{18}O_{water}$ (dashed grey line). Assumptions from the *N. pachyderma* (s) results can be used to reconstruct water temperature from the data generated in this study (solid black line). The black triangles depict the time when major climatic events were registered at the Fladen Ground (see text).

By synchronising the first sudden stratification event observed in our Fourier $\delta^{13}C$ residuals with the Cree estuary SSLR we can infer the order of events that caused the temperature and $\delta^{18}O_{water}$ changes (events indicated by black triangles in Figure 5.4) in the North Sea: In 8270 ± 53 cal BP a SSLR caused stratified

106

conditions in the northern North Sea. This SSLR was caused by the second drainage of Lake Agassiz-Ojibway (Barber et al., 1999; Hoffman et al., 2012; Renssen et al., 2002, 2001) which forced the 8.2 ka event 30 yr later. This cold event inhibited summer stratification at the Fladen Ground and is associated with the southward extension of sub-Arctic waters. An incursion of fresher sub-Arctic waters into the North Sea (~0.03 ‰ SMOW) occurred 44 years after the SSLR, bringing with it the 20% *N. pachyderma* (s) isoline and a return to water-density driven stratified conditions. The water temperatures in the northern North Sea reached their minimum of 3.7 °C 55 years after the SSLR. Shortly thereafter, the sub-Arctic waters receded and background conditions with intermittently mixed warmer waters were established 70 years after the SSLR.

Due to the lack of highly-resolved marine archives during the 8.2 ka event, we are prevented from carrying out a direct comparison with adjacent oceanic records. We can, however, compare our reconstruction to the semi-annual Greenland ice core records (Thomas et al., 2007) and to a sub-annually-resolved speleothem $\delta^{18}O$ record from central/east China (Liu et al., 2013) that shows dry conditions during the event. These two records co-vary to a high degree and their age uncertainties are comparable with our reconstruction. The order of events and temperature variability suggested by our record is consistent with the "central 8.2 ka event" observed in Greenland ice cores (Thomas et al., 2007), both showing a duration of 70 years. The coldest conditions in both records are offset by 27 years in their respective age models, well within our possible radiocarbon dating range of ±106 years and the SSLR-synchronised dating range of ± 53 years. If the offset is manually eliminated then the two records show a significant positive correlation (r = 0.39, p<0.01). On the other hand, the driest conditions suggested by the U/Th-dated Chinese speleothem record and the coldest temperatures in our reconstruction are offset by 40 years, still within the SSLR-synchronised dating range. The dry event recorded in China also has a duration of 70 years. If the offset is manually eliminated then our temperature reconstruction shows a significant correlation with the Chinese $\delta^{18}O$ record of -0.55 (p<0.001).

The high level of synchrony between our temperature reconstruction and the Greenland ice core record implies that the date proposed by Thomas et al. (2007) as the start of the 8.2 ka event would differ from the SSLR-driven stratification in the North Sea by 1 year. Similarly, the start of the Greenland "central event" and the incursion of sub-Arctic waters into the North Sea would differ by 4 years. The small offset between our reconstruction, the Greenland record and the Chinese speleothem record and the high level of similarity between the three suggests that the GICC05 and the IntCal13 calibration curves are more synchronous than other authors have suggested (Torbenson et al., 2015).

In this study we have developed two *A. islandica* c.200-year-long floating GICs. Radiocarbon dating places these chronologies in the early Holocene and we developed annually-resolved $\delta^{18}O$ and $\delta^{13}C$ series from one of them which is centred around the 8.2 ka event. These series are currently the only high or mid-latitude marine records with such a high temporal resolution, and they suggest that two major water column stratification episodes, separated by 44 years, occurred in the North Sea between 8320 and 8220 cal BP. The first episode is likely to be coeval with a sudden sea level rise registered at the Cree Estuary caused by the second drainage of Lake Agassiz-Ojibway while the second episode was caused by the incursion of sub-Arctic waters into the North Sea. By utilising existing assumptions about water temperature and water mass changes we were able to determine that the bottom water temperature was ~3.8 °C between 8270 and 8160 cal BP, during the height of the 8.2 ka event. Finally, we determined that the drainage of Lake Agassiz-Ojibway, the initial temperature drop, the incursion and the recession of sub-Arctic waters into the North Sea were separated by 30, 14 and 26 years, respectively.

Our reconstruction is highly coherent with Greenland ice core records and provides an insight into the expression of the 8.2 ka event in shelf seas. By using the stratigraphic template provided by the *A. islandica* GIC, it is possible to reconstruct the chronological order of major events with high precision. This information is significant in understanding the reaction times to perturbations of the Atlantic Meridional Overturning Circulation.

5.7.1   8.7 ka chronology
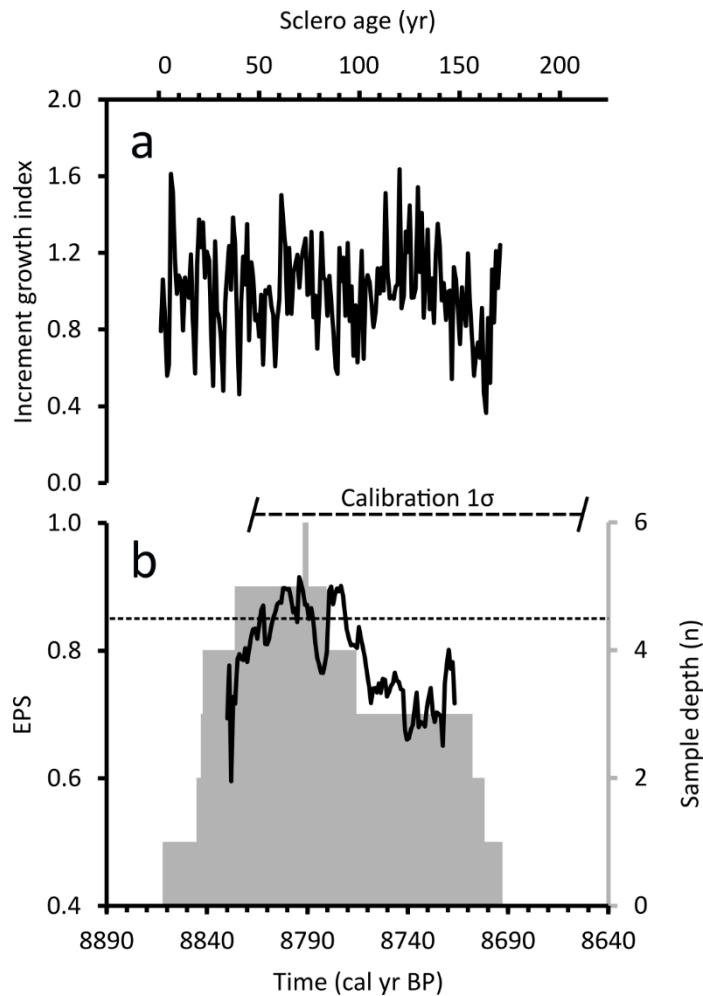
Figure 5.5 8.7 ka chronology (a) and associated statistics (b).

5.7.2   Subsample signal strength of the 8.2 ka chronology

The SSS mirrors the EPS for the complete duration of the record but it is shifted toward more positive values and never crosses below the 0.85 threshold (Figure 5.6). This is due to the relatively small number of shells that make up 8.2kC. The reason that the SSS never reaches negative values lies on its mathematical definition (Section 2.6). Solving the SSS equation for $\bar{r}$ shows that for a chronology composed of 4 shells with the same average sample depth as 8.2kC (3 shells), an $\bar{r}$ value of 0.18 is necessary to obtain an SSS of 0.85. The $\bar{r}$ value for 8.2kC is never smaller than 0.20.
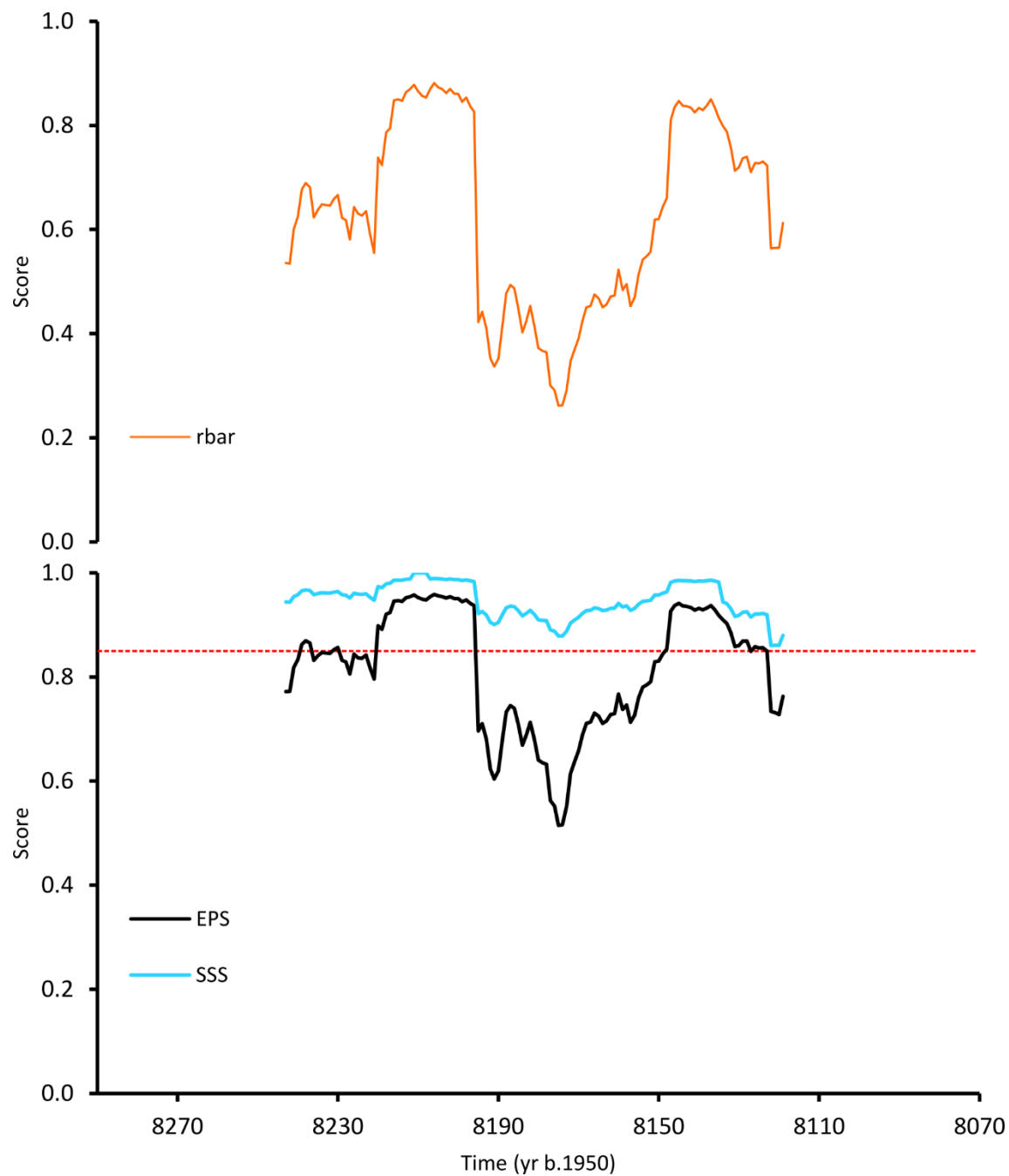
Figure 5.6 Subsample signal strength in relation to r̄ and expressed population signal of the 8.2 ka chronology. The SSS mirrors the EPS for the complete duration of the calculation but its value is always greater than 0.85.

6. SYNTHESIS AND CONCLUSIONS

Primarily, the work within this thesis is dedicated to the reconstruction of past environmental variability in the northern North Sea. The information contributed to the body of knowledge includes the extension of one of the Fladen Ground chronologies developed by Butler et al. (2009a), making it now the longest of its kind in the North Sea. Two additional chronologies were developed using fossil material dated to the early Holocene epoch. Accompanying two of the three chronologies are series of stable isotope geochemical data that allow the probing of the climate and ecosystem functioning of the past. In this section I will discuss the main results of the work presented in this thesis and put in perspective the role of *A. islandica* in high-resolution palaeoceanographic reconstructions. In doing this, I will present evidence that points to the achievement of the objectives presented in Section 1.3.

6.1 MANUSCRIPT SUMMARIES

In Manuscript I (Chapter 3), $\delta^{13}C$ from *A. islandica* shells was examined as a possible proxy for Atlantic herring recruitment in the North Sea. To do so it was first necessary to extend one of the modern *A. islandica* Fladen Ground growth increment chronologies to use it as an age model.

From $\delta^{13}C$ values extracted from the annual increments, it was evident that the anthropogenically-driven ^{13}C depletion in the North Sea, the oceanic Suess effect, started manifesting itself in the 1850s, approximately 100 years after the beginning of the Industrial Revolution. The high frequency variability of the $\delta^{13}C$ series was emphasised by mathematically subtracting the oceanic Suess effect. A significant linear regression between the $\delta^{13}C$/oceanic Suess effect residuals ($\delta^{13}C\dot{S}$) and the $\log_{10}$-transformed maximum diatom count (MD) was found, which was used as a proxy for primary production (Brzezinski et al., 1998; Irigoien et al., 2002). The causal link between $\delta^{13}C\dot{S}$ and MD was determined to be the effect that MD has over the $\delta^{13}C$ of the environmental dissolved inorganic carbon ($\delta^{13}C_{DIC}$) through the preferential uptake of ^{12}C during photosynthesis. This relationship was used to construct an equation that relates $\delta^{13}C\dot{S}$ and MD to

herring recruitment. It was determined that access to nutrition served as the causal link between these quantities. By doing this Objective 1 of Section 1.3 was achieved.

The equation built was successful in reproducing the North Sea herring recruitment levels estimated for the 20th century, shown by comparison with two independent studies. Additionally, the reconstruction was consistent with historical catch statistics from different countries bordering the North Sea going as far back as the 1500s.

This is the very first herring recruitment reconstruction attempted for periods prior to 1950 and, unlike models developed by other researchers, it includes a food web-based mechanism that supports it. This work provides the longer time scale needed to understand the interaction between climatic parameters and stock densities and demonstrates that molluscan sclerochronological records can contribute to the study of ecosystem functioning.

In Manuscript II (Chapter 4) $\delta^{18}O$ from *A. islandica* shells was examined as a water temperature proxy. Although $\delta^{18}O$ in sea water reflects both water temperature and the particular $\delta^{18}O$ signature of the water mass, the assumption of a constant water mass was used. This was based on indications from a comprehensive study at the surface and bottom of the North Sea (Berx and Hughes, 2009) and on instrumental data for the 20th century (ICES, 2014). As the material used for $\delta^{18}O$ analysis comes from the same shells presented in Chapter 3, the age model and uncertainties associated with it are the same. Nevertheless, an additional test of the crossmatch between shell pairs is presented. This test agrees well with the temporal uncertainties estimated in Chapter 3.

The temperature derived from $\delta^{18}O$ was determined to have an average 7.20 °C with a standard deviation of 0.63 °C for the past c. 500 years. This is in good agreement with Berx and Hughes (2009), who found that the waters at the bottom of the Fladen Ground had an annual average temperature between 7.0 and 7.5 °C with a monthly amplitude of 1.0 °C or less. Through this investigation it was possible to suggest a minor correction of the late 19th to late 20th century warming trend of the bottom waters of the North Sea from 0.09 °C ± 0.02 °C decade^{-1} to 0.08 °C ± 0.02 °C decade^{-1}. One additional warming period was found in the bottom water temperature reconstruction between 1640 and 1740 at a rate of 0.05 °C ± 0.02 °C decade^{-1}, while a cooling at a rate of -0.11 °C ± 0.02 °C decade^{-1} was found for the duration of the 19th century. A source for this centennial variability was not found.

The analyses made in Chapter 4 were mainly focussed on examining the effects of atmospheric pressure gradients on the average bottom water temperatures and on the seasonal thermal stratification. The results suggested that only persistent multiyear winter NAO conditions (rather than year-on-year changes in

NAO) affect the average BWT at the Fladen Ground. This analysis assessed the ideas of Alexander and Deser (1995), Curry and McCartney (2001), and Petrie (2007), tested them for past climatic conditions, and obtained equivalent results. This achieves Objective 2 as stated in Section 1.3.

Further, it was determined that the thermal stratification in the northern sectors of the North Sea is not resilient to local storms. These storms, however, need to be strong and frequent to completely mix the water column. This analysis, however, is limited to the extent of sea surface temperature data. A robust, preferentially seasonally resolved sea surface temperature reconstruction would be required to test the persistence of the thermal stratification.

In Manuscript III (Chapter 5) fossil *A. islandica* shells were examined to reconstruct the climatic conditions of the northern North Sea during the 8.2 ka event, a time of abrupt cooling in the Northern Hemisphere. In the development of this investigation, two increment width chronologies were developed, one for about 300 years before and one during the 8.2 ka event. The extension of the chronologies and the uncertainty of radioisotope dating was not sufficient to connect these chronologies. Nevertheless, these chronologies are the first molluscan increment-width chronologies to be developed exclusively from material pre-dating the Common Era.

Stable isotope geochemistry ($\delta^{18}O$ and $\delta^{13}C$) derived from the shells covering the 8.2 ka event suggested that the waters of the North Sea became stratified, re-mixed and stratified again in a short time span. It was found that this pattern was consistent with a sudden sea level rise detected in western Scotland (Lawrence et al., 2016). By synchronising the *A. islandica* geochemistry to this sea level rise and using a qualitative reconstruction from the Norwegian Margin (Klitgaard-Kristensen et al., 1998), it was possible to establish a plausible order of events that took place in the North Sea in and around the 8.2 ka event.

Moreover, by applying existing assumptions about water masses in the North Sea, it was possible to partially disentangle the water mass effect from the effects of water temperature on the $\delta^{18}O$ derived from the *A. islandica* shells. This resulted in a temperature reconstruction that suggested that the waters in the northern North Sea were 0.66 °C warmer prior to the 8.2 ka than they were in the period from 1551-2004. During the 8.2 ka event, the waters cooled by nearly 2 °C but the temperatures quickly rose after sub-Arctic waters receded. The temperature and oceanographic reconstruction done in this Chapter achieved Objective 3 as stated in section 1.3. It was determined that this environmental reconstruction was highly coherent with Greenland ice core records and a Chinese stalagmite, two of the very few archives that show the 8.2 ka event with comparable resolution to the record developed in Chapter 5. This information is significant in understanding the reaction times to perturbations of the Atlantic Meridional Overturning Circulation.

The Holocene
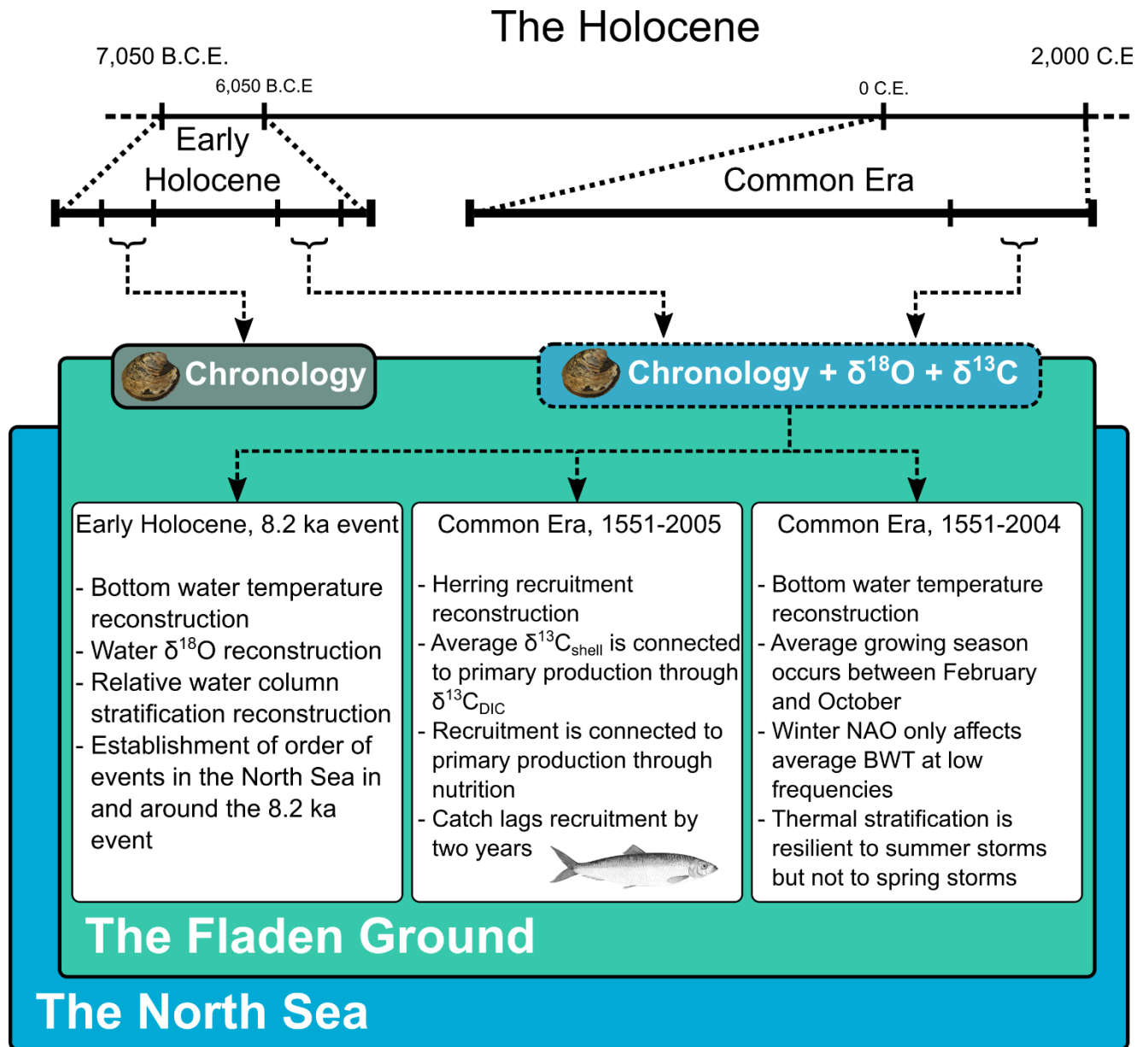
Figure 6.1 Schematic summarising the main results of this thesis.

Figure 6.1 summarises the results presented in this thesis and shows how all chapters are connected. All the material used in this thesis comes from the Fladen Ground in the northern North Sea. The methodology used to study past climatic conditions is also common across all chapters. The material studied was used to probe the climate during two widely separated periods during the Holocene: (a) the last quarter of the Common Era, a time when the waters of the northern North Sea were fully seasonally stratified, and (b) the Early Holocene, a time when the seasonal stratification would have been less resilient to mixing action due to lower sea level and a more turbulent overall climate. Through these studies I have demonstrated how factors like sea level, water mass and storminess can all contribute to the strength of the seasonal water

column stratification and how primary production affects the $\delta^{13}C$ of the dissolved inorganic carbon and the herring recruitment.

6.2 CHALLENGES

The main challenge encountered during the development of this dissertation was the extension of the FGB chronology. Many of the shells measured did not show clear increments. Many acetate peel replicas were produced before I started in Bangor and a good number of these were unusable. The provenance of the ^{14}C dates of the shells was not always clear (was it measured in the umbo or in the ventral margin?) due to clerical shortcomings. Many of the shells measured that had a good possibility of extending the chronology ended up crossmatching in the 19th or 20th centuries, again because of the unclear provenance of the ^{14}C dates. This ended up consuming a significant amount of time and in times resulted in comparing shells that had very low possibilities of successfully being crossmatched.

Another challenge was the perverse offset in the $\delta^{18}O$ values of the shells in the second half of the 20th century. At first, not knowing if the offset was real or not, this resulted in the misinterpretation of the 20th century BWTs. They were much lower than what the instrumental values suggested. This led to hypotheses being proposed by my co-authors and I ranging from extended changes in the $\delta^{18}O$ of the water (unlikely), to previously unknown vital effects, to diagenesis. Finally, Occam's razor prevailed when I proposed that there was a problem with the storage. I knew from experience that carbonate powder is prone to humidity absorption if improperly stored. This was the main reason to use silica desiccant for later storage of aragonite powder.

All of this is in contrast to the study developed for Chapter 5. During the course of the investigation there were virtually no problems. The four 8.2 ka shells crossmatched very well on the first try (umbo measurements) and a slightly longer chronology was obtained with a second attempt (ventral margin measurements). The previous experience with the $\delta^{18}O$ offset also meant that great care was taken when storing the powder produced for the geochemical analysis.

6.3 FUTURE PATHS AND OPEN QUESTIONS

Many open questions in high resolution palaeoceanographic studies of the high latitudes can be addressed using available shell material. Cross-matched *A. islandica* material dated to prior the 8.2 ka event exist that would allow the determination of climatic conditions of the much shallower northern North Sea

coming out of the Last Glacial Maximum. The additional testing and calibration of Sr/Ca and Mg/Ca ratios in the shells studied would also serve as a water mass-independent temperature reconstruction (Schöne et al., 2011b).

A. islandica shells in the stored in the archives the University of Exeter and the University of Bergen also provide an unmatched opportunity to study the primary production and (possibly) the herring recruitment variability in Icelandic, Norwegian and Irish waters. Previous works that found atmospheric and oceanic links to European herring recruitment were unsuccessful at explaining those links (i.e., finding a mechanism). These works were also hindered by the relatively short duration of the recruitment records. This means that the results from these investigations are susceptible to the "shifting baseline syndrome." (SBS) This assumes that fisheries studied using data from the relatively recent past are responding to external factors in a normal way when, in fact, the observed response might be due to unduly environmental pressures. This puts in doubt the usefulness of the results in predicting future herring populations.

As demonstrated in Chapter 3, it is possible to solve the shifting baseline syndrome by reconstructing recruitment using proportions of stable isotopes of carbon extracted from shells of *A. islandica*. Large populations of quahogs are found in the same areas where European herring reproduce. A successful reconstruction of herring recruitment would show the spatiotemporal variation in herring population dynamics. With this information a recruitment model based on atmospheric, oceanographic and environmental factors can be developed. The model can be tested under past scenarios of low, medium and high fishing pressures while taking into consideration the climatic variability at short, medium and long timescales.

7. BIBLIOGRAPHY

Adefisoye, J., Golam Kibria, B., George, F., 2016. Performances of several univariate tests of normality: An empirical study. J. Biom. Biostat. 07. https://doi.org/10.4172/2155-6180.1000322

Akimova, A., Núñez-Riboni, I., Kempf, A., Taylor, M.H., 2016. Spatially-resolved influence of temperature and salinity on stock and recruitment variability of commercially important fishes in the North Sea. PLoS One 11, 1–25. https://doi.org/10.1371/journal.pone.0161917

Alexander, M.A., Deser, C., 1995. A mechanism for the recurrence of wintertime midlatitude SST anomalies. J. Phys. Oceanogr. 25, 122–137. https://doi.org/10.1175/1520-0485(1995)025<0122:AMFTRO>2.0.CO;2

Alheit, J., Hagen, E., 1996. The Bohuslän herring periods: Are they controlled by climate variation or local phenomena? Ices C. 1996/O6.

Andersen, K.K., Svensson, A., Johnsen, S.J., Rasmussen, S.O., Bigler, M., Röthlisberger, R., Ruth, U., Siggaard-Andersen, M.-L., Peder Steffensen, J., Dahl-Jensen, D., 2006. The Greenland Ice Core Chronology 2005, 15–42ka. Part 1: constructing the time scale. Quat. Sci. Rev. 25, 3246–3257. https://doi.org/10.1016/j.quascirev.2006.08.002

Arreguín-Sánchez, F., 1996. Catchability: A key parameter for fish stock assessment. Rev. Fish Biol. Fish. 6. https://doi.org/10.1007/BF00182344

Ascough, P.L., Church, M.J., Cook, G.T., 2017. Marine radiocarbon reservoir effects for the Mesolithic and Medieval periods in the western isles of Scotland. Radiocarbon 59, 17–31. https://doi.org/10.1017/RDC.2016.99

Austin, W.E.N., Scourse, J.D., 1997. Evolution of seasonal stratification in the Celtic Sea during the Holocene. J. Geol. Soc. London. 154, 249–256. https://doi.org/10.1144/gsjgs.154.2.0249

Axenrot, T., Hansson, S., 2003. Predicting herring recruitment from young-of-the-year densities, spawning

stock biomass, and climate. Limnol. Oceanogr. 48, 1716–1720. https://doi.org/10.4319/lo.2003.48.4.1716

Baillie, M.G.L., Pilcher, J.R., 1973. A simple crossdating program for tree-ring research. Tree-Ring Bull. 33, 7–14.

Balson, P., Butcher, A., Holmes, R., Johnson, H., Lewis, M., Musson, R., 2001. North Sea geology, in: Strategic Environmental Assessment 2 (SEA2). Department of Trade and Industry, London, pp. 1–48.

Barber, D.C., Jennings, A.E., Andrews, J.T., Dyke, A., Kerwin, M.W., Hillarie-Marcel, C., Morehead, M.D., Bilodeau, G., McNeely, R., Southon, J., Gagnon, J.-M., 1999. Forcing of the cold event of 8,200 years ago by catastrophic drainage of Laurentide lakes. Nature 400, 13–15.

Becker, G.A., Schulz, A., 2000. Atlas of North Sea surface temperatures. Weekly and monthly means for the period 1969 to 1993. Dtsch. Hydrogr. Zeitschrift 51, 5–79. https://doi.org/10.1007/BF02933585

Beirne, E.C., Wanamaker Jr., A.D., Feindel, S.C., 2012. Experimental validation of environmental controls on the $\delta^{13}C$ of *Arctica islandica* (ocean quahog) shell carbonate. Geochim. Cosmochim. Acta 84, 395–409. https://doi.org/10.1016/j.gca.2012.01.021

Berx, B., Hughes, S.L., 2009. Climatology of surface and near-bed temperature and salinity on the north-west European continental shelf for 1971-2000. Cont. Shelf Res. 29, 2286–2292. https://doi.org/10.1016/j.csr.2009.09.006

Blaas, M., Kerkhoven, D., de Swart, H., 2001. Large-scale circulation and flushing characteristics of the North Sea under various climate forcings. Clim. Res. 18, 47–54. https://doi.org/10.3354/cr018047

Black, B.A., Griffin, D., van der Sleen, P., Wanamaker Jr., A.D., Speer, J.H., Frank, D.C., Stahle, D.W., Pederson, N., Copenheaver, C.A., Trouet, V., Griffin, S., Gillanders, B.M., 2016. The value of crossdating to retain high-frequency variability, climate signals, and extreme events in environmental proxies. Glob. Chang. Biol. 22, 2582–2595. https://doi.org/10.1111/gcb.13256

Bogstad, B., Dingsør, G.E., Ingvaldsen, R.B., Gjøsæter, H., 2013. Changes in the relationship between sea temperature and recruitment of cod, haddock and herring in the Barents Sea. Mar. Biol. Res. 9, 895–907. https://doi.org/10.1080/17451000.2013.775451

Bozec, Y., Thomas, H., Schiettecatte, L.-S., Borges, A. V, Elkalay, K., de Baar, H.J.W., 2006. Assessment of the processes controlling seasonal variations of dissolved inorganic carbon in the North Sea. Limnol.

Ocean. 51, 2746–2762. https://doi.org/10.1002/jqs.2931

Brand, A., Allen, L., Altman, M., Hlava, M., Scott, J., 2015. Beyond authorship: Attribution, contribution, collaboration, and credit. Learn. Publ. 28, 151–155. https://doi.org/10.1087/20150211

Brand, W.A., Coplen, T.B., Vogl, J., Rosner, M., Prohaska, T., 2014. Assessment of international reference materials for isotope-ratio analysis (IUPAC Technical Report). Pure Appl. Chem. 86, 425–467. https://doi.org/10.1515/pac-2013-1023

Bronk Ramsey, C., 2009. Bayesian analysis of radiocarbon dates. Radiocarbon 51, 337–360. https://doi.org/10.1017/S0033822200033865

Bronk Ramsey, C., van der Plicht, J., Weninger, B., 2001. 'Wiggle matching' radiocarbon dates. Radiocarbon 43, 381–389. https://doi.org/10.1017/S0033822200038248

Brzezinski, M.A., Villareal, T.A., Lipschultz, F., 1998. Silica production and the contribution of diatoms to new and primary production in the central North Pacific. Mar. Ecol. Ser. 167, 89–104. https://doi.org/10.3354/meps167089

Büntgen, U., Frank, D.C., Nievergelt, D., Esper, J., 2006. Summer temperature variations in the European Alps, A.D. 755-2004. J. Clim. 19, 5606–5623. https://doi.org/10.1175/JCLI3917.1

Buras, A., 2017. A comment on the expressed population signal. Dendrochronologia 44, 130–132. https://doi.org/10.1016/j.dendro.2017.03.005

Burd, A.C., 1978. Long-term changes in North Sea herring stocks. Rapp. Proces-Verbaux des Reun. Cons. Int. pour l'Exploration la Mer 172, 137–153.

Burningham, H., French, J., 2013. Is the NAO winter index a reliable proxy for wind climate and storminess in northwest Europe? Int. J. Climatol. 33, 2036–2049. https://doi.org/10.1002/joc.3571

Burrows, M., Thorpe, S.A., 1999. Drifter observations of the Hebrides slope current and nearby circulation patterns. Ann. Geophys. 17, 280–302. https://doi.org/10.1007/s00585-999-0280-5

Burt, W.J., Thomas, H., Hagens, M., Pätsch, J., Clargo, N.M., Salt, L.A., Winde, V., Böttcher, M.E., 2016. Carbon sources in the North Sea evaluated by means of radium and stable carbon isotope tracers. Limnol. Oceanogr. 61, 666–683. https://doi.org/10.1002/lno.10243

Busschers, F.S., Kasse, C., van Balen, R.T., Vandenberghe, J., Cohen, K.M., Weerts, H.J.T., Wallinga, J.,

Johns, C., Cleveringa, P., Bunnik, F.P.M., 2007. Late Pleistocene evolution of the Rhine-Meuse system in the southern North Sea basin: Imprints of climate change, sea-level oscillation and glacio-isostacy. Quat. Sci. Rev. 26, 3216–3248. https://doi.org/10.1016/j.quascirev.2007.07.013

Butler, P.G., 2009. Establishing the *Arctica islandica* archive: Development of the definite shell-based proxy for the North Atlantic shelf seas. Bangor University.

Butler, P.G., Richardson, C.A., Scourse, J.D., Wanamaker Jr., A.D., Shammon, T.M., Bennell, J.D., 2010. Marine climate in the Irish Sea: Analysis of a 489-year marine master chronology derived from growth increments in the shell of the clam *Arctica islandica*. Quat. Sci. Rev. 29, 1614–1632. https://doi.org/10.1016/j.quascirev.2009.07.010

Butler, P.G., Richardson, C.A., Scourse, J.D., Witbaard, R., Schöne, B.R., Fraser, N.M., Wanamaker Jr., A.D., Bryant, C.L., Harris, I., Robertson, I., 2009a. Accurate increment identification and the spatial extent of the common signal in five *Arctica islandica* chronologies from the Fladen Ground, northern North Sea. Paleoceanography 24, PA2210. https://doi.org/10.1029/2008PA001715

Butler, P.G., Scourse, J.D., Richardson, C.A., Wanamaker Jr., A.D., Bryant, C.L., Bennell, J.D., 2009b. Continuous marine radiocarbon reservoir calibration and the ^{13}C Suess effect in the Irish Sea: Results from the first multi-centennial shell-based marine master chronology. Earth Planet. Sci. Lett. 279, 230–241. https://doi.org/10.1016/j.epsl.2008.12.043

Butler, P.G., Wanamaker Jr., A.D., Scourse, J.D., Richardson, C. a., Reynolds, D.J., 2013. Variability of marine climate on the North Icelandic Shelf in a 1357-year proxy archive based on growth increments in the bivalve *Arctica islandica*. Palaeogeogr. Palaeoclimatol. Palaeoecol. 373, 141–151. https://doi.org/10.1016/j.palaeo.2012.01.016

Butler, P.G., Wanamaker Jr., A.D., Scourse, J.D., Richardson, C.A., Reynolds, D.J., 2011. Long-term stability of δ^{13}C with respect to biological age in the aragonite shell of mature specimens of the bivalve mollusk *Arctica islandica*. Palaeogeogr. Palaeoclimatol. Palaeoecol. 302, 21–30. https://doi.org/10.1016/j.palaeo.2010.03.038

Came, R.E., Oppo, D.W., McManus, J.F., 2007. Amplitude and timing of temperature and salinity variability in the subpolar North Atlantic over the past 10 k.y. Geology 35, 315–318. https://doi.org/10.1130/G23455A.1

Capuzzo, E., Lynam, C.P., Barry, J., Stephens, D., Forster, R.M., Greenwood, N., McQuatters-Gollop, A.,

Silva, T., van Leeuwen, S.M., Engelhard, G.H., 2018. A decline in primary production in the North Sea over 25 years, associated with reductions in zooplankton abundance and fish stock recruitment. Glob. Chang. Biol. 24, e352–e364. https://doi.org/10.1111/gcb.13916

Chavez, F.P., Messié, M., Pennington, J.T., 2011. Marine primary production in relation to climate variability and change. Ann. Rev. Mar. Sci. 3, 227–260. https://doi.org/10.1146/annurev.marine.010908.163917

Clark, G.R., 1968. Mollusk shell: Daily growth lines. Science (80-.). 161, 800–802. https://doi.org/10.1126/science.161.3843.800

Cochran, J.K., Kallenberg, K., Landman, N.H., Harries, P.J., Weinreb, D., Turekian, K.K., Beck, A., Cobban, W.A., 2010. Effect of diagenesis on the Sr, O, and C isotope composition of late cretaceous mollusks from the western interior seaway of North America. Am. J. Sci. 310, 69–88. https://doi.org/10.2475/02.2010.01

Colonese, A.C., Netto, S.A., Francisco, A.S., DeBlasis, P., Villagran, X.S., de Almeida Rocha Ponzoni, R., Hancock, Y., Hausmann, N., Eloy de Farias, D.S., Prendergast, A., Schöne, B.R., da Cruz, F.W., Giannini, P.C.F., 2017. Shell sclerochronology and stable isotopes of the bivalve *Anomalocardia flexuosa* (Linnaeus, 1767) from southern Brazil: Implications for environmental and archaeological studies. Palaeogeogr. Palaeoclimatol. Palaeoecol. 484, 7–21. https://doi.org/10.1016/j.palaeo.2017.01.006

Cook, E.R., Krusic, P.J., 2014. ARSTAN: A tree-ring standardization program based on detrending and autoregressive time series modeling, with interactive graphics.

Cook, E.R., Pederson, N., 2011. Uncertainty, emergence, and statistics in dendrochronology, in: Encyclopedia of Quaternary Science: Second Edition. pp. 77–112. https://doi.org/10.1007/978-1-4020-5725-0_4

Cook, E.R., Peters, K., 1997. Calculating unbiased tree-ring indices for the study of climatic and environmental change. The Holocene 7, 361–370. https://doi.org/10.1177/095968369700700314

Coplen, T.B., Hopple, J.A., Böhlke, J.K., Peiser, H.S., Rieder, S.E., Krouse, H.R., Rosman, K.J.R., Ding, T., Vocke Jr., R.D., Revesz, K.M., Lamberty, A., Taylor, P., De Bievre, P., 2002. Compilation of minimum and maximum isotope ratios of selected elements in naturally occurring terrestrial materials and reagents. Reston, Virginia. https://doi.org/10.3133/wri014222

Cordes, E.E., Jones, D.O.B., Schlacher, T.A., Amon, D.J., Bernardino, A.F., Brooke, S., Carney, R., DeLeo, D.M., Dunlop, K.M., Escobar-Briones, E.G., Gates, A.R., Génio, L., Gobin, J., Henry, L.-A., Herrera,

S., Hoyt, S., Joye, M., Kark, S., Mestre, N.C., Metaxas, A., Pfeifer, S., Sink, K., Sweetman, A.K., Witte, U., 2016. Environmental impacts of the deep-water oil and gas industry: A review to guide management strategies. Front. Environ. Sci. 4. https://doi.org/10.3389/fenvs.2016.00058

Corten, A., 2013. Recruitment depressions in North Sea herring. ICES J. Mar. Sci. 70, 1–15. https://doi.org/10.1093/icesjms/fss187

Corten, A., 2001. Northern distribution of North Sea herring as a response to high water temperatures and/or low food abundance. Fish. Res. 50, 189–204. https://doi.org/10.1016/S0165-7836(00)00251-4

Corten, A., 1999. A proposed mechanism for the Bohuslän herring periods. ICES J. Mar. Sci. 56, 207–220. https://doi.org/10.1006/jmsc.1998.0429

Coull, J.R., 1990. The Scottish herring fishery in the inter-war years, 1919-1939: Ordeal and retrenchment. Int. J. Marit. Hist. 2, 55–81.

Coull, J.R., 1986. The Scottish herring fishery 1800–1914: Development and intensification of a pattern of resource use. Scott. Geogr. Mag. 102, 4–17. https://doi.org/10.1080/00369228618736643

Curry, R.G., McCartney, M.S., 2001. Ocean gyre circulation changes associated with the North Atlantic Oscillation*. J. Phys. Oceanogr. 31, 3374–3400. https://doi.org/10.1175/1520-0485(2001)031<3374:OGCCAW>2.0.CO;2

Cushing, D.H., 1989. A difference in structure between ecosystems in strongly stratified waters and in those that are only weakly stratified. J. Plankton Res. 11, 1–13. https://doi.org/10.1093/plankt/11.1.1

Cushing, D.H., 1968. The east anglian herring fishery in the eighteenth century. ICES J. Mar. Sci. 31, 323–329. https://doi.org/10.1093/icesjms/31.3.323

Dahlgren, T.G., Weinberg, J.R., Halanych, K.M., 2000. Phylogeography of the ocean quahog (*Arctica islandica*): Influences of paleoclimate on genetic diversity and species range. Mar. Biol. 137, 487–495. https://doi.org/10.1007/s002270000342

Dickey-Collas, M., 2016. North Sea herring: Longer term perspective on management science behind the boom, collapse and recovery of the North Sea herring fishery, in: Edwards, C.T.T., Dankel, D.J. (Eds.), Management Science in Fisheries: An Introduction to Simulation-Based Methods. Routledge, London, pp. 365–408. https://doi.org/10.4324/9781315751443

Dickey-Collas, M., Nash, R.D.M., Brunel, T., Van Damme, C.J.G., Marshall, C.T., Payne, M.R., Corten, A., Geffen, A.J., Peck, M.A., Hatfield, E.M.C., Hintzen, N.T., Enberg, K., Kell, L.T., Simmonds, E.J., 2010. Lessons learned from stock collapse and recovery of North Sea herring: A review. ICES J. Mar. Sci. 67, 1875–1886. https://doi.org/10.1093/icesjms/fsq033

Dong, B., Sutton, R.T., Woollings, T., Hodges, K., 2013. Variability of the North Atlantic summer storm track: Mechanisms and impacts on European climate. Environ. Res. Lett. 8, 034037. https://doi.org/10.1088/1748-9326/8/3/034037

Dow, J., 1969. Scottish trade with Sweden 1580-1622. Scott. Hist. Rev. 48, 124–150.

Dunca, E., Mutvei, H., Göransson, P., Mörth, C.M., Schöne, B.R., Whitehouse, M.J., Elfman, M., Baden, S.P., 2009. Using ocean quahog (Arctica islandica) shells to reconstruct palaeoenvironment in Öresund, Kattegat and Skagerrak, Sweden. Int. J. Earth Sci. 98, 3–17. https://doi.org/10.1007/s00531-008-0348-6

Edwards, K.J., Whittington, G., 2001. Lake sediments, erosion and landscape change during the Holocene in Britain and Ireland. Catena 42, 143–173. https://doi.org/10.1016/S0341-8162(00)00136-3

Eiriksson, J., Cage, A.G., Gudmundsdóttir, E.R., Klitgaard-Kristensen, D., Marret, F., Rodrigues, T., Abrantes, F., Austin, W.E.N., Jiang, H., Knudsen, K., Sejrup, H.-P., 2006. Variability of the North Atlantic Current during the last 2000 years based on shelf bottom water and sea surface temperatures along an open ocean/shallow marine transect in Western Europe. The Holocene 7, 1017–1029. https://doi.org/10.1177/0959683606hl991rp

Ellett, D.J., Edwards, A., 1983. Oceanography and inshore hydrography of the Inner Hebrides. Proc. R. Soc. Edinburgh. Sect. B. Biol. Sci. 83, 144–160. https://doi.org/10.1017/S0269727000013385

Ellison, C.R.W., Chapman, M.R., Hall, I.R., 2006. Surface and deep ocean interactions during the cold climate event 8200 years ago. Science (80-.). 312, 1929–1932. https://doi.org/10.1126/science.1127213

Epplé, V.M., Brey, T., Witbaard, R., Kuhnert, H., Pätzold, J., 2006. Sclerochronological records of *Arctica islandica* from the inner German Bight. The Holocene 16, 763–769. https://doi.org/10.1191/0959683606hl970rr

Erisman, B.E., Allen, L.G., Claisse, J.T., Pondella, D.J., Miller, E.F., Murray, J.H., 2011. The illusion of plenty: Hyperstability masks collapses in two recreational fisheries that target fish spawning aggregations. Can. J. Fish. Aquat. Sci. 68, 1705–1716. https://doi.org/10.1139/f2011-090

Esper, J., Frank, D.C., Wilson, R.J.S., Büntgen, U., Treydte, K., 2007. Uniform growth trends among central Asian low- and high-elevation juniper tree sites. Trees - Struct. Funct. 21, 141–150. https://doi.org/10.1007/s00468-006-0104-0

Estrella-Martínez, J., Schöne, B.R., Thurstan, R.H., Capuzzo, E., Scourse, J.D., Butler, P.G., 2019. Reconstruction of Atlantic herring (*Clupea harengus*) recruitment in the North Sea for the past 455 years based on the $\delta^{13}C$ from annual shell increments of the ocean quahog (*Arctica islandica*). Fish Fish. 20, 537–551. https://doi.org/10.1111/faf.12362

Feldstein, S.B., 2007. The dynamics of the North Atlantic Oscillation during the summer season. Q. J. R. Meteorol. Soc. 133, 937–948. https://doi.org/10.1002/qj.107

Folland, C.K., Knight, J., Linderholm, H.W., Fereday, D., Ineson, S., Hurrel, J.W., 2009. The summer North Atlantic oscillation: Past, present, and future. J. Clim. 22, 1082–1103. https://doi.org/10.1175/2008JCLI2459.1

Foster, L.C., Allison, N., Finch, A.A., Andersson, C., 2009. Strontium distribution in the shell of the aragonite bivalve *Arctica islandica*. Geochemistry, Geophys. Geosystems 10, n/a-n/a. https://doi.org/10.1029/2007GC001915

Foster, L.C., Andersson, C., Høie, H., Allison, N., Finch, A.A., Johansen, T., 2008. Effects of micromilling on $\delta^{18}O$ in biogenic aragonite. Geochemistry Geophys. Geosystems 9, 1–6. https://doi.org/10.1029/2007GC001911

Frederiksen, M., Edwards, M., Richardson, A.J., Halliday, N.C., Wanless, S., 2006. From plankton to top predators: Bottom-up control of a marine food web across four trophic levels. J. Anim. Ecol. 75, 1259–1268. https://doi.org/10.1111/j.1365-2656.2006.01148.x

Füllenbach, C.S., Schöne, B.R., Mertz-Kraus, R., 2015. Strontium/lithium ratio in aragonitic shells of *Cerastoderma edule* (Bivalvia) - A new potential temperature proxy for brackish environments. Chem. Geol. 417, 341–355. https://doi.org/10.1016/j.chemgeo.2015.10.030

Garstang, W., 1900. The impoverishment of the sea. A critical summary of the experimental and statistical evidence bearing upon the alleged depletion of the trawling grounds. J. Mar. Biol. Assoc. United Kingdom 6, 1–69. https://doi.org/10.1017/S0025315400072374

Graham, A.G.C., Stoker, M.S., Lonergan, L., Bradwell, T., Stewart, M.A., 2011. The Pleistocene glaciations of the North Sea basin. Dev. Quat. Sci. 15, 261–278. https://doi.org/10.1016/B978-0-444-53447-

7.00021-0

Gray, S.T., Graumlich, L.J., Betancourt, J.L., Pederson, G.T., 2004. A tree-ring based reconstruction of the Atlantic Multidecadal Oscillation since 1567 A.D. Geophys. Res. Lett. 31, 2–5. https://doi.org/10.1029/2004GL019932

Grey, S.M., Haines, K., Troccoli, A., 2000. A study of temperature changes in the Upper North Atlantic: 1950-94. J. Clim. 13, 2697–2711. https://doi.org/10.1175/1520-0442(2000)013<2697:ASOTCI>2.0.CO;2

Gröger, J.P., Kruse, G.H., Rohlf, N., 2010. Slave to the rhythm: How large-scale climate cycles trigger herring (*Clupea harengus*) regeneration in the North Sea. ICES J. Mar. Sci. 67, 454–465. https://doi.org/10.1093/icesjms/fsp259

Grossman, E.L., Ku, T.-L., 1986. Oxygen and carbon isotope fractionation in biogenic aragonite: Temperature effects. Chem. Geol. Isot. Geosci. Sect. 59, 59–74. https://doi.org/10.1016/0168-9622(86)90057-6

Gruber, N., Keeling, C.D., Bacastow, R.B., Guenther, P.R., Lueker, T.J., Wahlen, M., Meijer, H. a J., Mook, W.G., Stocker, T.F., 1999. Spatiotemporal patterns of carbon-13 in the global surface oceans and the oceanic suess effect. Global Biogeochem. Cycles 13, 307–335. https://doi.org/10.1029/1999GB900019

Guimares Nobre, G., Jongman, B., Aerts, J., Ward, P.J., 2017. The role of climate variability in extreme floods in Europe. Environ. Res. Lett. 12. https://doi.org/10.1088/1748-9326/aa7c22

Hald, M., Salomonsen, G.R., Husum, K., Wilson, L.J., 2011. A 2000 year record of Atlantic Water temperature variability from the Malangen Fjord, northeastern North Atlantic. The Holocene 21, 1049–1059. https://doi.org/10.1177/0959683611400457

Halsband, C., Hirche, H.J., 2001. Reproductive cycles of dominant calanoid copepods in the North Sea. Mar. Ecol. Prog. Ser. 209, 219–229. https://doi.org/10.3354/meps209219

Hammer, Ø., Harper, D.A.T., Ryan, P.D., 2001. PAST: Paleontological Statistics Software Package for Education and Data Analysis. Palaeontol. Electron. 4.

Hansen, B., Bech, G., 1996. Bacteria associated with a marine planktonic copepod in culture. I. Bacterial genera in seawater, body surface, intestines and fecal pellets and succession during fecal pellet

degradation. J. Plankton Res. 18, 257–273. https://doi.org/10.1093/plankt/18.2.257

Harley, S.J., Myers, R.A., Dunn, A., 2001. Is catch-per-unit-effort proportional to abundance? Can. J. Fish. Aquat. Sci. 58, 1760–1772. https://doi.org/10.1139/f01-112

Harris, B., 2000. Scotland's herring fisheries and the prosperity of the nation, c.1660–1760. Scott. Hist. Rev. 79, 39–60. https://doi.org/10.3366/shr.2000.79.1.39

Harwood, A.J.P., Dennis, P.F., Marca, A.D., Pilling, G.M., Millner, R.S., 2008. The oxygen isotope composition of water masses within the North Sea. Estuar. Coast. Shelf Sci. 78, 353–359. https://doi.org/10.1016/j.ecss.2007.12.010

Heath, M., Richardson, K., 1989. Comparative study of early-life survival variability of herring *Clupea harengus*, in the north-eastern Atlantic. J. Fish Biol. 35, 49–57. https://doi.org/10.1111/j.1095-8649.1989.tb03045.x

Hebbeln, D., Knudsen, K.L., Gyllencreutz, R., Kristensen, P., Klitgaard-Kristensen, D., Backman, J., Scheurle, C., Jiang, H., Gil, I., Smelror, M., Jones, P.D., Sejrup, H.P., 2006. Late Holocene coastal hydrographic and climate changes in the eastern North Sea. Holocene 16, 987–1001. https://doi.org/10.1177/0959683606hl989rp

Helama, S., Schöne, B.R., Black, B.A., Dunca, E., 2006. Constructing long-term proxy series for aquatic environments with absolute dating control using a sclerochronological approach: Introduction and advanced applications. Mar. Freshw. Res. 57, 591. https://doi.org/10.1071/MF05176

Herrle, J.O., Bollmann, J., Gebühr, C., Schulz, H., Sheward, R.M., Giesenberg, A., 2018. Black Sea outflow response to Holocene meltwater events. Sci. Rep. 8, 1–6. https://doi.org/10.1038/s41598-018-22453-z

Hiriart-Baer, V.P., Milne, J.E., Marvin, C.H., 2011. Temporal trends in phosphorus and lacustrine productivity in Lake Simcoe inferred from lake sediment. J. Great Lakes Res. 37, 764–771. https://doi.org/10.1016/j.jglr.2011.08.014

Hoffman, J.S., Carlson, A.E., Winsor, K., Klinkhammer, G.P., LeGrande, A.N., Andrews, J.T., Strasser, J.C., 2012. Linking the 8.2 ka event and its freshwater forcing in the Labrador Sea. Geophys. Res. Lett. 39, 971. https://doi.org/10.1029/2012GL053047

Höglund, H., 1978. Long-term variations in the Swedish herring fishery off Bohuslän and their relation to

North Sea herring, in: Hempel, G. (Ed.), North Sea Fish Stocks-Recent Changes and Their Causes: A Symposium Held in Aarhus. Conseil International Pour L'Exploration De La Mer, Copenhagen, pp. 175–186.

Hurrell, J.W., 1995. Decadal trends in the North Atlantic Oscillation: Regional temperatures and precipitation. Science (80-.). 269, 676–679. https://doi.org/10.1126/science.269.5224.676

Hurrell, J.W., Kushnir, Y., Ottersen, G., Visbeck, M., 2003. An overview of the North Atlantic Oscillation, in: Hurrell, J.W., Kushnir, Y., Ottersen, G., Visbeck, M. (Eds.), The North Atlantic Oscillation: Climatic Significance and Environmental Impact. American Geophysical Union, Washington, D.C., pp. 1–35. https://doi.org/10.1029/134GM01

Hut, G., 1987. Consultants' group meeting on stable isotope reference samples for geochemical and hydrological investigations. Vienna.

ICES, 2018. ICES Stock Assessment Database. International Council for the Exploration of the Sea, Copenhagen.

ICES, 2017. Herring Assessment Working Group for the Area South of 62° N (HAWG), 14-22 March 2017. Copenhagen.

ICES, 2016. ICES Report on Ocean Climate 2015, in: Larsen, K.M.H., Gonzalez-Pola, C., Fratantoni, P., Beszczynska-Möller, A., Hughes, S.L. (Eds.), ICES Cooperative Research Report No. 331. International Council for the Exploration of the Sea, Copenhagen, p. 79.

ICES, 2014. ICES Dataset on Ocean Hydrography. International Council for the Exploration of the Sea, Copenhagen.

ICES, 1983. Flushing times of the North Sea. ICES Coop. Res. Rep. 123, 86-94.

IOC, IHO, BODC, 2003. Centenary edition of the GEBCO Digital Atlas, published on CD-ROM on behalf of the Intergovernmental Oceanographic Commission and the International Hydrographic Organization as part of the General Bathymetric Chart of the Oceans.

Irigoien, X., Harris, R.P., Verheye, H.M., Joly, P., Runge, J., Starr, M., Pond, D., Campbell, R., Shreeve, R., Ward, P., Smith, A.N., Dam, H.G., Peterson, W., Tirelli, V., Koski, M., Smith, T., Harbour, D., Davidson, R., 2002. Copepod hatching success in marine ecosystems with high diatom concentrations. Nature 419, 387–389. https://doi.org/10.1038/nature01055

Irigoien, X., Head, R.N., Harris, R.P., Cummings, D., Harbour, D., Meyer-Harms, B., 2000. Feeding selectivity and egg production of Calanus helgolandicus in the English Channel. Limnol. Oceanogr. 45, 44–54. https://doi.org/10.4319/lo.2000.45.1.0044

Jenkins, J.T., 1913. The British Sea fisheries: Their present condition and future prospects. J. R. Soc. Arts 61, 231–242.

Jennings, S., Wilson, R.W., 2009. Fishing impacts on the marine inorganic carbon cycle. J. Appl. Ecol. 46, 976–982. https://doi.org/10.1111/j.1365-2664.2009.01682.x

Johns, D., 2016. Total diatom, dinoflagelates, eye-count copepoda, trav copepoda and PCI for B2 and C2, Fladen area, monthly means, 1958-2015 as recorded by the Continuous Plankton Recorder, Sir Alister Hardy Foundation for Ocean Science. Plymouth, United Kingdom. https://doi.org/10.7487/2017.79.1.1043

Jones, D.S., 1981. Annual growth increments in shells of *Spisula solidissima* record marine temperature variability. Science (80-.). 211, 165–167. https://doi.org/http://dx.doi.org/10.1016/B978-0-444-42277-4.50012-0

Jones, D.S., Arnold, B., Quitmyer, I., Schöne, B.R., Surge, D., 2007. 1st International Sclerochronology Conference [WWW Document]. URL https://conference.ifas.ufl.edu/sclerochronology/ (accessed 11.11.18).

Jones, P., Cathcart, A., Speirs, D.C., 2016. Early evidence of the impact of preindustrial fishing on fish stocks from the mid-west and southeast coastal fisheries of Scotland in the 19th century. ICES J. Mar. Sci. J. du Cons. 73, 1404–1414. https://doi.org/10.1093/icesjms/fsv189

Jouzel, J., 2013. A brief history of ice core science over the last 50 yr. Clim. Past 9, 2525–2547. https://doi.org/10.5194/cp-9-2525-2013

Kabel, K., Moros, M., Porsche, C., Neumann, T., Adolphi, F., Andersen, T.J., Siegel, H., Gerth, M., Leipe, T., Jansen, E., Sinninghe Damsté, J.S., 2012. Impact of climate change on the Baltic Sea ecosystem over the past 1,000 years. Nat. Clim. Chang. 2, 871–874. https://doi.org/10.1038/nclimate1595

Kilada, R.W., Campana, S.E., Roddick, D., 2007. Validated age, growth, and mortality estimates of the ocean quahog (*Arctica islandica*) in the western Atlantic. ICES J. Mar. Sci. 64, 31–38. https://doi.org/10.1093/icesjms/fsl001

Kleiven, H.F., Kissel, C., Laj, C., Ninnemann, U.S., Richter, T.O., Cortijo, E., 2008. Reduced North Atlantic deep water coeval with the glacial Lake Agassiz freshwater outburst. Science (80-.). 319, 60–64. https://doi.org/10.1126/science.1148924

Klitgaard-Kristensen, D., Sejrup, H.P., Haflidason, H., 2001. The last 18 kyr fluctuations in Norwegian sea surface conditions and implications for the magnitude of climatic change: Evidence from the North Sea. Paleoceanography 16, 455–467. https://doi.org/10.1029/1999PA000495

Klitgaard-Kristensen, D., Sejrup, H.P., Haflidason, H., Johnsen, S., Spurk, M., 1998. A regional 8200 cal. yr BP cooling event in northwest Europe, induced by final stages of the Laurentide ice-sheet deglaciation? J. Quat. Sci. 13, 165–169. https://doi.org/10.1002/(SICI)1099-1417(199803/04)13:2<165::AID-JQS365>3.3.CO;2-R

Kürten, B., Painting, S.J., Struck, U., Polunin, N.V.C., Middelburg, J.J., 2013. Tracking seasonal changes in North Sea zooplankton trophic dynamics using stable isotopes. Biogeochemistry 113, 167–187. https://doi.org/10.1007/s10533-011-9630-y

Lachniet, M.S., 2009. Climatic and environmental controls on speleothem oxygen-isotope values. Quat. Sci. Rev. 28, 412–432. https://doi.org/10.1016/j.quascirev.2008.10.021

Lamb, R.M., Harding, R., Huuse, M., Stewart, M., Brocklehurst, S.H., 2018. The early Quaternary North Sea Basin. J. Geol. Soc. London. 175, 275–290. https://doi.org/10.1144/jgs2017-057

Lampitt, R.S., Noji, T., von Bodungen, B., 1990. What happens to zooplankton faecal pellets? Implications for material flux. Mar. Biol. 104, 15–23. https://doi.org/10.1007/BF01313152

Last, J.M., 1989. The food of herring, *Clupea harengus*, in the North Sea, 1983–1986. J. Fish Biol. 34, 489–501. https://doi.org/10.1111/j.1095-8649.1989.tb03330.x

Lawrence, T., Long, A.J., Gehrels, W.R., Jackson, L.P., Smith, D.E., 2016. Relative sea-level data from southwest Scotland constrain meltwater-driven sea-level jumps prior to the 8.2 kyr BP event. Quat. Sci. Rev. 151, 292–308. https://doi.org/10.1016/j.quascirev.2016.06.013

Leblanc, K., Arístegui, J., Armand, L., Assmy, P., Beker, B., Bode, A., Breton, E., Cornet, V., Gibson, J., Gosselin, M.-P., Kopczynska, E., Marshall, H., Peloquin, J., Piontkovski, S., Poulton, A.J., Quéguiner, B., Schiebel, R., Shipe, R., Stefels, J., van Leeuwe, M.A., Varela, M., Widdicombe, C., Yallop, M., 2012. A global diatom database – abundance, biovolume and biomass in the world ocean. Earth Syst. Sci.

Data 4, 149–165. https://doi.org/10.5194/essd-4-149-2012

Linderholm, H.W., Folland, C.K., 2017. Summer North Atlantic Oscillation (SNAO) variability on decadal to palaeoclimate time scales. Past Glob. Chang. Mag. 25, 57–60. https://doi.org/10.22498/pages.25.1.57

Liu, Y.-H., Henderson, G.M., Hu, C.-Y., Mason, A.J., Charnley, N., Johnson, K.R., Xie, S.-C., 2013. Links between the East Asian monsoon and North Atlantic climate during the 8,200 year event. Nat. Geosci. 6, 117–120. https://doi.org/10.1038/ngeo1708

Lusseau, S.M., Gallego, A., Rasmussen, J., Hatfield, E.M.C., Heath, M., 2014. North Sea herring (*Clupea harengus* L.) recruitment failure may be indicative of poor feeding success. ICES J. Mar. Sci. 71, 2026–2041. https://doi.org/10.1093/icesjms/fsu070

Luterbacher, J., Xoplaki, E., Dietrich, D., Jones, P.D., Davies, T.D., Portis, D., Gonzalez-Rouco, J.F., von Storch, H., Gyalistras, D., Casty, C., Wanner, H., 2001. Extending North Atlantic Oscillation reconstructions back to 1500. Atmos. Sci. Lett. 2, 114–124. https://doi.org/10.1006/asle.2001.004

Lutz, R.A., Mann, R., Goodsell, J.G., Castagna, M., 1982. Larval and early post-larval development of *Arctica islandica*. J. Mar. Biol. Assoc. United Kingdom 62, 745. https://doi.org/10.1017/S0025315400070314

Mann, M.E., Zhang, Z., Rutherford, S., Bradley, R.S., Hughes, M.K., Shindell, D., Ammann, C., Faluvegi, G., Ni, F., 2009. Global Signatures and Dynamical Origins of the Little Ice Age and Medieval Climate Anomaly. Science (80-.). 326, 1256–1260. https://doi.org/10.1126/science.1177303

Mann, R., Wolf, C., 1983. Swimming behaviour of larvae of the ocean quahog *Arctica islandica* in response to pressure and temperature. Mar. Ecol. Prog. Ser. 13, 211–218. https://doi.org/10.3354/meps013211

Marchitto, T.M., Jones, G.A., Goodfriend, G.A., Weidman, C.R., 2000. Precise temporal correlation of Holocene mollusk shells using sclerochronology. Quat. Res. 53, 236–246. https://doi.org/10.1006/qres.1999.2107

Mariani, S., Hutchinson, W.F., Hatfield, E.M.C., Ruzzante, D.E., Simmonds, E.J., Dahlgren, T.G., Andre, C., Brigham, J., Torstensen, E., Carvalho, G.R., 2005. North Sea herring population structure revealed by microsatellite analysis. Mar. Ecol. Prog. Ser. 303, 245–257. https://doi.org/10.3354/meps303245

Marin, F., Le Roy, N., Marie, B., 2012. The formation and mineralization of mollusk shell. Front. Biosci. S4, 321. https://doi.org/10.2741/s321

Mette, M.J., Wanamaker Jr., A.D., Carroll, M.L., Ambrose, W.G., Retelle, M.J., 2016. Linking large-scale climate variability with *Arctica islandica* shell growth and geochemistry in northern Norway. Limnol. Oceanogr. 61, 748–764. https://doi.org/10.1002/lno.10252

Miettinen, A., Divine, D., Koç, N., Godtliebsen, F., Hall, I.R., 2012. Multicentennial variability of the sea surface temperature gradient across the subpolar North Atlantic over the last 2.8 kyr. J. Clim. 25, 4205–4219. https://doi.org/10.1175/JCLI-D-11-00581.1

Miettinen, A., Koç, N., Hall, I.R., Godtliebsen, F., Divine, D., 2011. North Atlantic sea surface temperatures and their relation to the North Atlantic Oscillation during the last 230 years. Clim. Dyn. 36, 533–543. https://doi.org/10.1007/s00382-010-0791-5

Moore, M.D., Charles, C.D., Rubenstone, J.L., Fairbanks, R.G., 2000. U/Th-dated sclerosponges from the Indonesian Seaway record subsurface adjustments to west Pacific Winds. Paleoceanography 15, 404. https://doi.org/10.1029/1999PA000396

Morton, B., 2011. The biology and functional morphology of Arctica islandica (bivalvia: arcticidae) – A gerontophilic living fossil. Mar. Biol. Res. 7, 540–553. https://doi.org/10.1080/17451000.2010.535833

Munro, D., Blier, P.U., 2012. The extreme longevity of *Arctica islandica* is associated with increased peroxidation resistance in mitochondrial membranes. Aging Cell 11, 845–855. https://doi.org/10.1111/j.1474-9726.2012.00847.x

Murawski, S.A., Ropes, J.W., Serchuk, F.. M., 1982. Growth of the ocean quahog, *Arctica islandica*, in the Middle Atlantic Bight. Fish. Bull. 80, 21–34.

Neuendorf, K.K.E., Mehl Jr., J.P., Jackson, J.A. (Eds.), 2005. Glossary of Geology, 5th ed. American Geological Institute, Alexandria, Virginia.

Nielsen, J., 2004. Taphonomy in the light of intrinsic shell properties and life habits: Marine bivalves from the Eemian of northern Russia. Paläontologische Zeitschrift 78, 53–72. https://doi.org/10.1007/bf03009130

Nielsen, T.G., Richardson, K., 1989. Food chain structure of the North Sea plankton communities: seasonal variations of the role of the microbial loop. Mar. Ecol. Prog. Ser. 56, 75–87. https://doi.org/10.3354/meps056075

Nishida, K., Ishimura, T., 2017. Grain-scale stable carbon and oxygen isotopic variations of the international

reference calcite, IAEA-603. Rapid Commun. Mass Spectrom. 31, 1875–1880. https://doi.org/10.1002/rcm.7966

O'Reilly, C.H., Woollings, T., Zanna, L., 2017. The dynamical influence of the Atlantic Multidecadal Oscillation on continental climate. J. Clim. 30, 7213–7230. https://doi.org/10.1175/JCLI-D-16-0345.1

Oeschger, R., Storey, K.B., 1993. Impact of anoxia and hydrogen sulphide on the metabolism of *Arctica islandica* L. (bivalvia). J. Exp. Mar. Bio. Ecol. 170, 213–226. https://doi.org/10.1016/0022-0981(93)90153-F

OSPAR, 2000. Geography, hydrography and climate, in: Quality Status Report 2000 Region II North Sea. OSPAR Commission, London, pp. 4–25.

Otto, L., Zimmerman, J.T.F., Furnes, G.K., Mork, M., Saetre, R., Becker, G., 1990. Review of the physical oceanography of the North Sea. Netherlands J. Sea Res. 26, 161–238. https://doi.org/10.1016/0077-7579(90)90091-T

Pace, S.M., Powell, E.N., Mann, R., Long, M.C., Klinck, J.M., 2017. Development of an age-frequency distribution for ocean quahogs (*Arctica islandica*) on Georges Bank. J. Shellfish Res. 36, 41–53. https://doi.org/10.2983/035.036.0106

Paul, D., Skrzypek, G., 2006. Flushing time and storage effects on the accuracy and precision of carbon and oxygen isotope ratios of sample using the Gasbench II technique. Rapid Commun. Mass Spectrom. 20, 2033–2040. https://doi.org/10.1002/rcm.2559

Peterson, C.H., Kennicutt II, M.C., Green, R.H., Montagna, P., Harper, Jr., D.E., Powell, E.N., Roscigno, P.F., 1996. Ecological consequences of environmental perturbations associated with offshore hydrocarbon production: A perspective on long-term exposures in the Gulf of Mexico. Can. J. Fish. Aquat. Sci. 53, 2637–2654. https://doi.org/10.1139/f96-220

Petrie, B., 2007. Does the North Atlantic Oscillation affect hydrographic properties on the Canadian Atlantic Continental Shelf? Atmos. - Ocean 45, 141–151. https://doi.org/10.3137/ao.450302

Pinnegar, J.K., Engelhard, G.H., Jones, M.C., Cheung, W.W.L., Peck, M.A., Rijnsdorp, A.D., Brander, K.M., 2016. Socio-economic impacts—Fisheries, in: Quante, M., Colijn, F. (Eds.), North Sea Region Climate Change Assessment. Springer International Publishing, Cham, pp. 375–395. https://doi.org/10.1007/978-3-319-39745-0_12

Pitcher, T.J., Lam, M.E., 2014. Fish commoditization and the historical origins of catching fish for profit. Marit. Stud. 14. https://doi.org/10.1186/s40152-014-0014-5

Poulsen, B., 2010. The variability of fisheries and fish populations prior to industrialized fishing: An appraisal of the historical evidence. J. Mar. Syst. 79, 327–332. https://doi.org/10.1016/j.jmarsys.2008.12.011

Poulsen, B., 2008. Dutch herring: An environmental history, c. 1600-1860. Aksant Academic Publishers, Amsterdam.

Poulsen, R.T., Holm, P., 2007. What can fisheries historians learn from marine science? The concept of catch per unit effort (CPUE). Int. J. Marit. Hist. 19, 89–112. https://doi.org/10.1177/084387140701900205

Purton, L., Brasier, M., 1997. Gastropod carbonate $\delta^{18}O$ and $\delta^{13}C$ values record strong seasonal productivity and stratification shifts during the late Eocene in England. Geology 25, 871–874. https://doi.org/10.1130/0091-7613(1997)025<0871:GCOACV>2.3.CO;2

Quillmann, U., Marchitto, T.M., Jennings, A.E., Andrews, J.T., Friestad, B.F., 2012. Cooling and freshening at 8.2ka on the NW Iceland Shelf recorded in paired $\delta^{18}O$ and Mg/Ca measurements of the benthic foraminifer *Cibicides lobatulus*. Quat. Res. 78, 528–539. https://doi.org/10.1016/j.yqres.2012.08.003

Rahaman, A., Grassian, V.H., Margulis, C.J., 2008. Dynamics of water adsorption onto a calcite surface as a function of relative humidity. J. Phys. Chem. C 112, 2109–2115. https://doi.org/10.1021/jp077594d

Rasmussen, S.O., Vinther, B.M., Clausen, H.B., Andersen, K.K., 2007. Early Holocene climate oscillations recorded in three Greenland ice cores. Quat. Sci. Rev. 26, 1907–1914. https://doi.org/10.1016/j.quascirev.2007.06.015

Rayner, N.A., Parker, D.E., Horton, E.B., Folland, C.K., Alexander, L. V., Rowell, D.P., 2003. Global analyses of sea surface temperature, sea ice, and night marine air temperature since the late nineteenth century. J. Geophys. Res. 108, 4407. https://doi.org/10.1029/2002JD002670

Reimer, P.J., Bard, E., Bayliss, A., Beck, J.W., Blackwell, P.G., Ramsey, C.B., Buck, C.E., Cheng, H., Edwards, R.L., Friedrich, M., Grootes, P.M., Guilderson, T.P., Haflidason, H., Hajdas, I., Hatté, C., Heaton, T.J., Hoffmann, D.L., Hogg, A.G., Hughen, K.A., Kaiser, K.F., Kromer, B., Manning, S.W., Niu, M., Reimer, R.W., Richards, D.A., Scott, E.M., Southon, J.R., Staff, R.A., Turney, C.S.M., van der Plicht, J., 2013. IntCal13 and Marine13 radiocarbon age calibration curves 0–50,000 years cal BP. Radiocarbon 55, 1869–1887. https://doi.org/10.2458/azu_js_rc.55.16947

Renssen, H., Goosse, H., Fichefet, T., 2002. Modeling the effect of freshwater pulses on the early Holocene climate: The influence of high-frequency climate variability. Paleoceanography 17, 10-1-10–16. https://doi.org/10.1029/2001PA000649

Renssen, H., Goosse, H., Fichefet, T., Campin, J.-M., 2001. The 8.2 kyr BP event simulated by a global atmosphere-sea-ice-ocean model. Geophys. Res. Lett. 28, 1567–1570. https://doi.org/10.1029/2000GL012602

Reynolds, D.J., Hall, I.R., Scourse, J.D., Richardson, C.A., Wanamaker, A.D., Butler, P.G., 2017a. Biological and climate controls on North Atlantic marine carbon dynamics over the last millennium: Insights from an absolutely dated shell-based record from the north Icelandic shelf. Global Biogeochem. Cycles 31, 1718–1735. https://doi.org/10.1002/2017GB005708

Reynolds, D.J., Hall, I.R., Slater, S.M., Scourse, J.D., Halloran, P.R., Sayer, M.D.J., 2017b. Reconstructing past seasonal to multicentennial-scale variability in the NE Atlantic Ocean Using the long-lived marine bivalve mollusk *Glycymeris glycymeris*. Paleoceanography 1–21. https://doi.org/10.1002/2017PA003154

Reynolds, D.J., Scourse, J.D., Halloran, P.R., Nederbragt, A.J., Wanamaker Jr., A.D., Butler, P.G., Richardson, C.A., Heinemeier, J., Eiríksson, J., Knudsen, K.L., Hall, I.R., 2016. Annually resolved North Atlantic marine climate over the last millennium. Nat. Commun. 7, 13502. https://doi.org/10.1038/ncomms13502

Richardson, L., 2017. UK Sea Fisheries Statistics 2016, Marine Management Organisation. London.

Ricker, W.E., 1975. Computation and interpretation of biological statistics of fish populations. Bull. Fish. Res. Board Canada 191, 1–382.

Ropes, J.J.W., 1984. Procedures for preparing acetate peels and evidence validating the annual periodicity of growth lines formed in the shells of ocean quahogs, *Arctica islandica*. Mar. Fish. Rev. 46, 27–35.

Ropes, J.W., Murawski, S.A., Serchuk, F.. M., 1984. Size, age, sexual maturity, and sex ratio in ocean quahogs, *Arctica islandica* Linne, off Long Island, New York. Fish. Bull. 82, 253–267.

Rorke, M., 2005. The Scottish herring trade, 1470–1600. Scott. Hist. Rev. 84, 149–165. https://doi.org/10.3366/shr.2005.84.2.149

Rorke, M., 2001. Scottish overseas trade, 1275/86-1597. University of Edigburgh.

Ryhter, J.H., 1969. Photosynthesis and fish production in the sea. Science (80-.). 166, 71–76.

Schloesser, R.W., Rooker, J.R., Louchuoarn, P., Neilson, J.D., Secor, D.H., 2009. Interdecadal variation in seawater $\delta^{13}C$ and δ18O recorded in fish otoliths. Direct 54, 1665–1668.

Schöne, B.R., 2013. *Arctica islandica* (Bivalvia): A unique paleoenvironmental archive of the northern North Atlantic Ocean. Glob. Planet. Change 111, 199–225. https://doi.org/10.1016/j.gloplacha.2013.09.013

Schöne, B.R., Fiebig, J., Pfeiffer, M., Gleß, R., Hickson, J., Johnson, A.L.A., Dreyer, W., Oschmann, W., 2005a. Climate records from a bivalved Methuselah (*Arctica islandica*, Mollusca; Iceland). Palaeogeogr. Palaeoclimatol. Palaeoecol. 228, 130–148. https://doi.org/10.1016/j.palaeo.2005.03.049

Schöne, B.R., Freyre Castro, A.D., Fiebig, J., Houk, S.D., Oschmann, W., Kröncke, I., 2004. Sea surface water temperatures over the period 1884–1983 reconstructed from oxygen isotope ratios of a bivalve mollusk shell (*Arctica islandica*, southern North Sea). Palaeogeogr. Palaeoclimatol. Palaeoecol. 212, 215–232. https://doi.org/10.1016/j.palaeo.2004.05.024

Schöne, B.R., Houk, S.D., Freyre, A.D., Castro, J.F., Oschmann, W., Kröncke, I., Dreyer, W., Gosselck, F., 2005b. Daily growth rates in shells of *Arctica islandica*: Assessing sub-seasonal environmental controls on a long-lived bivalve mollusk. Palaios 20, 78–92. https://doi.org/10.2110/palo.2003.p03-101

Schöne, B.R., Oschmann, W., Rössler, J., Freyre Castro, A.D., Houk, S.D., Kröncke, I., Dreyer, W., Janssen, R., Rumohr, H., Dunca, E., 2003. North Atlantic Oscillation dynamics recorded in shells of a long-lived bivalve mollusk. Geology 31, 1037–1040. https://doi.org/10.1130/G20013.1

Schöne, B.R., Pfeiffer, M., Pohlmann, T., Siegismund, F., 2005c. A seasonally resolved bottom-water temperature record for the period AD 1866-2002 based on shells of *Arctica islandica* (Mollusca, North Sea). Int. J. Climatol. 25, 947–962. https://doi.org/10.1002/joc.1174

Schöne, B.R., Schmitt, K., Maus, M., 2017. Effects of sample pretreatment and external contamination on bivalve shell and Carrara marble $\delta^{18}O$ and $\delta^{13}C$ signatures. Palaeogeogr. Palaeoclimatol. Palaeoecol. 484, 22–32. https://doi.org/10.1016/j.palaeo.2016.10.026

Schöne, B.R., Wanamaker Jr., A.D., Fiebig, J., Thébault, J., Kreutz, K., 2011a. Annually resolved $\delta^{13}C_{shell}$ chronologies of long-lived bivalve mollusks (*Arctica islandica*) reveal oceanic carbon dynamics in the temperate North Atlantic during recent centuries. Palaeogeogr. Palaeoclimatol. Palaeoecol. 302, 31–42. https://doi.org/10.1016/j.palaeo.2010.02.002

Schöne, B.R., Zhang, Z., Radermacher, P., Thébault, J., Jacob, D.E., Nunn, E. V., Maurer, A.F., 2011b. Sr/Ca and Mg/Ca ratios of ontogenetically old, long-lived bivalve shells (Arctica islandica) and their function as paleotemperature proxies. Palaeogeogr. Palaeoclimatol. Palaeoecol. 302, 52–64. https://doi.org/10.1016/j.palaeo.2010.03.016

Scourse, J., Austin, W.E.N., Long, B.T., Assinder, D.J., Huws, D., 2002. Holocene evolution of seasonal stratification in the Celtic Sea: Refined age model, mixing depths and foraminiferal stratigraphy. Mar. Geol. 191, 119–145. https://doi.org/10.1016/S0025-3227(02)00528-5

Scourse, J., Richardson, C., Forsythe, G., Harris, I., Heinemeier, J., Fraser, N., Briffa, K., Jones, P., 2006a. First cross-matched floating chronology from the marine fossil record: data from growth lines of the long-lived bivalve mollusc *Arctica islandica*. The Holocene 16, 967–974. https://doi.org/10.1177/0959683606hl987rp

Scourse, J., Sejrup, H.P., Jones, P.D., HOLSMEER Project Participants, 2006b. Late Holocene oceanographic and climate change from the western European margin: The results of the HOLSMEER project. The Holocene 16, 931–935. https://doi.org/10.1177/0959683606hl984ed

Segers, F., Dickey-Collas, M., Rijnsdorp, A.D., 2007. Prey selection by North Sea herring (*Clupea harengus*), with special reference to fish eggs. ICES J. Mar. Sci. 64, 60–68. https://doi.org/10.1093/icesjms/fsl002

Sharp, Z., 2017. Principles of stable isotope geochemistry, 2nd ed. https://doi.org/10.5072/FK2GB24S9F

Simmonds, E.J., 2007. Comparison of two periods of North Sea herring stock management: Success, failure, and monetary value. ICES J. Mar. Sci. 64, 686–692. https://doi.org/10.1093/icesjms/fsm045

Sims, D.W., Genner, M.J., Southward, A.J., Hawkins, S.J., 2001. Timing of squid migration reflects North Atlantic climate variability. Proc. R. Soc. B Biol. Sci. 268, 2607–2611. https://doi.org/10.1098/rspb.2001.1847

Smylie, M., 1999. Traditional fishing boats of Britain and Ireland. Waterline, Shrewsbury.

Sprintall, J., Cronin, M.F., 2001. Upper Ocean Vertical Structure, in: Encyclopedia of Ocean Sciences. Elsevier, pp. 3120–3128. https://doi.org/10.1006/rwos.2001.0149

Sturt, F., Garrow, D., Bradley, S., 2013. New models of North West European Holocene palaeogeography and inundation. J. Archaeol. Sci. 40, 3963–3976. https://doi.org/10.1016/j.jas.2013.05.023

Sündermann, J., Pohlmann, T., 2011. A brief analysis of North Sea physics. Oceanologia 53, 663–689. https://doi.org/10.5697/oc.53-3.663

Sušelj, K., Sood, A., Heinemann, D., 2010. North Sea near-surface wind climate and its relation to the large-scale circulation patterns. Theor. Appl. Climatol. 99, 403–419. https://doi.org/10.1007/s00704-009-0149-2

Swart, P.K., Greer, L., Rosenheim, B.E., Moses, C.S., Waite, A.J., Winter, A., Dodge, R.E., Helmle, K., 2010. The ^{13}C Suess effect in scleractinian corals mirror changes in the anthropogenic CO_2 inventory of the surface oceans. Geophys. Res. Lett. 37, 1–5. https://doi.org/10.1029/2009GL041397

Tester, A.L., 1955. Estimation of recruitment and natural mortality rate from age-composition and catch data in British Columbia herring populations. J. Fish. Res. Board Canada 12, 649–681. https://doi.org/10.1139/f55-035

Thomas, E.R., Wolff, E.W., Mulvaney, R., Steffensen, J.P., Johnsen, S.J., Arrowsmith, C., White, J.W.C., Vaughn, B., Popp, T., 2007. The 8.2 ka event from Greenland ice cores. Quat. Sci. Rev. 26, 70–81. https://doi.org/10.1016/j.quascirev.2006.07.017

Thompson, I., Jones, D.S., Dreibelbis, D., 1980. Annual internal growth banding and life history of the ocean quahog *Arctica islandica* (Mollusca: Bivalvia). Mar. Biol. 57, 25–34. https://doi.org/10.1007/BF00420964

Thorarinsdóttir, G.G., Gunnarsson, K., Bogason, E., 2009. Mass mortality of ocean quahog, Arctica islandica, on hard substratum in Lonafjördur, north-eastern Iceland after a storm. Mar. Biodivers. Rec. 2, e55. https://doi.org/10.1017/S1755267209000736

Thorarinsdóttir, G.G., Jacobson, L.D., 2005. Fishery biology and biological reference points for management of ocean quahogs (*Arctica islandica*) off Iceland. Fish. Res. 75, 97–106. https://doi.org/10.1016/j.fishres.2005.04.010

Thornalley, D.J.R., Elderfield, H., McCave, I.N., 2009. Holocene oscillations in temperature and salinity of the surface subpolar North Atlantic. Nature 457, 711–714. https://doi.org/10.1038/nature07717

Torbenson, M.C.A., Plunkett, G., Brown, D.M., Pilcher, J.R., Leuschner, H.H., 2015. Asynchrony in key Holocene chronologies: Evidence from Irish bog pines. Geology 43, 799–802. https://doi.org/10.1130/G36914.1

Treydte, K.S., Schleser, G.H., Helle, G., Frank, D.C., Winiger, M., Haug, G.H., Esper, J., 2006. The twentieth century was the wettest period in northern Pakistan over the past millennium. Nature 440, 1179–1182. https://doi.org/10.1038/nature04743

Trofimova, T., Milano, S., Andersson, C., Bonitz, F.G.W., Schöne, B.R., 2018. Oxygen isotope composition of *Arctica islandica* aragonite in the context of shell architectural organization: Implications for paleoclimate reconstructions. Geochemistry, Geophys. Geosystems 19, 453–470. https://doi.org/10.1002/2017GC007239

Turekian, K.K., Cochran, J.K., Nozaki, Y., Thompson, I., Jones, D.S., 1982. Determination of shell deposition rates of *Arctica islandica* from the New York Bight using natural [228]Ra and [228]Th and bomb-produced [14]C[1]. Limnol. Oceanogr. 27, 737–741. https://doi.org/10.4319/lo.1982.27.4.0737

Turrell, W.R., Slesser, G., Payne, R., Adams, R.D., Gillibrand, P.A., 1996. Hydrography of the East Shetland Basin in relation to decadal North Sea variability. ICES J. Mar. Sci. 53, 899–916. https://doi.org/1054–3139/96/060899+18

Tyler-Walters, H., Sabatini, M., 2017. *Arctica islandica* Icelandic cyprine, in: Tyler-Walters, H., Hiscock, K. (Eds.), Marine Life Information Network: Biology and Sensitivity Key Information Reviews. Marine Biological Association of the United Kingdom, Plymouth.

Ungvari, Z., Ridgway, I., Philipp, E.E.R., Campbell, C.M., McQuary, P., Chow, T., Coelho, M., Didier, E.S., Gelino, S., Holmbeck, M.A., Kim, I., Levy, E., Sosnowska, D., Sonntag, W.E., Austad, S.N., Csiszar, A., 2011. Extreme longevity is associated with increased resistance to oxidative stress in *Arctica islandica*, the longest-living non-colonial animal. Journals Gerontol. Ser. A Biol. Sci. Med. Sci. 66A, 741–750. https://doi.org/10.1093/gerona/glr044

Vaganov, E.A., Grachev, A.M., Shishov, V. V., Panyushkina, I.P., Leavitt, S.W., Knorre, A.A., Chebykin, E.P., Menyailo, O. V., 2013. Elemental composition of tree rings: A new perspective in biogeochemistry. Dokl. Biol. Sci. 453, 375–379. https://doi.org/10.1134/S0012496613060203

van Leeuwen, S., Tett, P., Mills, D., van der Molen, J., 2015. Stratified and nonstratified areas in the North Sea: Long-term variability and biological and policy implications. J. Geophys. Res. Ocean. 120, 4670–4686. https://doi.org/10.1002/2014JC010485

Vieten, R., Warken, S., Winter, A., Schröder-Ritzrau, A., Scholz, D., Spötl, C., 2018. Hurricane Impact on Seepage Water in Larga Cave, Puerto Rico. J. Geophys. Res. Biogeosciences 123, 879–888.

https://doi.org/10.1002/2017JG004218

Viitasalo, M., Rosenberg, M., Heiskanen, A.-S., Koski, M., 1999. Sedimentation of copepod fecal material in the coastal northern Baltic Sea: Where did all the pellets go? Limnol. Oceanogr. 44, 1388–1399. https://doi.org/10.4319/lo.1999.44.6.1388

Vindenes, H., Orvik, K.A., Søiland, H., Wehde, H., 2018. Analysis of tidal currents in the North Sea from shipboard acoustic Doppler current profiler data. Cont. Shelf Res. 162, 1–12. https://doi.org/10.1016/j.csr.2018.04.001

Wang, X.L., Zwiers, F.W., Swail, V.R., Feng, Y., 2009. Trends and variability of storminess in the Northeast Atlantic region, 1874–2007. Clim. Dyn. 33, 1179–1195. https://doi.org/10.1007/s00382-008-0504-5

Warrach, K., 1998. Modelling the thermal stratification in the North Sea. J. Mar. Syst. 14, 151–165. https://doi.org/10.1016/S0924-7963(98)00007-4

Warton, D.I., Wright, I.J., Falster, D.S., Westoby, M., 2006. Bivariate line-fitting methods for allometry. Biol. Rev. Camb. Philos. Soc. 81, 259–291. https://doi.org/10.1017/S1464793106007007

Weidman, C.R., Jones, G.A., Lohman, K.C., 1994. The long-lived mollusc *Arctica islandica*: A new paleoceanographic tool for the reconstruction of bottom temperatures for the continental shelves of the northern North Atlantic Ocean. J. Geophys. Res. 99, 18305. https://doi.org/10.1029/94JC01882

Wigley, T.M.L., Briffa, K.R., Jones, P.D., 1984. On the average value of correlated time series, with applications in dendroclimatology and hydrometeorology. J. Clim. Appl. Meteorol. https://doi.org/10.1175/1520-0450(1984)023<0201:OTAVOC>2.0.CO;2

Winter, A., Zanchettin, D., Miller, T., Kushnir, Y., Black, D., Lohmann, G., Burnett, A., Haug, G.H., Estrella-Martínez, J., Breitenbach, S.F.M., Beaufort, L., Rubino, A., Cheng, H., 2015. Persistent drying in the tropics linked to natural forcing. Nat. Commun. 6, 7627. https://doi.org/10.1038/ncomms8627

Winther, N.G., Johannessen, J.A., 2006. North Sea circulation: Atlantic inflow and its destination. J. Geophys. Res. Ocean. 111, 1–12. https://doi.org/10.1029/2005JC003310

Witbaard, R., 1997. Tree of the sea: The use of the internal growth lines in the shell of Arctica islandica (Bivalvia, Mollusca) for the retrospective assessment of marine environmental change. University of Groningen.

Witbaard, R., 1996. Growth variations in *Arctica islandica* L. (mollusca): A reflection of hydrography-related food supply. ICES J. Mar. Sci. 53, 981–987. https://doi.org/10.1006/jmsc.1996.0122

Witbaard, R., Bergman, M.J.N., 2003. The distribution and population structure of the bivalve *Arctica islandica* L. in the North Sea: What possible factors are involved? J. Sea Res. 50, 11–25. https://doi.org/10.1016/S1385-1101(03)00039-X

Witbaard, R., Duineveld, G.C.A., 1990. Shell-growth of the bivalve *Arctica islandica* (L.) and its possible use for evaluating the status of the benthos in the subtidal North Sea. Basteria 54, 801–816.

Witbaard, R., Duineveld, G.C.A., de Wilde, P.A.W.J., 1999. Geographical differences in growth rates of *Arctica islandica* (mollusca: bivalvia) from the North Sea and adjacent waters. J. Mar. Biol. Assoc. United Kingdom 79, 907–915.

Witbaard, R., Duineveld, G.C.A., De Wilde, P.A.W.J., 1997. A long-term growth record derived from *Arctica islandica* (mollusca, bivalvia) from the Fladen Ground (Northern North Sea). J. Mar. Biol. Assoc. United Kingdom 77, 801. https://doi.org/10.1017/S0025315400036201

Witbaard, R., Jansma, E., Sass Klaassen, U., 2003. Copepods link quahog growth to climate. J. Sea Res. 50, 77–83. https://doi.org/10.1016/S1385-1101(03)00040-6

Witbaard, R., Jenness, M.I., Van Der Borg, K., Ganssen, G., 1994. Verification of annual growth increments in *Arctica islandica* L. from the North Sea by means of oxygen and carbon isotopes. Netherlands J. Sea Res. 33, 91–101. https://doi.org/10.1016/0077-7579(94)90054-X

Woosley, R.J., Millero, F.J., Grosell, M., 2012. The solubility of fish-produced high magnesium calcite in seawater. J. Geophys. Res. Ocean. 117, 1–5. https://doi.org/10.1029/2011JC007599

Worbes, M., 2002. One hundred years of tree-ring research in the tropics - A brief history and an outlook to future challenges. Dendrochronologia 20, 217–231. https://doi.org/10.1078/1125-7865-00018

Zettler, M.L., Bonsch, R., Gosselck, F., 2001. Distribution, abundance and some population characteristics of the ocean quahog, Arctica islandica (Linnaeus, 1767), in the Mecklenburg Bight (Baltic Sea). J. Shellfish Res. 20, 161–169.